5-2023

Development and Implementation of a Computational Modeling Tool for Evaluation of THA Component Position

Thang Dac Nguyen
tnguye83@vols.utk.edu

To the Graduate Council:

I am submitting herewith a dissertation written by Thang Dac Nguyen entitled "Development and Implementation of a Computational Modeling Tool for Evaluation of THA Component Position." I have examined the final electronic copy of this dissertation for form and content and recommend that it be accepted in partial fulfillment of the requirements for the degree of Doctor of Philosophy, with a major in Biomedical Engineering.

Richard D. Komistek, Major Professor

We have read this dissertation and recommend its acceptance:

Dr. Reinbolt, Dr. Toai Luong, Dr. Komistek, Dr. LaCour

Accepted for the Council:

Dixie L. Thompson

Vice Provost and Dean of the Graduate School

(Original signatures are on file with official student records.)

Development and Implementation of a Computational Modeling Tool

for Evaluation of THA Component Position

A Dissertation Presented for the

Doctor of Philosophy

Degree

The University of Tennessee, Knoxville

Thang Dac Nguyen

May 2023

DEDICATION

This dissertation is dedicated to my parents, Chuyên and Văn, for your undying support throughout my entire life. Your unconditional love and dedication to ensuring I receive the best opportunities has been a constant source of inspiration and motivation for me. You have always been there for me, both physically and emotionally, guiding me in the right direction from a young age while also trusting my decisions. It is because of your support that I was able to achieve my goals and eventually complete my PhD. I am excited for the future and am forever grateful for everything that you have done for me. To my brother, Đắc Sơn, I want to be someone you can look up to and be proud of, and I will always do my best to be a good role model for you.

This dissertation is also dedicated to Tống Thùy Nga, who has stood by me through thick and thin and waited for me patiently, no matter how long it took. Without your love and support from the beginning, I could not have completed this dissertation. You have been my constant companion, supporting me through the ups and downs of life. You trusted me with all your heart. Your invaluable support cannot be put into words, and the love that you have given me is second to none.

ACKNOWLEDGEMENTS

First and foremost, I would like to thank Dr. Komistek. Your expert guidance, insightful feedback, and unwavering support have been invaluable to me throughout my PhD journey with the Center of Musculoskeletal Research at University of Tennessee Knoxville. I am grateful for your patience, encouragement, and willingness to go above and beyond to help me achieve my goals. Your expertise and dedication to the field of biomedical and medical devices have been an inspiration to me, and I feel fortunate to have had the opportunity to work with you. Thank you, Dr. Komistek, for your guidance and mentorship.

I would also like to extend my gratitude to Dr. Michael LaCour. Throughout my academic journey, Michael has been an infinite source of support, guidance, and encouragement. You have not only provided me with invaluable insights and feedback on my research, but also have been a constant source of motivation and positivity. Most importantly, you have always prioritized my well-being, reminding me to take care of myself during the most challenging times both physically and mentally. Without your support, I would not have been able to complete my PhD in just 4 years. Thank you, Michael!

Thank you to Dr. Manh Ta, you have brought me an opportunity to pursue the doctoral degree at the University of Tennessee Knoxville. You have introduced me to Dr. Komistek and helped me speed up my PhD progress. Your knowledge and understanding

of living in the USA have been an invaluable resource for me. I also want to thank Mrs. Duyen, Dr. Manh Ta's wife, for your kindness, warmth, and hospitality.

Thank you to Dr. Jeffrey Reinbolt for your mentorship and your help in graduate school and your feedback on my research. You have provided me with valuable guidance and feedback on both my dissertation and my internship.

Thank you to my colleagues at CMR, Jarrod, Seth, Garett, Lauren, Milad, and Viet for not just being my colleagues, but also my classmates and friends. My experience at UTK has been so much more memorable with all of you. I really enjoyed the time we ate pizza at Garett's home and played Top Golf together.

Thank you to Viet for helping me with my work. You have been there for me during both the ups and downs of my PhD journey, providing encouragement and support when I needed it most. I feel fortunate to have had such an exceptional mentor and best friend.

Thank you to Carter and Cyris, you guys are my first American friends and roommates. You helped me improve my English and made me feel home here in the United States. I always remember all the memories we had together in Tennessee. Hope to see you soon.

Thank you to Karli, Aaron, and Karli's and Aaron's parents. You have always welcomed me into your home with open arms, treating me like family and making me feel at home. Your generosity, kindness, and warm hospitality have made my experience in

Knoxville unforgettable. Your friendship and support have been a source of strength and encouragement during my most challenging times.

I would like to thank my JointVue co-workers John, Dan, Alan, Maja, Jarrod, Manh Ta, and Dr. Komistek. You all have provided me with valuable insights and feedback, challenging me to push beyond my limits and to strive for excellence. Thank you for being such an important part of my journey before and after graduation.

I would like to thank all my Vietnamese friends in Vietnam Gang. Your friendship and support have been instrumental in making my time at Knoxville and UTK feel like I was back in Vietnam.

Thank you to all my friends in Nhóm Healthy, who have been there for me since we met in high school. You have become a second family where I can always turn to for support and comfort. I am truly blessed to have you in my life. Thank you for being there for me, through thick and thin, and for making my life so much richer and happier.

Finally, I would like to thank Độ Phùng, and Mimosa Chu Việt Dũng. Watching your streams every day has been a cherished habit of mine for a very long time. Your engaging content and positive attitude helped me unwind and stay motivated, even when things felt overwhelming. I am grateful for the joy you have brought to my mental health. Thank you anh Độ and Mimosa.

ABSTRACT

The human body is a complicated structure with muscles, ligaments, bones, and joints. Modeling human body with computational tools are becoming a trend [1]. More importantly, using computational tools to evaluate human body is a non-invasive technique that could help surgeons and researchers evaluate implant products [2]. Therefore, the development of a model which can analyze both implant sizing suggestion and kinematics of subject specific data could prove valuable. For total hip arthroplasty, one common complication is in vivo separation and dislocation of the femoral head within the acetabular cup [3] [4]. Developing a successful computational tool to address this issue includes developing a dynamic model of hip joint, implementing implant sizing suggestion algorithms and computing component alignments. Due to advancement in technology, the current focus has been to develop patient-specific solutions, a combined program of both hip model and implant suggestion model has been developed.

In this dissertation, the primary objective is to develop a fully functional hip analysis software that not only can suggestion and template the implant sizing and position, but the software can also utilize the patient specific data to run simulation with different activities. The second objective of this dissertation is to conduct hip analysis studies using hip analysis software. Overall, the results in this dissertation discuss the effect of different stem positions and surgeon preferences on the outcome of the Total Hip Arthroplasty.

TABLE OF CONTENTS

LIST OF TABLES

LIST OF FIGURES

CHAPTER 1: INTRODUCTION

1.1. Hip anatomy

The hip joint is a large ball-and-socket joint, encompassing of the femoral and the pelvis bones [5] [6]. The hip joint is one of the most important joints in the human body, comprised of some of the largest muscles in the body, providing support and mobility in multiple directions, for everyday activities such as walking, running, jumping, and sitting. The anatomy and the biomechanics of the hip joint has been well studied and documented in many journal articles [5] [6] [7] [8] [9]. The structure of the hip joint consists of several bones, muscles, and ligaments. As stated earlier, the bones that make up the hip joint are the femoral, which is the thigh bone, and the pelvis bone having an acetabulum, which is the socket that the femoral seats within (Figure 1-1). The muscles that surround the hip joint are divided into six groups based on their functionalities: flexion, extension, adduction, abduction, internal rotation, and external rotation. Some major muscles include the gluteal muscles, which are located in the buttocks and are responsible for extending the hip, the adductor muscles, which are located on the inner thigh and are responsible for bringing the leg towards the midline of the body, and the Iliopsoas muscle, which is located in the front of the hip and is responsible for flexing the hip (Figure 1-2 and Figure 1-3).

The ligaments are important constraint forces that support the hip joint, encapsulating the femoral head with the acetabulum, include the iliofemoral ligament, which is located on the front of the joint and prevents the hip from hyperextending, the pubofemoral ligament, which is located on the front of the joint and prevents the hip from

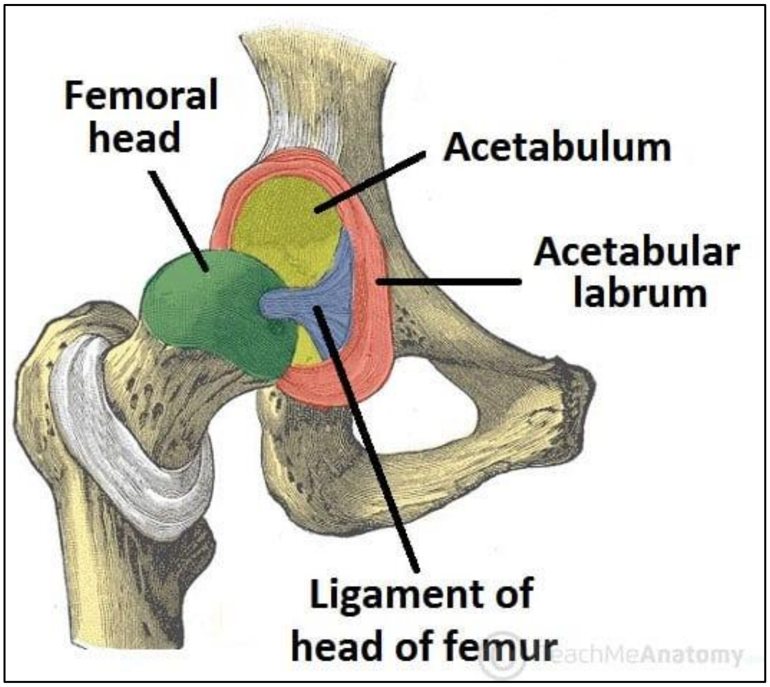

Figure 1-1: The articulating surfaces of the hip joint – pelvic acetabulum and head of the femur (image from: teachmeanatomy.info/lower-limb/joints/hip-joint/).

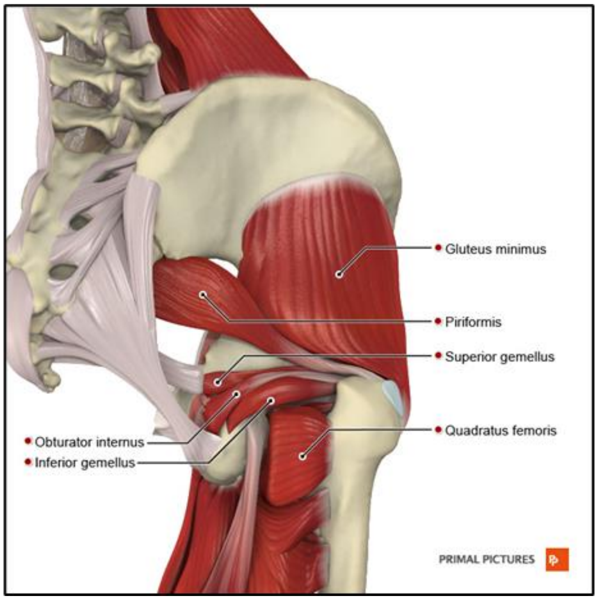

Figure 1-2: Hip muscles (image from: physio-pedia.com/Hip_Anatomy).

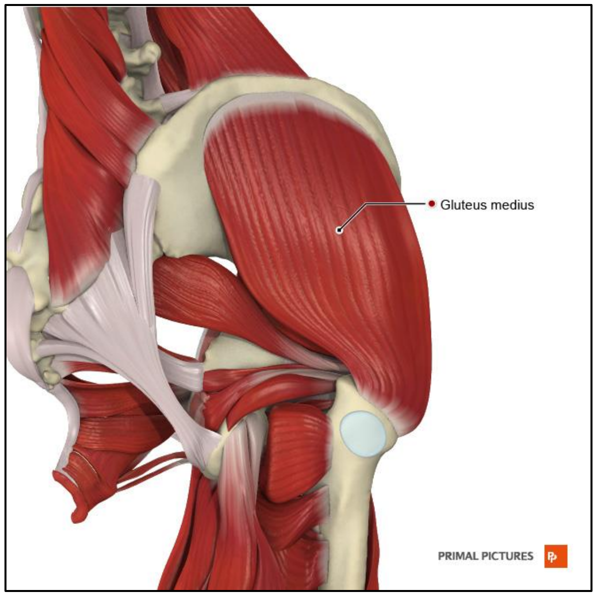

Figure 1-3: Gluteus Medius muscles (image from: physio-pedia.com/Hip_Anatomy).

abducting too far, and the ischiofemoral ligament, which is located on the back of the joint and prevents the hip from hyperextending (Figure 1-4). The femoral head interacting within the acetabulum of the hip joint is essential for both mobility and stability in the human body. As a pure ball and socket joint, there is freedom for all three degrees of rotation, but this joint must also be stabilized to resist unwanted movement. Therefore, the hip joint allows for a wide range of motion, including flexion, extension, abduction, adduction, and rotation. The freedom of rotation in the hip joint, allows for movements to occur, unlike any other joint in the body, so activities to occur, which include lower flexion activities such as walking and running, and also higher flexion activities, such as bending down and sitting. The hip joint also provides stability to the pelvis and lower back, making it an important joint for maintaining posture and balance.

1.2. Total hip arthroplasty

Total hip arthroplasty (THA), a resurfacing procedure, also known as hip replacement surgery, is a surgical procedure in which a damaged or diseased hip joint is replaced with an artificial joint [10]. The artificial joint, called a prosthesis, is typically made up of a metal ball attached to a stem fit within the femoral canal and mated to a socket that is fit in the acetabulum and both are held in place with either bone cement or a bone in-growth material that induces bone to grown within this rougher surface material (Figure 1-5). This procedure is often performed to relieve pain and improve function for patients with severe hip conditions, such as osteoarthritis, rheumatoid arthritis, or hip fractures. Total hip arthroplasty is a major surgery that requires careful planning and preparation and is typically performed under general or regional anesthesia [11] [12].

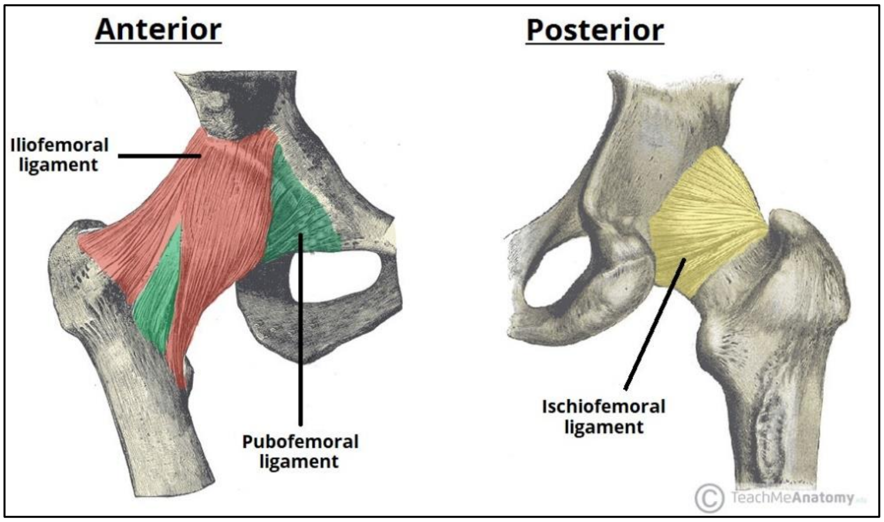

Figure 1-4: The extracapsular ligaments of the hip joint; iliofemoral, pubofemoral and ischiofemoral ligaments (image from: https://teachmeanatomy.info/lower-limb/joints/hip-joint/).

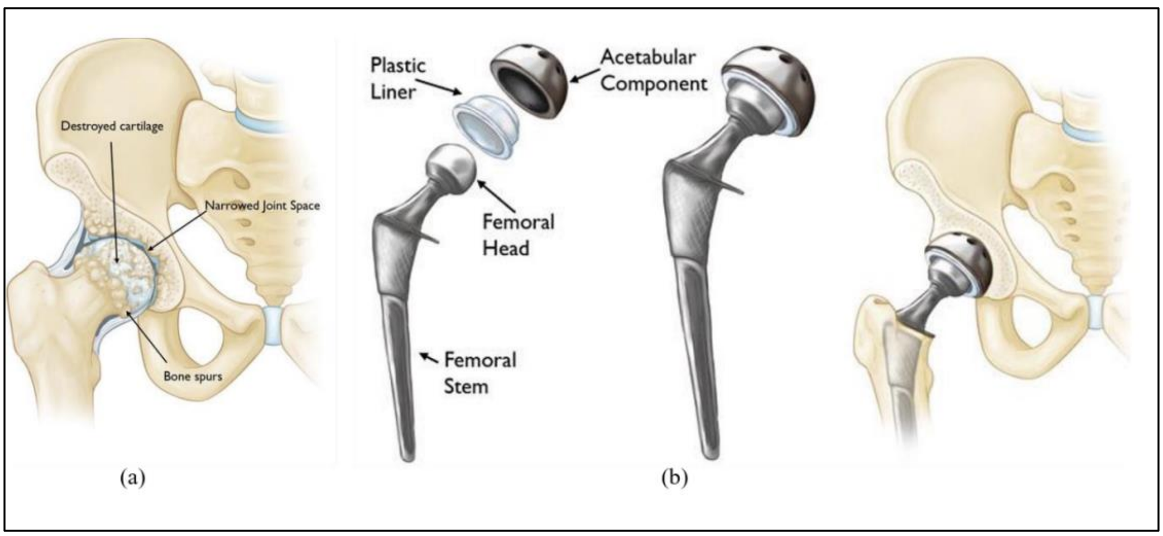

Figure 1-5: (a) An osteoarthritic hip joint and (b) artificial hip joint components. Image from (orthoinfo.aaos.org)

Following the surgery, patients must undergo a period of rehabilitation to regain strength and mobility in the hip joint. While total hip arthroplasty is generally considered a safe and effective procedure [13], there are risks and potential complications associated with any surgery, including infection [14] [15], blood clots [16], implant failure [17] and with hip implants specifically anterior hip pain [18] [19]. Although THA is a very successful procedure, it has recently been documented that over 20% of patients are not happy with their implant because more recently patients are expecting more out of their implant than just pain relief [20].

More recently, mathematical modeling of the hip joint has been the focus of extensive research, aiming to improve our understanding of hip biomechanics and develop effective treatments for various hip conditions including further advancement of THA [21] [22]. Computational models have been developed to predict the mechanics of hip implants, leading to the improvement of implant design, and reducing complications associated with total hip arthroplasty [4] [10] [23]. THA is generally considered a safe and effective treatment option for patients with severe hip conditions, with high success rates and low complication rates. In an article published in 1997 on the Journal of Arthroplasty, Carol A. Mancuso, et al. [24] reported a satisfaction rate of 89% among 180 THA patients after 2 to 3 years follow up. However, a more recent study published on Arthroplasty in 2019, Okafor Lauren, et al. stated that at least 7% of patients are dissatisfied with the outcome of their THA [25], while others have reported an even higher rate [20]. Overall, THA shown to improve mobility, reduce pain, and improve overall quality of life [26], yet

THA is not without limitations. Therefore, careful patient selection and proper surgical technique are crucial for achieving optimal outcomes.

While the risk of serious complications is generally low, the risks associated with anesthesia, bleeding, infection, and other complications is routinely discussed with the patient by the surgeon before the procedure. Additionally, THA is a major surgery that requires a period of recovery and rehabilitation, and patients must follow specific precautions to avoid complications such as dislocation of the hip joint. In an article published in the Journal of Orthopaedic & Sports Physical Therapy, by Deborah M. Kennedy, et al. 2011 [27] they conducted a study to assess the rate of recovery from THA patients. The authors used the Lower Extremity Functional Scale (LEFS) and the 6-minute walk test (6MWT) and found that patients rapidly recover in the first 12 to 15 weeks after THA (Figure 1-6). Moreover, if the patients continued to do their exercises, they will be expected to see more improvements after the first year of surgery. Therefore, consistent with the recovery physical therapy after surgery is a very important factor that contributes to the success of THA. Patients with certain medical conditions or underlying issues may not be good candidates for THA, and cost and access may also be limitations for some patients seeking the procedure.

In conclusion, while research pertaining to the hip joint, THA and mathematical modeling has provided valuable insights into the biomechanics of the hip joint, there remains a subset of THA patients who experience discomfort. Overall, THA remains a highly successful procedure for relieving pain and improving function in patients with severe hip conditions. However, it is important for healthcare providers to carefully

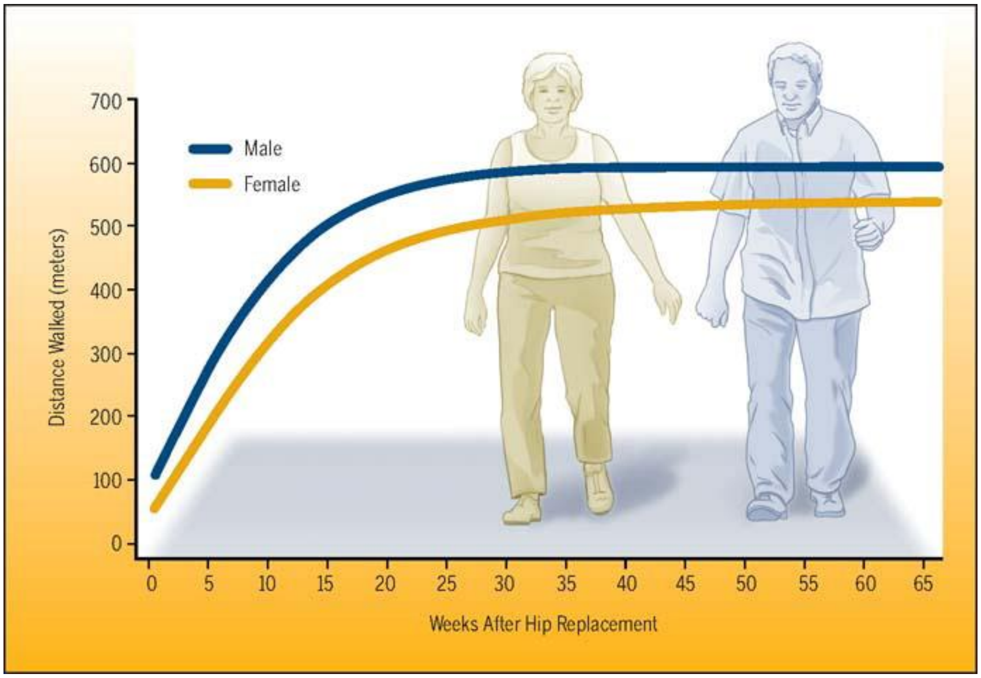

Figure 1-6: The 6-minute walk test results in THA patients. Image from Journal of Orthopaedic & Sports Physical Therapy [28].

evaluate patients and discuss the risks, benefits, and limitations of THA to help patients decide if the procedure is appropriate for them.

CHAPTER 2: BACKGROUND

Advancements related to THA have occurred primarily due to the improvement and advancements related to enhanced technology, some within orthopaedics and others from technology transfer from other fields. The first documented hip arthroplasty was performed in Germany over 130 years ago in 1891 [29], where ivory was used to replace the damaged femoral heads. The modern era of total hip arthroplasty started when Sir John Charnley introduced the low friction arthroplasty that based on three ideas of using low friction, high density, and fixed components to bone [30]. Then, the metal-on-metal hip arthroplasty was developed by an English surgeon George McKee [29]. The metal-on-metal prosthesis had a good survive rate, but it had a huge flaw as the metal on metal contact created small metallic debris that overtime released toxic materials to the surrounded area and causes tissue necrosis [31] [32] [33]. The next generation of the hip prosthesis used a polyethylene liner between the cup and the femoral head to prevent the metal-on-metal contact to occur. With the discovery of radiation in 1896 [34], the advancements of the X-ray technology allow surgeons to view a patient's joint before, during and after surgery. Specifically, in vivo hip fluoroscopy has become a popular method among medical industry.

During the work of this dissertation, the 3D bone models of the hip joint were created using Computed Tomography (CT) scan images and segmentation. More recently, ultrasound technology has also been used as an alternative method to create the 3D bone models which is safer for the patient as they are not subjected to radiation. This background chapter will include the state of the arts technology of CT/ultrasound scan technology, in vivo hip fluoroscopy, popular musculoskeletal modeling methods and software, mathematical modeling using Kane's dynamics, and current implant templating methods that are being used in surgical planning process.

2.1. Computed Tomography and Ultrasound 3D Bone Models

The use of medical imaging has revolutionized the field of medicine and has become an indispensable tool in the diagnosis and treatment of various diseases and injuries. One of the most important applications of medical imaging for orthopaedics is the creation of 3D bone models of within the human body. These models are useful in a wide range of aspects related to orthopaedics, including surgical planning, intra-operative procedures using a robot, and anatomical education. The purpose of this background review is to discuss the state-of-the-art technologies pertaining to CT and Ultrasound for creating 3D bone models.

Computed Tomography (Figure 2-1) scanning is a widely used medical imaging technique that uses X-rays to create detailed images of the internal structures of the body [35] [36] [37]. CT scans are particularly because they provide high-resolution images of the anatomy. CT scans use a computer algorithm to reconstruct a 3D image of the scanned object from a series of 2D images. In recent years, there has been a significant increase in the use of CT scans to create 3D bone models in the human body. One of the areas where CT scan technology has been particularly useful is in the creation of 3D bone models of the hip and knee joints. Dennis et al. (2005) [38] used CT scans to create a 3D model of the implanted knee and normal knee joint for the purpose of studying the weight-bearing kinematics differences between normal knee and anterior cruciate ligament-deficient knee. The researchers found that the 3D model accurately represented the anatomy of the joint

Figure 2-1: An example of CT scan machine. (Image from us.medica.canon)

and could be used to simulate various mechanical loads on the joint [38]. LaCour et al. (2020) [39] used 3D bone models of the hip joint created from CT scans to input to the mathematical hip computational model and surgical planning tools for hip replacement surgeries. The researchers found that the 3D bone models provided accurate information about the anatomy of the hip joint, which helped the researchers to validate the forward dynamics mathematical model of the hip [39].

Ultrasound imaging (Figure 2-2) is a medical imaging technique that uses high-frequency sound waves to create images of the internal structures of the body [40] [41]. Ultrasound imaging has become particularly useful for creating 3D models of anatomical structures for high risk patients that are difficult to image with CT scans, such as children and pregnant woman. More recently, there has been an increasing interest in the use of ultrasound technology to create 3D bone models of the hip and knee joints. Mahfouz et al. (2021) reviewed the current techniques and future directions of 3D ultrasound imaging of the knee joint. The authors stated that ultrasound imaging is a non-invasive, time saving, and low-cost alternative to CT scans for creating 3D bone models of the knee joint [42]. In another study by Riglet et al. (2022), the authors developed a novel method for measuring the orientation of the liner in the dual mobility cup in the THA using ultrasound. The researchers compared the results between ultrasound imaging and 3D laser scan for submerged dual mobility cup. They found the mean difference between the two imaging methods for liner orientation with respect to the shell is 1.2° [43]. The authors concluded that their study validated the feasibility of using ultrasound to measure the liner orientation in the shell of submerged dual mobility cup ex vivo. Their study did not conduct in vivo

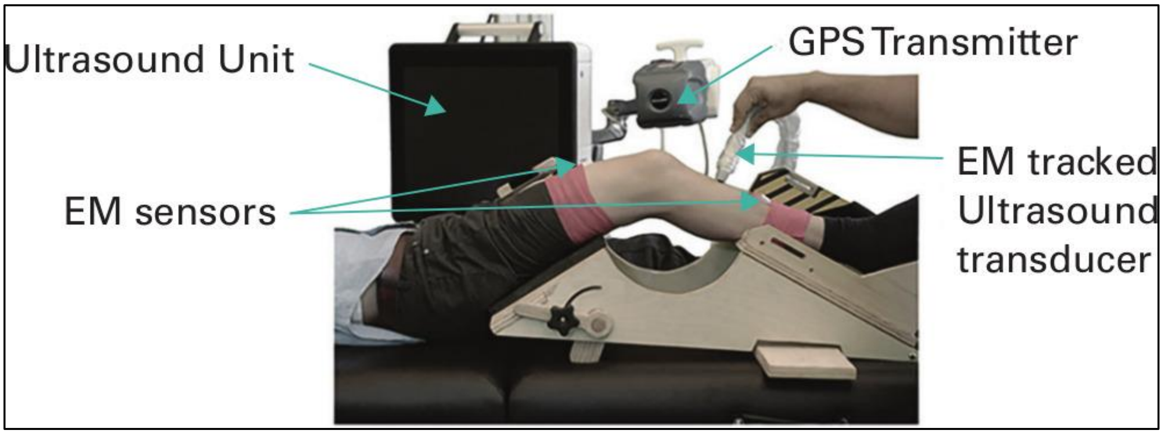

Figure 2-2: An example of an ultrasound machine scanning subject's knee. (Image from Mahfouz et al. (2021) [42])

experiments and they suggested that in vivo experiments should be conducted in the future to further assess the feasibility of their 3D ultrasound method. However, the authors noted that there are still limitations to ultrasound imaging, such as limited depth penetration and difficulty imaging bone structures, but these can be overcome by using a different wand or changing the settings on the ultrasound unit [43].

There has been some reviews in the literature regarding the relative advantages and disadvantages of CT scan technology and ultrasound technology for creating 3D object models of anatomical structures in the human body [44] [45] [46]. In general, while CT scans provide higher resolution images than ultrasound imaging, they also expose the patient to ionizing radiation, which can be a concern in certain populations such as children and pregnant women. Additionally, CT scans can be more expensive and time-consuming than ultrasound imaging and the patient is subjected to two different medical office visits, which becomes a concern for elderly patients during the Covid pandemic. Limiting the number of office visits a patient has to take, minimizes their exposure to various diseases. On the other hand, ultrasound imaging is a non-invasive and low-cost alternative to CT scans. Ultrasound imaging is also able to capture dynamic images of anatomical structures, which can be useful in certain applications such as assessing joint mobility.

In conclusion, CT scan technology and ultrasound technology are both effective tools for creating 3D bone models of anatomical structures in the human body. CT scans provide high-resolution images and are particularly useful for imaging bone structures, while ultrasound imaging is a non-invasive and low-cost alternative that is able to capture dynamic images of anatomical structures. Both technologies have been used successfully in various clinical applications, such as surgical planning and biomechanical studies. The choice of which technology to use depends on the specific application and the patient population being imaged. Further research is needed to improve the accuracy and efficiency of both CT scan technology and ultrasound technology for creating 3D object models in the human body.

2.2. Fluoroscopy and Magnetic Resonance Imaging

In vivo hip fluoroscopy is a medical imaging technique that uses low-dose X-rays to create real-time images of the hip joint while a person is in motion. It involves the use of a fluoroscope (Figure 2-3), a special type of X-ray machine that produces real-time moving images of any human joint [47]. This allows healthcare professionals to view the joint as it is moving in real-time, enabling them to identify any abnormalities or injuries that may be causing pain or discomfort. Another popular medical imaging technology is Magnetic Resonance Imaging (MRI). The MRI machine (Figure 2-4) consists of a large, circular magnet that creates a strong magnetic field around the body. The patient needs to lie inside the machine to create highly detailed images of the body's tissues and organs. Fluoroscopy, on the other hand, produces images that are not as detailed as MRI but is useful for real-time imaging in two-dimension, which can be converted to 3D using a model-fitting technique, during certain procedures. Fluoroscopy is a minimally invasive procedure that is usually shorter and can be completed in a matter of minutes. It can also be used during hip surgeries to ensure accurate placement of implants or other devices.

Figure 2-3: An example of fluoroscope machine. (Image from medicalequipment-msl.com)

Figure 2-4: An MRI machine. (Image from simonmed.com)

In vivo hip fluoroscopy has several clinical applications, including the assessment of hip joint mechanics, implant performance, and the diagnosis of hip pathologies such as femoroacetabular impingement [48], hip separation [49], and osteoarthritis [50]. In a study conducted by Komistek, et al. (2001) [49], 20 subjects with different hip conditions were analyzed using fluoroscopy videos to investigate the effects of hip ligaments absence after THA (Figure 2-5). The error analysis for the fluoroscopy found that the accuracy of the measurements using fluoroscopy was under 0.75 mm [51] (Figure 2-6). The fluoroscopy has been proven as an accurate method to analyze the hip joint with minimal measurement errors.

Since fluoroscopy can provide real-time images of the hip joint during movement, it is a suitable method to extract kinematics data from implanted patients. That kinematics data then can be used as input for advanced computational modeling. For example, Mahfouz, et al. (2003) [52] used fluoroscopy to analyze knee kinematics under in vivo conditions. The authors used fluoroscopy images in a perspective projection, 3D models of knee implants were then overlayed to the X-ray images (Figure 2-7). The kinematics data were then used to reconstruct the motion of the knee joint during weight-bearing activities such as gait, step up, step down, deep knee bend, etc. The kinematics data were analyzed under weight-bearing conditions and the authors were able to determine in vivo motions and detect any abnormalities [52].

Overall, fluoroscopy is a valuable medical imaging tool for assessing hip and knee joint mechanics and pathology. Its ability to provide real-time images of the hip joint during movement makes it a valuable addition to the diagnostic arsenal of clinicians. However,

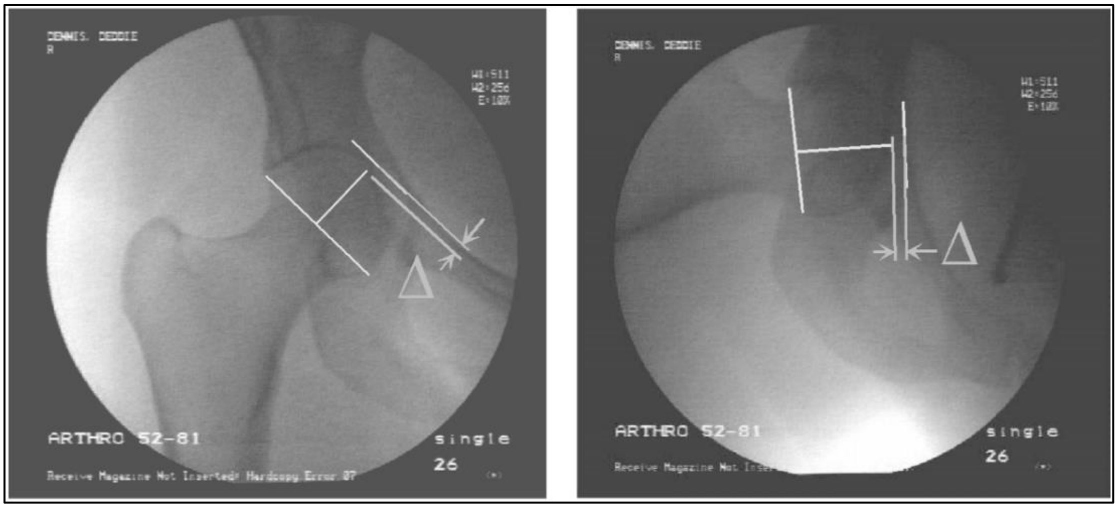

Figure 2-5: An example of a fluoroscopy video from a normal hip subject - Images from Komistek, et al. (2001).

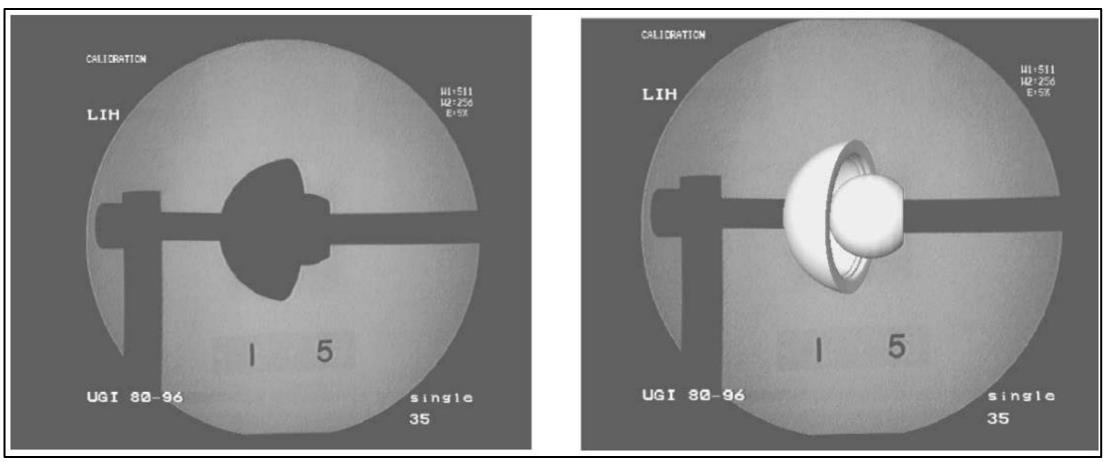

Figure 2-6: An example of overlaying process during error analysis - Images from Komistek, et al. (2001).

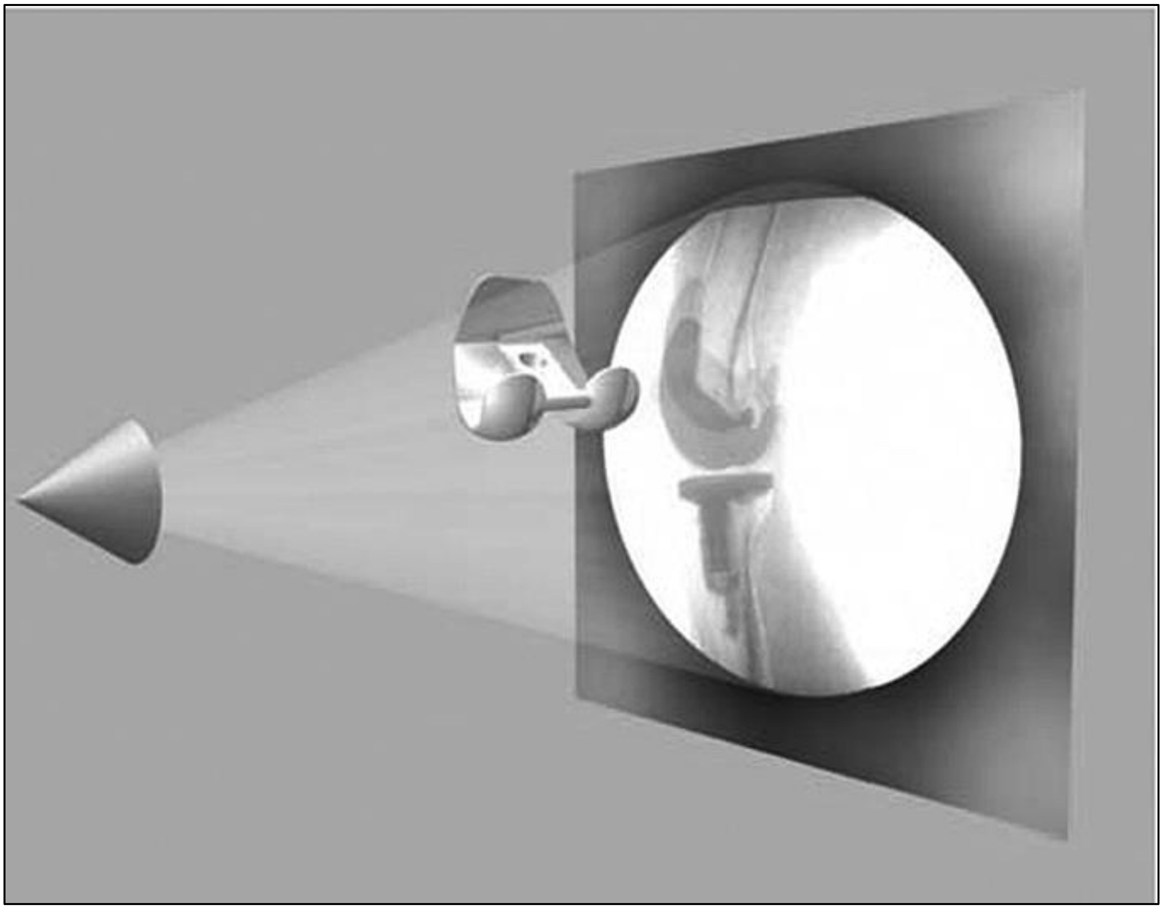

Figure 2-7: An example of perspective projection and overlaying process of the knee implant to an X-ray image (image from Mahfouz, et al. 2003).

fluoroscopy uses X-ray, which can be harmful with prolonged exposure. Thus, it is important to use the lowest possible radiation dose that is still effective for the procedure.

2.3. Visualization Toolkit framework

Visualization Toolkit (VTK) is an open-source software for manipulating and displaying scientific data. A Graphical User Interface (GUI) is a tool that was designed to help human to interact with computer more efficiently. This section will provide a deeper understanding of the VTK and GUI applications and how these tools are implemented to the hip model.

Since VTK is an open-source software, GUI implementation using VTK is highly documented online. VTK examples can be found online at ketware.github.io and most of examples are written in C++, Java, and Python. Although there are not many examples of VTK algorithms written in MATLAB, we can still use C++ or Java examples as references when we implement VTK in MATLAB. Overall, VTK offers many advanced features from 3D manipulation such as subject color changes, lighting conditions and shading to 3D visualizing algorithms such as vector, scalar, volumetric calculation, mesh-mesh distances, and Boolean operations. Step by step to implement VTK to Windows system and MATLAB will be discussed in the following paragraph. Figure 2-8 pertains to the structure of VTK visualization pipeline. Conceptually, the structure of VTK pipeline includes four main objects classes: (1) data object class that represents data; (2) algorithm object class that transforms, projects, filters data; (3) displaying control object class execute the visualization; and (4) interactor object class which is generally a bridge between User and VTK render window.

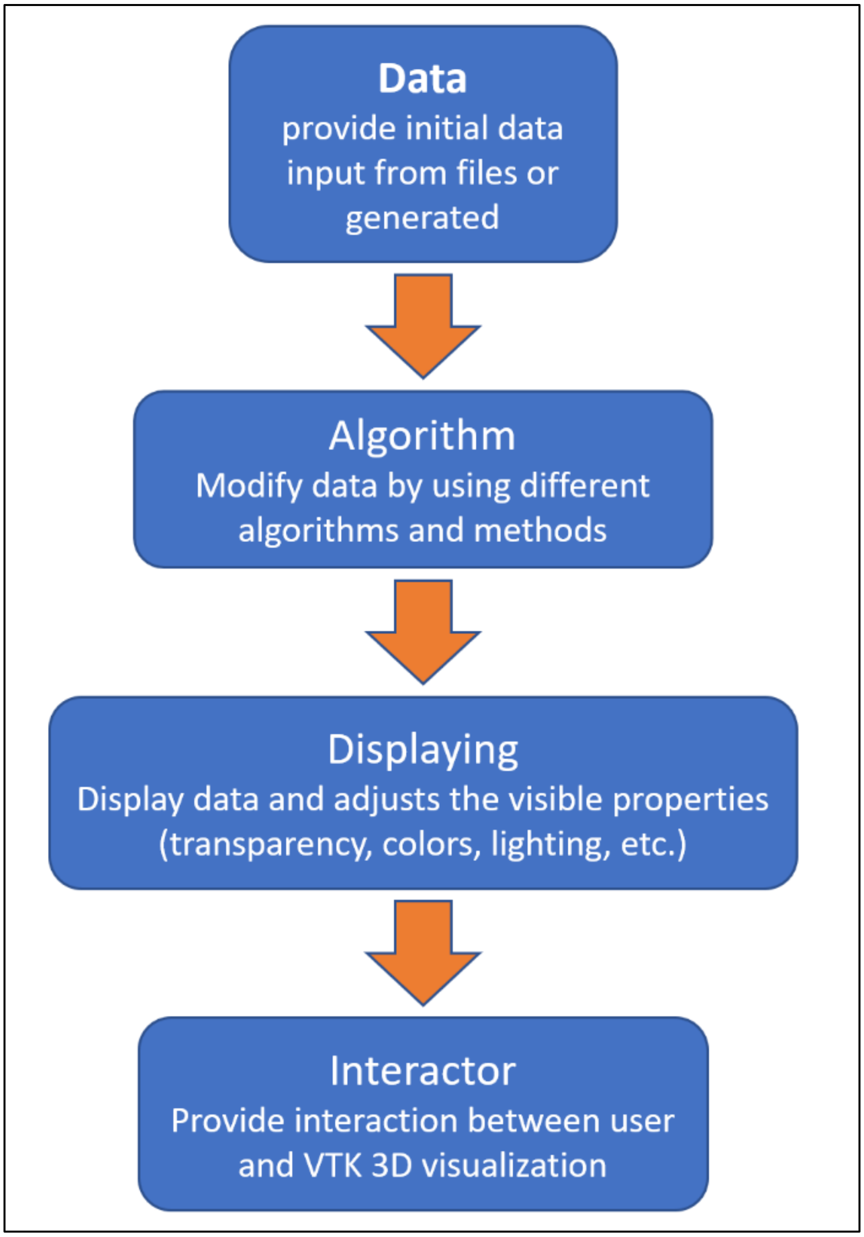

Figure 2-8: VTK pipeline.

Although the VTK pipeline structure is simple with just four main object classes, using VTK properly and efficiently is quite challenging because of the highly hierarchical and complex structures of VTK objects. For example, vtkTransformPolyDataFilter class is the child class of vtkPolyDataAlgorithm class, that means vtkTransformPolyDataFilter inherited all properties and methods in vtkPolyDataAlgorithm class and can be use in any function that the input is a vtkPolyDataAlgorithm class object. The information about classes inheritance can be found in VTK documentation online. The vtkPolyDataAlgorithm class is also a child class of vtkAlgorithm class, and vtkAlgorithm class is a child class of an even more abstract class – vtkObject class (Figure 2-9).

In this section, implementation of VTK in MATLAB will be introduced briefly by discussing different examples. Since VTK visualization and algorithms have involved in many aspects of this dissertation, there is not enough room available to fully discuss every aspect. Therefore, only the most important and fundamental aspects of VTK which were used in this dissertation will be introduced. The following code example was implemented in MATLAB using VTK to create a sphere data that later can be used as an input for algorithm classes.

```
% create sphere data
sourcePoint = vtkSphereSource.New();
mapperPoint = vtkPolyDataMapper.New();
actorPoint = vtkActor.New();
% sphere setting
sourcePoint.SetRadius(Radius);
```

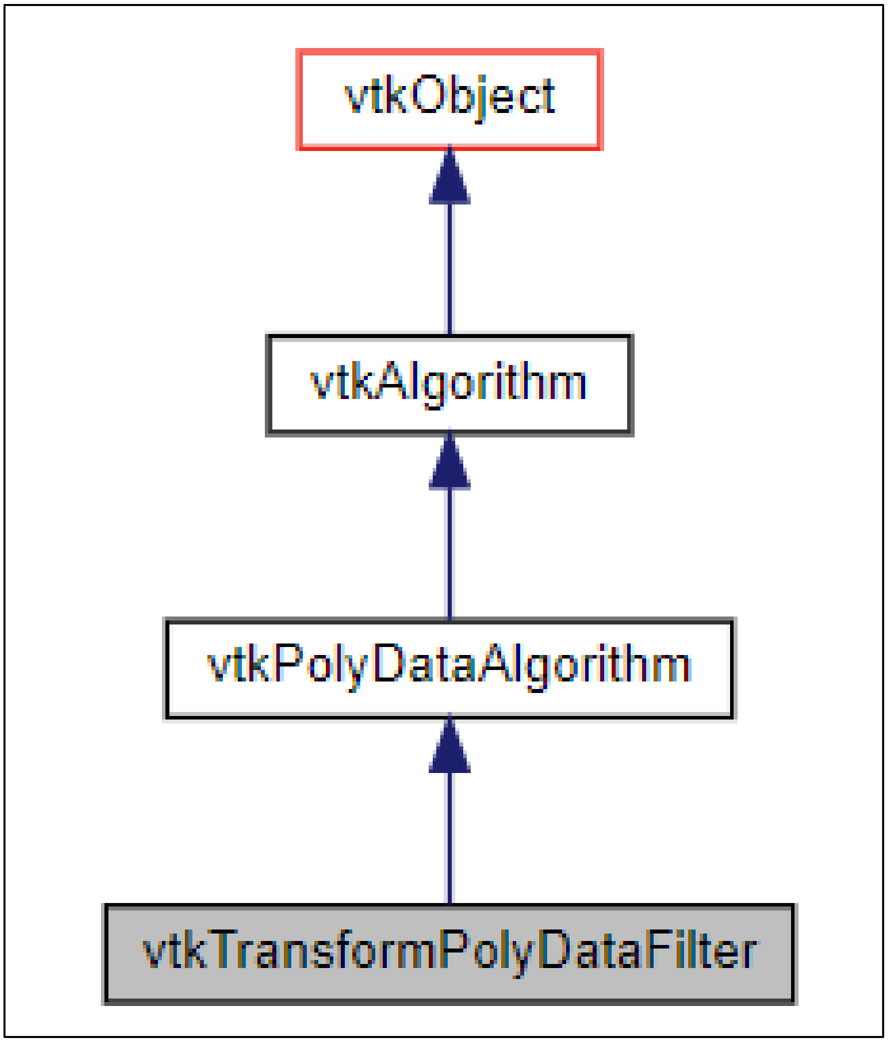

Figure 2-9: Inheritance diagram for vtkTransformPolyDataFilter class.

```
sourcePoint.SetCenter(Position(1), Position(2),
Position(3));

sourcePoint.SetPhiResolution(Resolution);

sourcePoint.SetThetaResolution(Resolution);

mapperPoint.SetInputConnection(sourcePoint.GetOutputPort())
;

actorPoint.SetMapper(mapperPoint);

% set properties

actorPoint.GetProperty().SetColor(Color(1), Color(2),
Color(3));

actorPoint.GetProperty().SetOpacity(1);

Usermatrix = vtkMatrix4x4.New();

actorPoint.SetUserMatrix(Usermatrix);

actor = actorPoint;
```

The sphere source is created using the command "`sourcePoint = vtkSphereSource.New();`". After having a sphere source object, the position and the resolution of the sphere can be adjusted by changing the setting of the sphere object. Having an actor of the sphere is just the first step of displaying the sphere on the screen. In the next step, the sphere actor will be placed to a renderer and render window. An interactor will be added to render window to allow User to interact with the sphere.

```
% Render window

RenderWindow = vtkRenderWindow.New();

renderer = vtkRenderer.New();

RenderWindow.AddRenderer(renderer);

renderer.SetBackground(0.8275,0.8314,0.9765);
```

```
% Add Interactor
renderWindowInteractor = vtkRenderWindowInteractor.New();
renderWindowInteractor.SetRenderWindow(RenderWindow);
renderWindowInteractor.GetInteractorStyle().SetCurrentStyle
ToTrackballCamera();
RenderWindow.SetSize(900,900);
%% add actor
renderer.AddActor(actor);
RenderWindow.Render();
```

The result is displayed in Figure 2-10. The color of the sphere is set to white, and the resolution value is set to 10. The process of displaying a single sphere object is already very lengthy and takes time to write the code correctly. Thus, a library of VTK functions written in MATLAB was created to minimize the manual and repeating coding process such as inputting data, creating object, mapper, renderer and render window. The whole process of displaying a sphere in Figure 2-10 can be shorten to just 3 lines of code below.

```
%% creating a sphere actor from AddPoint2 function
actor = AddPoint(Radius,Position, Color,Resolution);
%% add actor
renderer.AddActor(actor);
RenderWindow.Render();
```

In this example, all the manual code to set up sphere radius, position, color, and resolution are implemented in the "`AddPoint`" function. In this dissertation, there are many other functions related to VTK were created such as "`AddLine`", "`cutOBJBoolean`",

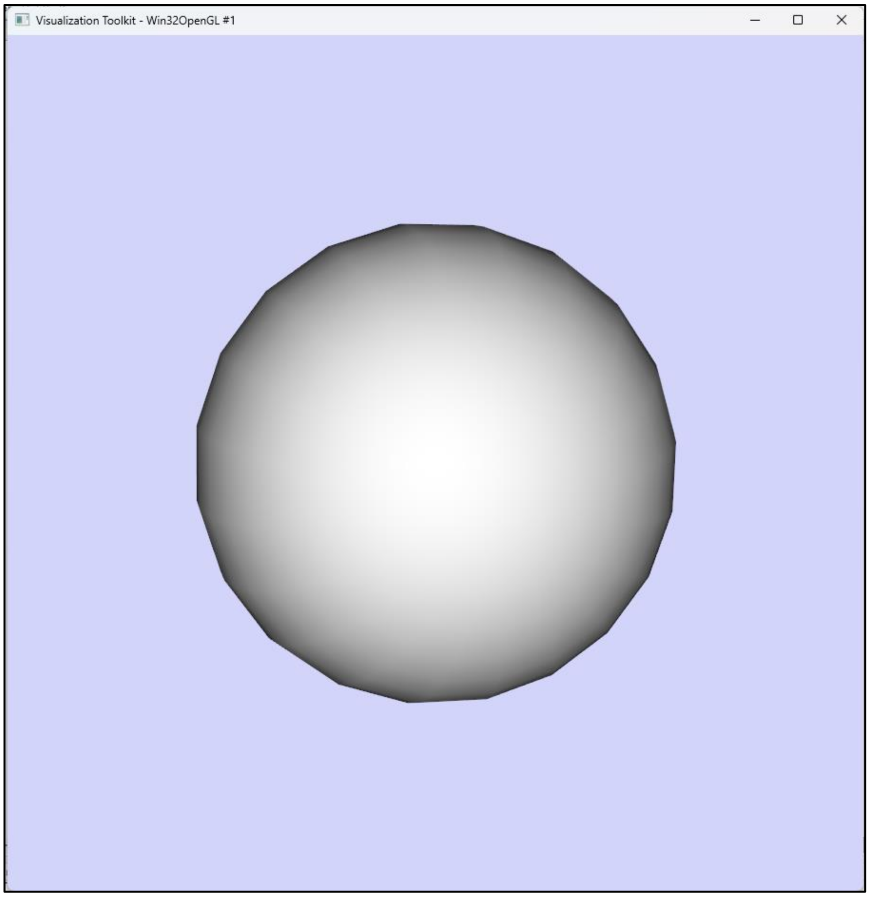

Figure 2-10: Sphere example result.

"SetTxFMatrix", etc. Accordingly, the following example demonstrates the complete code to display a femur.obj file using the VTK functions "displayOBJ". The input of the function includes the path to the .obj file that contains the femur bone 3D model, and the color that we want to display on the screen.

```
path = 'C:\Users\dacth\OneDrive - University of
Tennessee\Desktop\B_Femur.obj';

color = [0.7324,0.7451,0.4549];

displayOBJ(path,color);
```

Figure 2-11 shows the femur object using the "displayOBJ" function. The femur bone object has been displayed successfully by using only 3 lines of codes. It clearly shows the benefit of having a VTK functions library for this dissertation.

In summary, VTK visualization has been discussed briefly in this section. The more advanced VTK implementation will be shown in the next some sections. VTK is not only used to display 3D objects, but it also serves as an algorithm's library. Official VTK instructional documents are available online, and the author of this dissertation suggests anyone who desires to know more about VTK to visit VTK's website and online VTK communities.

2.4. Available musculoskeletal modeling methods and software

There are several popular methods used to analyze the musculoskeletal system of the human body, including finite element analysis (FEA), musculoskeletal modeling with software, such as OpenSim, and AnyBody. These methods are used to study the biomechanics of the human body, including the movement and forces acting on the bones,

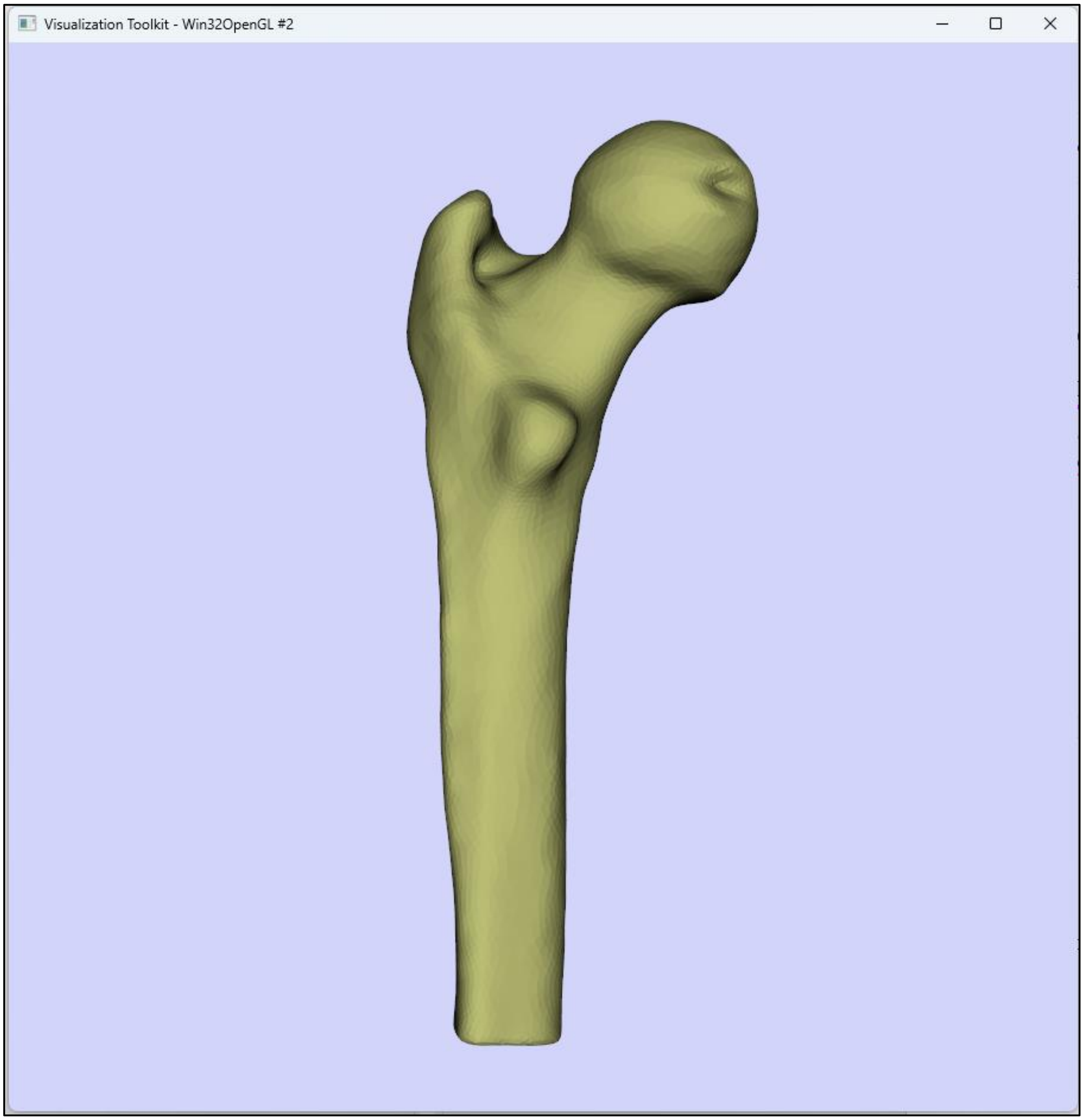

Figure 2-11: Displaying femur bone model with VTK.

muscles, and other structures. The general idea with respect to all modeling methods is to create a computational model of the body and simulating its movements during different activities and soft-tissue structure contributions. Musculoskeletal modeling has become an increasingly popular tool with respect to biomechanics research and has been used to study a wide range of topics, ranging from the mechanics of joint replacement implants to the function of specific muscles during movement [53] [54].

OpenSim [55] is an open-source software package developed by Simbios that allows researchers to create musculoskeletal models of the human body. The software includes a graphical User interface to create models of specific body segments or the entire body (Figure 2-12). OpenSim also includes a library of pre-built models and tools for analyzing data and simulating movements. One of the strengths of OpenSim is its ability to incorporate data from different sources, such as motion capture systems, force plates, and electromyography (EMG) sensors. This allows researchers to create realistic models of movement and study the forces acting on different structures in the body. OpenSim has been used to study a wide range of topics, from the mechanics of gait to the effects of aging on muscle function.

AnyBody [56] is another popular musculoskeletal modeling software package that allows researchers to create models of the human body and simulate movements. Like OpenSim, AnyBody includes a graphical User interface and a library of pre-built models (Figure 2-13). AnyBody also includes a powerful optimization engine that can be used to find the most efficient muscle activation patterns during movement. One of the unique features of AnyBody is its ability to incorporate detailed anatomical data, such as muscle

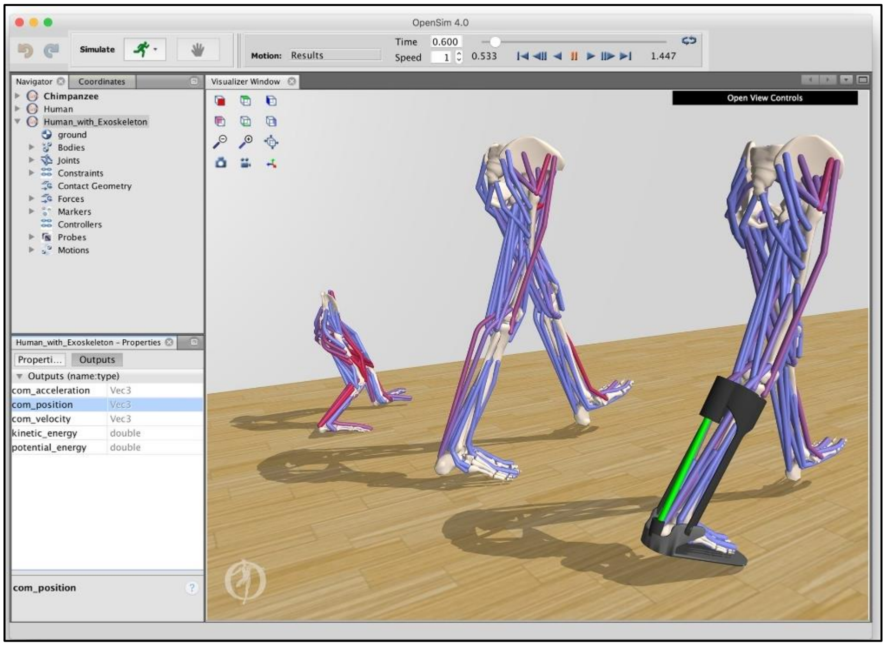

Figure 2-12: OpenSim 4.0 desktop application. (Image from Ajay Seth et al. 2018 [55])

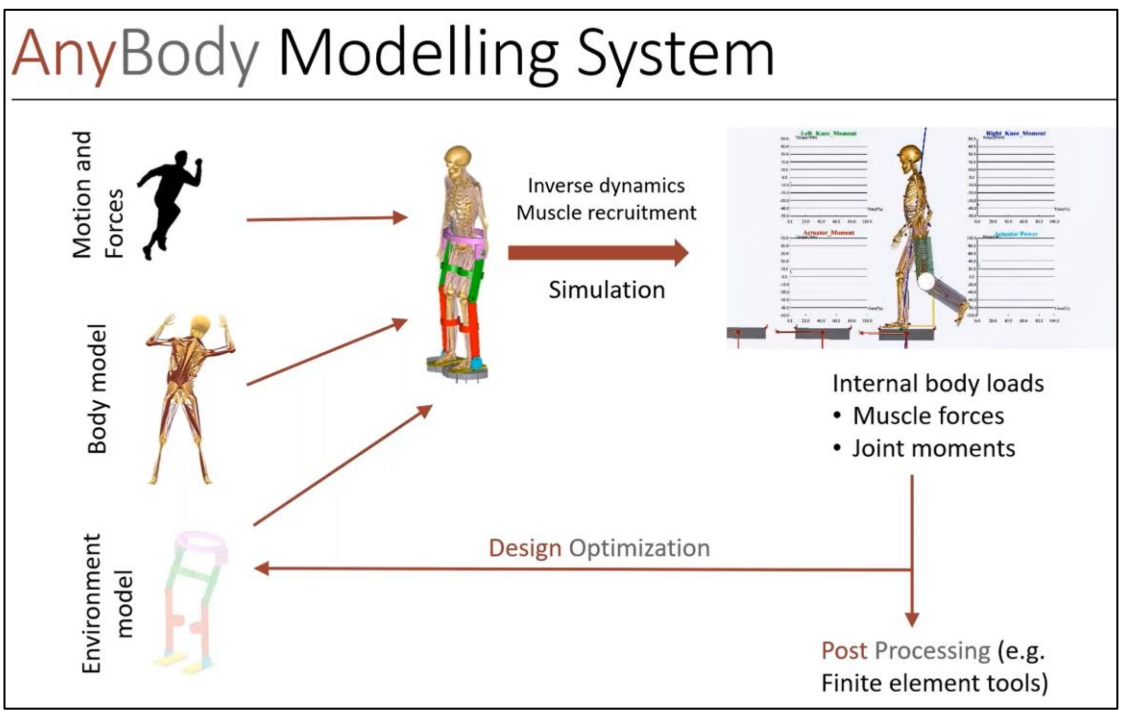

Figure 2-13: AnyBody modeling system. (Image from AnyBody Technology)

fiber directions and muscle attachment points, into its models. This allows researchers to create highly realistic models of the human body and study the forces acting on different structures during movement. AnyBody has been used to study different topics such as the mechanics of the spine to the function of specific muscles in the shoulder.

Another very popular modeling method is finite element method (FEM). The finite element method (FEM) is a powerful numerical technique that has been widely used to model and analyze the behavior of structures in engineering and science [57] [58] [59] [60]. In recent years, FEM has also been applied to the modeling of the human body, particularly in the fields of biomechanics and medical engineering [61] [62] [63] [64]. The methods used for generating FEM models of the human body typically involve medical imaging techniques, such as MRI or CT scans. These techniques produce 3D models of the internal structures of the body, which can be refined using computer-aided design (CAD) software to create a more detailed model (Figure 2-14). The models are then meshed using triangular or tetrahedral elements, with the density of the mesh adjusted to balance accuracy with computational cost (Figure 2-15). The material properties assigned to the model are critical for accurately simulating the behavior of the human body. Different tissues have different properties, such as stiffness and density, and these properties must be assigned appropriately to each element in the model. Material properties can be obtained from experimental data or from literature, and can vary depending on the age, sex, and health status of the individual being modeled. Boundary conditions are extremely important for FEM simulations pertaining to the interaction of the body with its environment. These include the forces and moments applied to joints and bones, as well as the contact forces

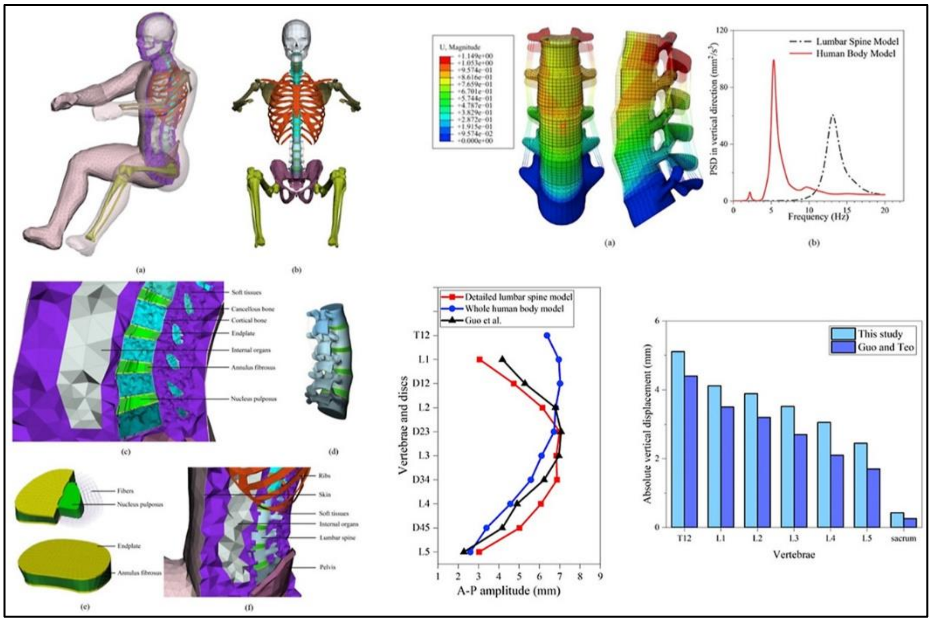

Figure 2-14: Whole human body finite element model with detailed lumbar spine. (Image from Li-Xin Guo, Chi Zhang 2022 [61])

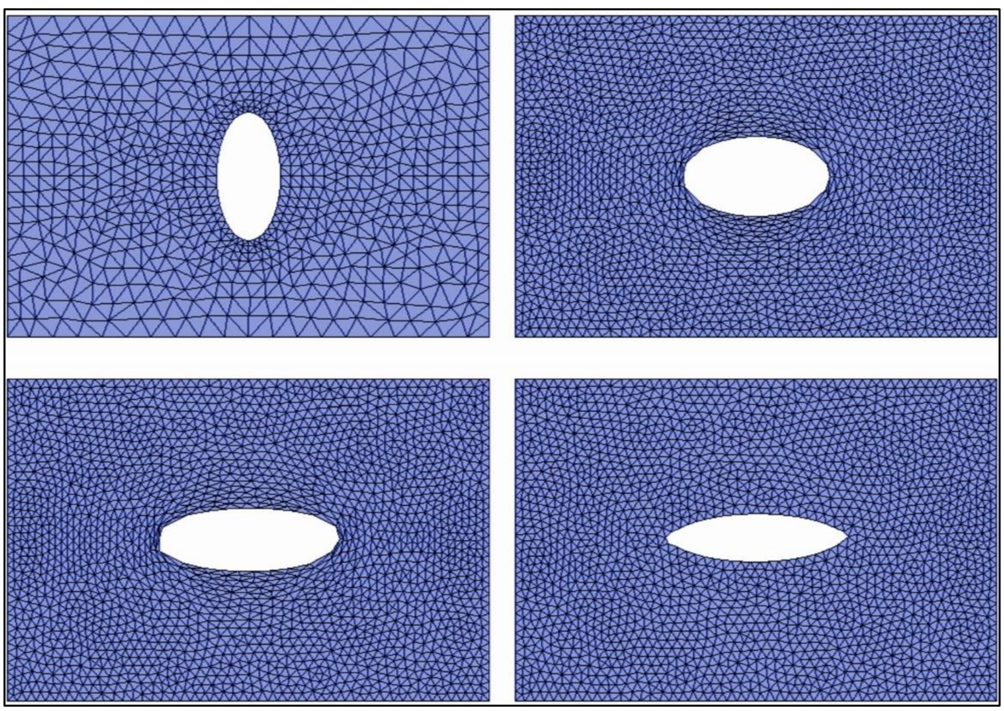

Figure 2-15: Triangular meshes with an optimize shape obstacle. (Image from Thi Thanh Mai Ta, Van Chien Le, Ha Thanh Pham 2018 [60])

between tissues. The FEM could be very accurate but incorrect input and/or boundary conditions could lead to misleading an incorrect result. Boundary conditions can be obtained from experimental data or from literature and can be adjusted to simulate different types of activities, such as walking or running. FEM has been used to design and optimize orthopedic implants, such as hip and knee replacements. By simulating the interaction of the implant with the surrounding bone and tissue, FEM can help to optimize the design to reduce stress concentrations and improve the longevity of the implant. Despite its many advantages, FEM also has some limitations. For example, the accuracy of the model depends on the accuracy of the input data, such as the material properties and boundary conditions. In addition, FEM requires significant computational resources, which can make it difficult to perform real-time simulations or to simulate large portions of the body.

Overall, musculoskeletal modeling is a powerful tool in biomechanics research that allows researchers to create computational models of the human body and simulate its movements during different activities. By studying the forces acting on different structures in the body, musculoskeletal modeling can help to improve our understanding of human movement and ultimately improve outcomes for patients. FEM, OpenSim, and AnyBody are all popular musculoskeletal modeling method used in research of musculoskeletal system of human body.

2.5. Kane’s dynamics in mathematical modeling for the hip joint

The previous section has discussed different computational modeling tools that currently exist such as OpenSim, AnyBody and Finite Element Method and each software package is powerful in its own way, but these are general models that may not be able to focus on a specific problem. Although there are considerable number of models that have been developed, very few of them concentrate on solving problem of hip joint specifically and are parametrically interchangeable and can be uniquely modifies for a specific solution. Choosing a mathematical method to model hip joint also requires understanding the limitations of other existing models. For example, finite element method is very efficient in solving single body problems; OpenSim is recognized for developing a model of musculoskeletal structures and dynamic simulations of movement. However, those models do not address the problem of hip joint instability and micromovement. Therefore, we decided to use Kane's dynamics and AutoLev to develop forward solution hip model that can solve some addressed problems above [23].

The three coding program languages that are used in this project are Autolev, C++ and Matlab. Autolev is a symbolic manipulation, developed by Thomas R. Kane and David A. Levinson [10]. C++ is a standard coding platform to generate executable simulation files, then we use Matlab to develop GUI program that User can interact with the model. Essentially, Autolev is a symbolic calculator that creates system equations. A total of six bones are modeled in the model (Figure 2-16): the foot, the tibial, the patella, the femur, the pelvis, and the torso. Each bone is represented in the model as a rigid body except the patella. Because the patella is very small compared to other bones, we modeled the patella as a frame. Each body has six degrees of freedom, three for translation and three for rotation.

Modeling of the bones in the system requires points to be added to the bodies, representing body mass centers, joints, ligaments, and muscles attachment sites. Initially,

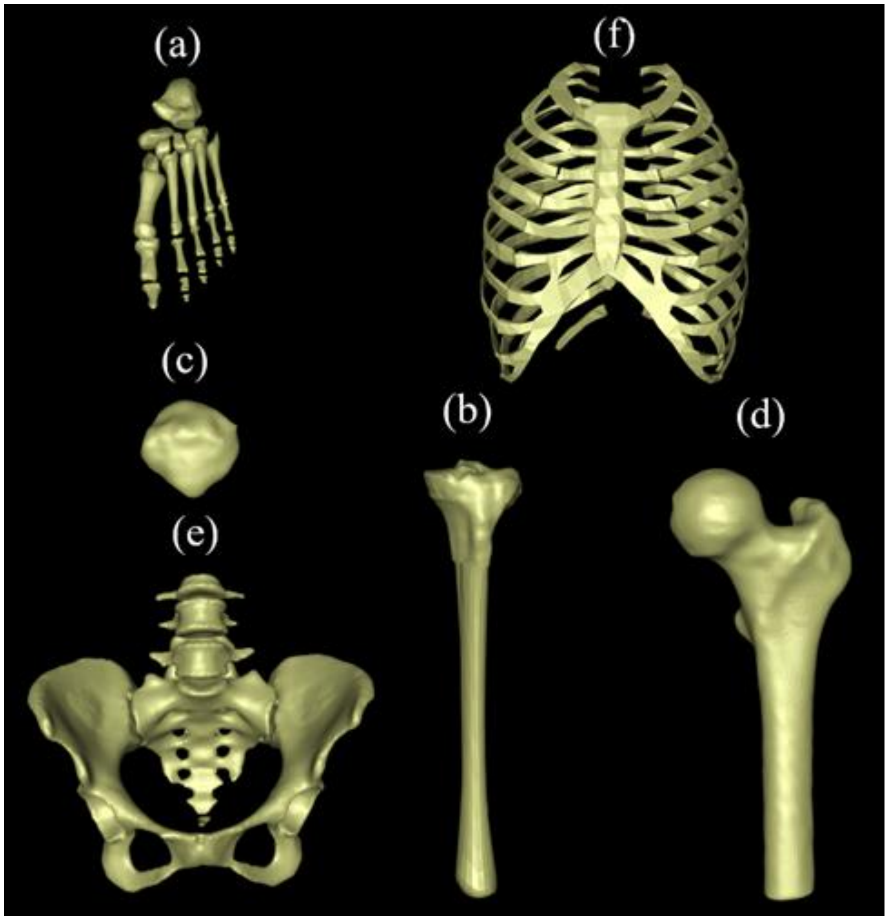

Figure 2-16: (a) foot, (b) tibial, (c) patella, (d) femur, (e) pelvis, and (f) torso bone representation.

these points are based on generic bone models obtained from the Center for Musculoskeletal Research (CMR) bone database, located at the University of Tennessee, Knoxville [23]. During the work of this dissertation, we have been deriving a patient specific database where all points are now included in this database within the CMR lab. More points can be also added to specific regions of interest, such as muscle bending points. The masses of the foot, tibial, femur, and pelvis are set as 1.4%, 4.6%, 10%, and 24% of the patient's body weight, respectively. As described previously, the mass of patella is small and can be considered negligible.

The ligaments modeled in this model are primarily hip capsular ligaments (Figure 2-17). The ligaments are modeled as non-linear system, where the ligament force changed dramatically when it reaches a certain length. The following equation shows the way ligament force is calculated in the model [23].

$$F = \begin{cases} 0 & if\ \Delta < 0, \\ k_1 * \Delta & if\ 0 < \Delta < \varepsilon, \\ k_1 * \varepsilon + k_2 * (\Delta - \varepsilon) & if\ \varepsilon < \Delta. \end{cases}$$

Where Δ is the length difference compared to the initial ligament length, ε is the threshold of the ligament where its tension coefficient changes dramatically, k_1 and k_2 are the stiffness of the ligaments. The ligament force is not a linear function, because the properties of the ligament tension change dramatically when Δ reaches a specific value.

2.6. Implant templating process and its limitations

Preoperative templating has become an essential part of the THA surgical process, as it helps a surgeon in the selection process of the appropriate size and orientation of the

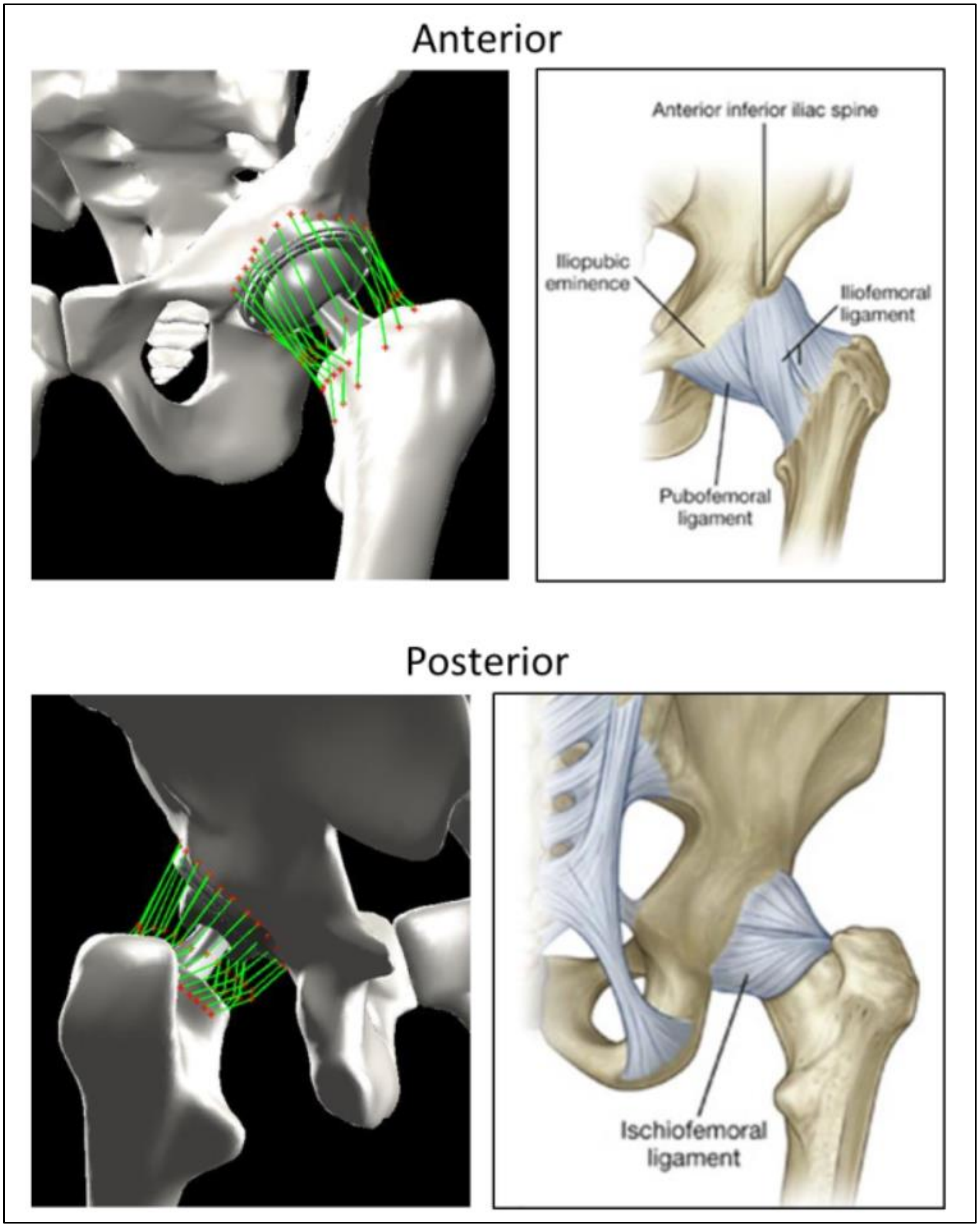

Figure 2-17: Anterior (iliofemoral and pubofemoral) and posterior (ischiofemoral) hip capsular ligaments included in the model. Right images from (basicmedicalkey.com).

implant to be used during the surgery. Over the last four decades, starting from the mid-1980s, there has been a discernible trend of a growing number of companies focusing on the development and implementation of surgical systems incorporating robotic and computer-guided technologies [65], such as Mako SmartRobotics™ from Stryker (Figure 2-18), VELYS™ Robotic-Assisted Solution system from DePuy Synthes (Figure 2-19), CORI Robotics system from Smith & Nephew's (Figure 2-20), and ROSA® Hip System from Zimmer Biommet (Figure 2-21). In all robotic-assisted surgery systems, the preoperative planning step plays a crucial role for determining the implant size and relative component positioning with respect to the bones. The pre-operatively planned surgery can then be performed intraoperatively. The precision of robotic during surgery has the potential to effectively transform preoperative planning from a theoretical step into an actual surgery. Therefore, enhancing the precision and efficacy of preoperative planning tools has become increasingly imperative. Additionally, accurate placement of implant components plays a critical role in ensuring optimal joint stability, function, and durability of newly implanted hip joints. Specifically, with respect to THA, predicting the stem position within the femoral canal is one of the main tasks of the templating process. The stem position depends on various factors, from the anatomical shape of the canal to the surgeon preferences pertaining to stem version, etc. Therefore, we need to take all the factor into consideration during the implementation of implant positioning process. To the best of our knowledge, there has been minimal attention given to the crucial aspect of implant positioning in relation to various factors.

Figure 2-18: Mako™ Robotic – Arm Assisted Surgery from Stryker. (Image from ubh.org)

Figure 2-19: VELYS™ Robotic-Assisted Solution system from DePuy Synthes. (Image from jnjmedtech.com)

Figure 2-20: Smith & Nephew's CORI Robotics system. (Image from medicaldevice-network.com)

Figure 2-21: ROSA® Hip System from Zimmer Biomet. (Image from zimmerbiomet.com).

One example of an attempt to suggest the optimal plan for THA is the study from Otomaru et al. (2012) [66]. The authors have developed an automated preoperative planning process using Atlas-based methods to calculate the average pattern of the contact map between the stem and the femoral canal. Based on the average pattern of the contact map, the authors calculated the “optimal reference plan” in which the stem is planned to fit the average contact pattern with the canal (Figure 2-22). However, their method only provides the average plan based on the training dataset. It does not mean their optimal plan satisfies the specific surgeon preferences since each surgeon has a different stem alignment preference. Moreover, even though their method used the patient’s canal shape to calculate the resulted contact map, the stem might not be in the canal fit position where the contact with the stem and the cortical bone is optimal.

Before implant templating process, imaging techniques such as 2D X-rays, CT scans, and MRI scans have been used to create a template of the patient's hip joint, which was then used to determine the size and orientation of the implant needed for the surgery. 2D X-ray images are commonly used for implant templating due to their availability and relatively low cost compared to more advanced imaging techniques. However, there are several limitations to using 2D X-ray images for implant templating that must be considered. One of the main limitations is that 2D X-rays only provide a two-dimensional view of the hip joint, which may not accurately represent the three-dimensional anatomy of the patient. This can make it difficult to accurately assess the size and orientation of the implant needed for optimal stability and function of the new joint. Surgeons must rely on

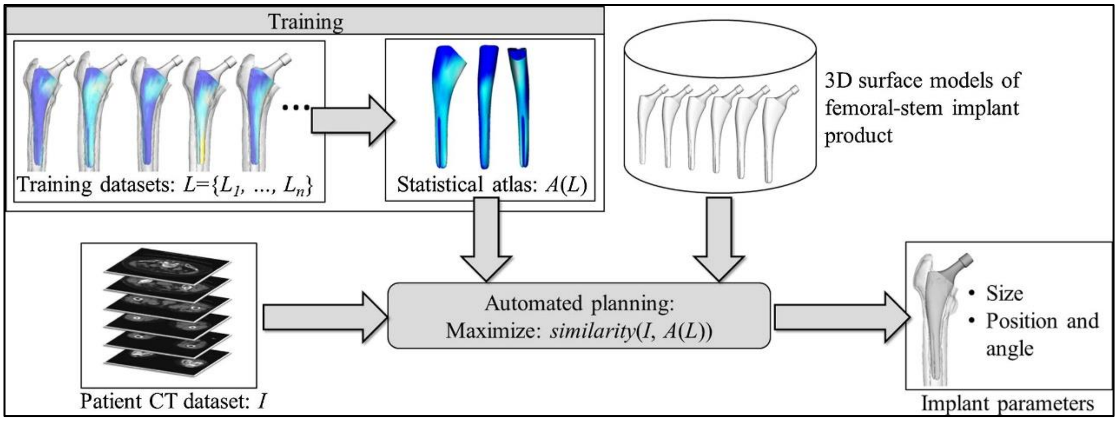

Figure 2-22: An image abstract of Otomaru et al. (2012) study.

their experience and knowledge of the anatomy of the hip joint to interpret 2D X-ray images accurately. They must also consider other factors such as the patient's age, sex, height, weight, and activity level when selecting the appropriate implant.

Another limitation of 2D X-ray images is that they may not provide enough information about the bone quality and density of the patient. This can impact the selection of the appropriate implant, as patients with osteoporosis or other bone conditions may require different implant options compared to those with normal bone density. In this particular case, surgeons may use other imaging techniques such as CT scans or MRI scans to obtain a more detailed view of the patient's bone structure and density. These imaging techniques can provide a more accurate assessment of the bone quality and help the surgeon select the best implant for the patient. 2D X-ray images may not accurately capture any deformities or abnormalities in the patient's hip joint, such as bone spurs or cysts, which can impact the surgical approach and the implant selection and can lead to suboptimal implant placement and increased risk of implant failure or revision surgery. To overcome this limitation, surgeons may need to rely on other imaging techniques or clinical assessments to identify any deformities or abnormalities in the hip joint before surgery. This can include physical examinations, medical history review, and other imaging techniques such as CT scans or MRI scans.

In conclusion, while 2D X-ray images are commonly used for implant templating in THA surgery due to their availability and relatively low cost, these previously described limitations should be considered. Further limitations include the two-dimensional nature of the images, the lack of information about bone quality and density, and the potential for inaccurate capture of deformities or abnormalities in the hip joint. Preoperative templating is typically done in two dimensions (2D) (Figure 2-23), and the stem version is often “driven” by the canal natural shape. A cross section analysis tool from our software can be used to visualize 2D X-ray templating. Looking from the AP view (Figure 2-24), the stem fit the canal very well with zero contact with the cortical bone. With respect to the SI view (Figure 2-25), the medial aspect of the femoral stem is in contact with the cortical bone. Thus, surgeons may not have complete control over stem position, particularly neck version and anterior/posterior tilt, and may have to ream into the cortical bone to achieve desired positions. Surgeons must rely on their experience and knowledge of the anatomy of the hip joint, use other imaging techniques as needed, and carefully consider the patient's individual characteristics to select the best implant for optimal joint stability, function, and longevity.

The implant positioning algorithm in this dissertation research study was developed to solve that problem and theoretically find the stem position within the canal with minimal contact with cortical bone. More detail about the implant positioning algorithm and the hip analysis software will be discussed in the following chapters.

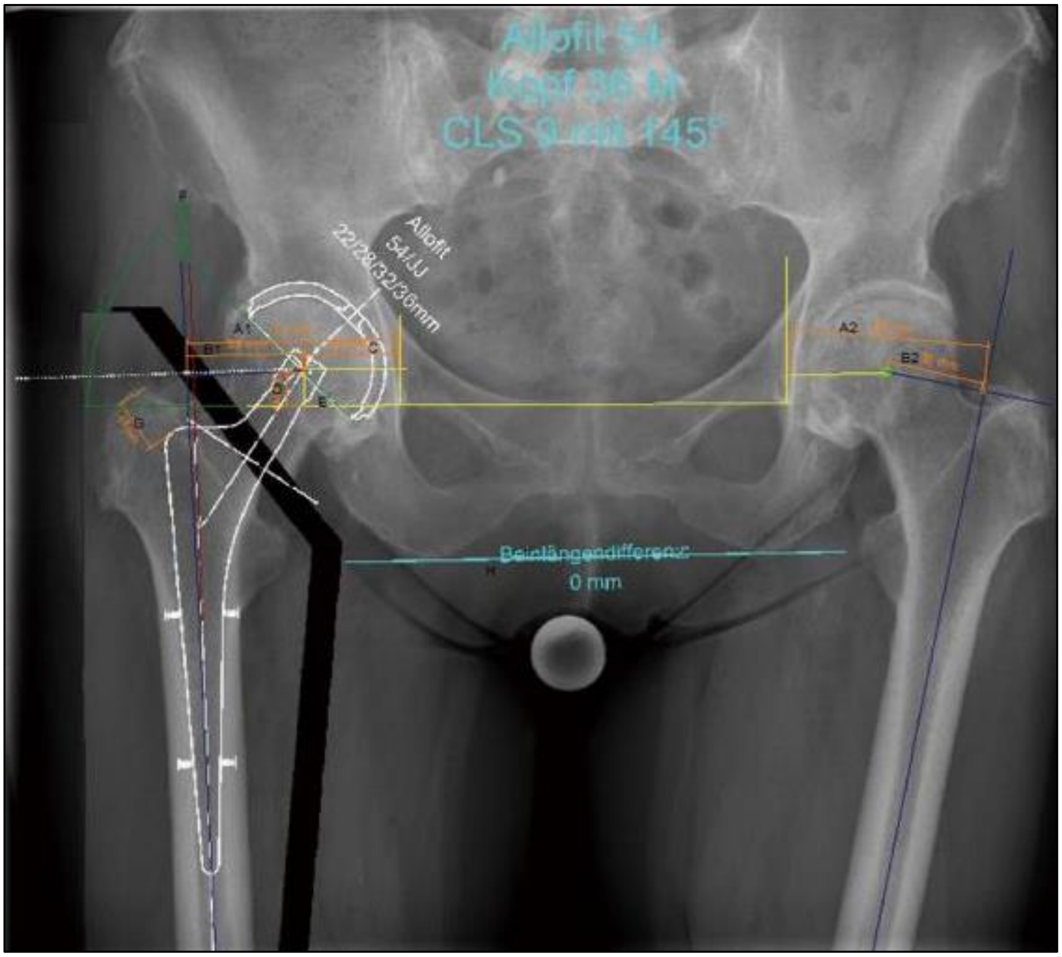

Figure 2-23: Surgeon templating using X-ray image.

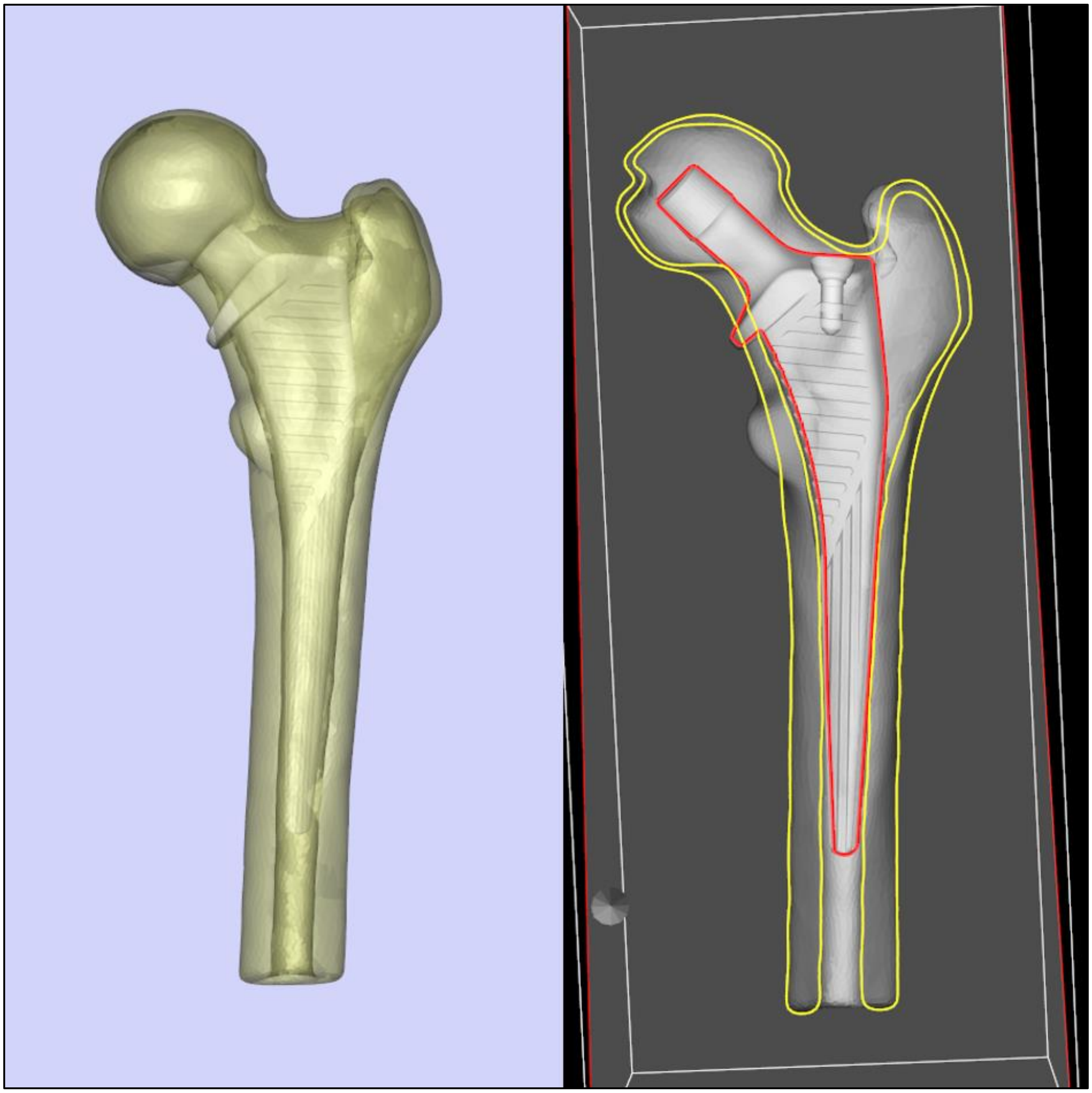

Figure 2-24: Cross section analysis for templating.

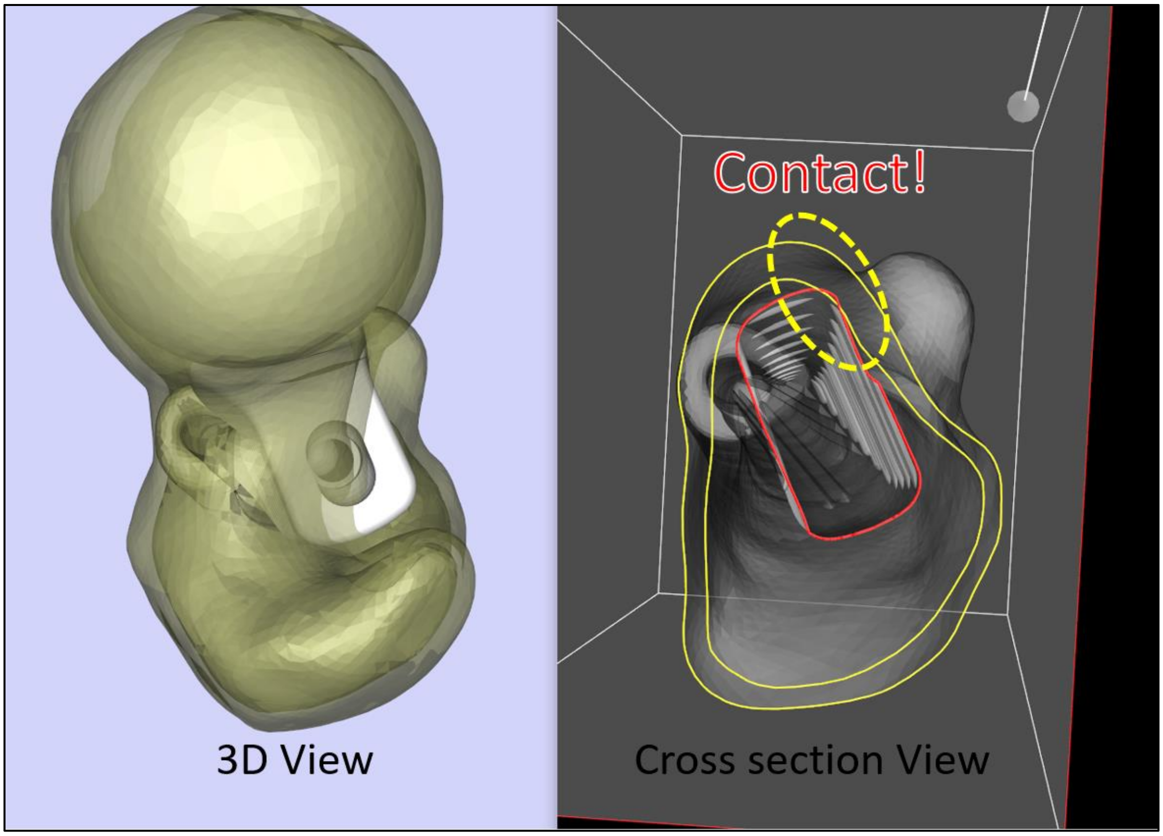

Figure 2-25: Implant cross section analysis view from different angle.

CHAPTER 3: OBJECTIVES

In the previous, Background chapter, the limitations of the existing implant templating techniques were outlined and the needs of having a dedicated hip analysis software was discussed. In this dissertation, the first objective is developing a fully functional hip analysis software package that can be used as a tool for healthcare professionals to analyze hip joint with patient specific data. The second objective of this dissertation is utilizing the hip model software to conduct comprehensive studies using the provided database. The objectives are not only for confirming our methodologies, but also to gain a better understanding of hip mechanics and enhance the outcome of THA.

The software, named “CMR_Hip_Model”, needs to be able to suggest hip prosthetic components sizes, calculate, and analyze components positions based on patient’s anatomy, and perform simulations with different activities such as gait or chair rise. The software aims to utilize mathematical modeling as a primary tool for analyzing and predicting hip joint mechanics and micro-movements, which can be achieved quickly and inexpensively. Accurately evaluating the postoperative function of total hip arthroplasty (THA) is crucial for improving THA performance [4] [10]. In order to achieve the main objectives of the dissertation, there are four tasks required to be done upon completion of the dissertation (Figure 3-1):

1) Creating patient specific data from patient’s 3D object models with template bones models.

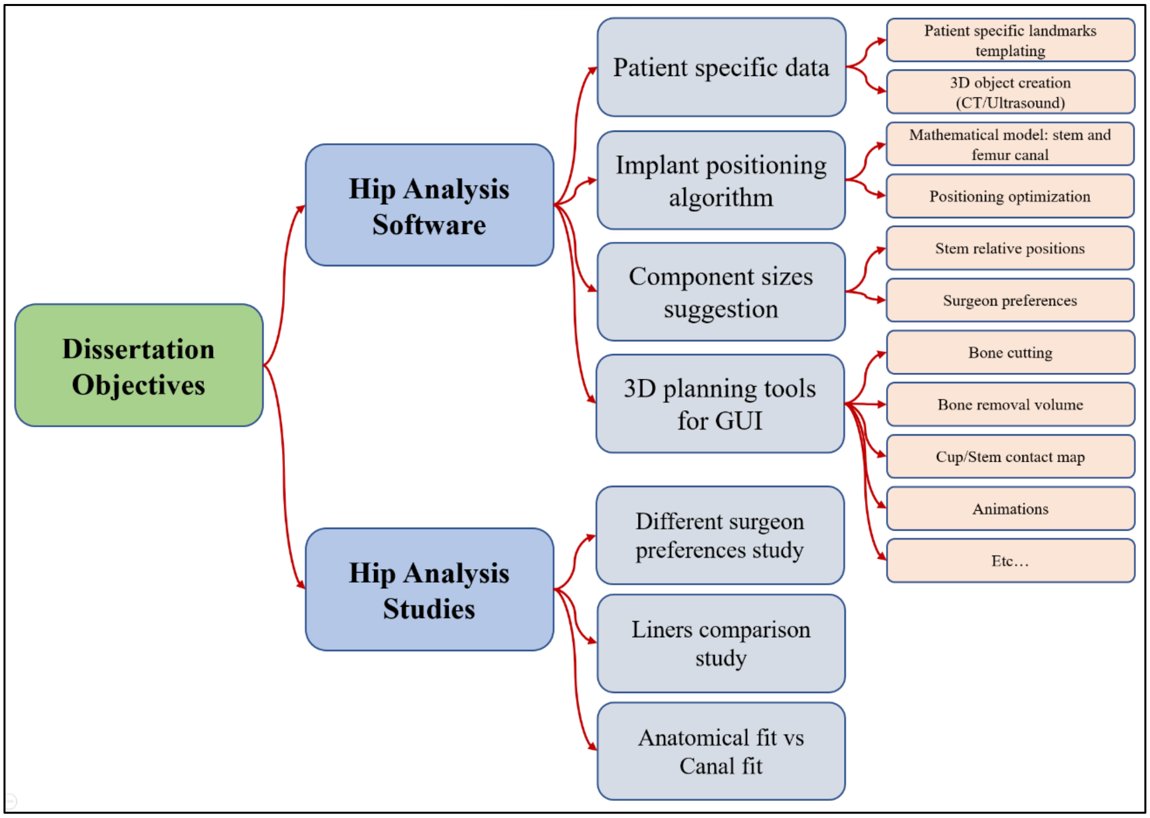

Figure 3-1: Dissertation main objectives and tasks breakdown.

2) Developing an algorithm that can predict the position of the stem within the canal (implant positioning algorithm).
3) Improving existing component sizes suggestion algorithm with patient specific data.
4) Developing 3D planning tools for use in the pre-operative planning process to refine and improve the model's graphical User interface (GUI), enable robust simulation and analysis.

Each of the four tasks above includes separate subtasks. Creating patient specific data involves obtaining the patent's bones models both pre-op or post-op by using CT or ultrasound scans and getting patient specific landmarks utilizing our template bones modeling algorithm. The implant positioning algorithm includes development of the dynamic mathematical model and optimizing the position of the stem within the canal of the femoral bone. Improvements pertaining to the implant sizing suggestion algorithm for both stem and cup requires calculation of the relative position between components in the model. The implant sizing suggestion is also based on surgeon preferences. The GUI improvements involve the implementation of bone cutting feature, contact map visualization, simulation results refinement, simulation animations, general clean-up of the User interface, and more (Figure 3-1).

With the completion of the hip analysis software, different studies were conducted utilizing every tool of the CMR_Hip_Model. The first study pertains to the comparison between different surgeon preferences for analyzing how the surgeon choices influence THA outcomes. The second study involves the canal fit and anatomical fit alignment tool for comparison. The study concentrated on how different stem alignments theoretically affect the kinematics of the THA for a patient postoperatively. The details pertaining to each task required to achieve the objectives of this dissertation will be discussed in the following chapters.

CHAPTER 4: METHOD

The first goal of this dissertation is to develop a fully functional hip analysis software package. The predecessors of this software package were the forward solution mathematical model, developed by Dr. LaCour, detailed in his dissertation [23], and the implant sizing suggestion algorithm developed by Dr. Manh Ta, which is described in his dissertation [4]. The first step of developing our hip analysis software is expanding and preparing the patient specific data. With the patient specific data, we were able to implement the methodology to determine the stem natural position within the canal. This method is defined as the implant positioning algorithm. The implant positioning algorithm is able to recognize even the slightest differences between various stem type designs and incorporate the stem design information with the canal shape analysis. The combination of the patient specific data and the implant positioning algorithm provides a comprehensive method to align the stem in the canal. We also defined the anatomical fit position of the stem to address different surgeon's preferences with the stem alignment.

After the completion of the patient specific data and the implant positioning algorithm, the next task was to develop a comprehensive graphical User interface (GUI) for our hip analysis software that not only can run hip simulations, but also analyze the patient specific data, suggest component sizes, calculate stem, cup positions within the canal. This includes developing and utilizing VTK, forward and inverse solution hip model, implant sizing suggestion algorithm, implant positioning algorithm, and all the hip analysis tools, such as 2D cup contact map, 3D cup contact map, stem contact map analysis, component alignment tools, new simulation activities, etc.

4.1. Expanding the subject database and patient specific data

After almost four years of development, the “implant suggestion” database has expanded to include over 100 formal bones and 20 sets of femoral and pelvis bones. Previously, only bone models from prior fluoroscopy studies and models that were provided to the project were used. Since then, 63 additional Statistical Shape Model bones were added (Figure 4-1) and we are continuing to add more Type A, Type B, and Type C bones. Furthermore, the “simulation” database has expanded to include a total of 10 subjects (Figure 4-2). These subjects were based directly on the bone models from a previous fluoroscopy study that was funded by DePuy-Synthes, A Johnson & Johnson Company. These 10 subjects are all patients that have been specifically processed. Hence, for these 10 subjects, we can do all the implant suggestion evaluations plus additional evaluations with the forward solution model.

Since the patient data we received from the segmented CT scans only has the bone anatomy structure, the data does not contain information about the muscle and ligament attachment sites. Thus, we need to process the segmented data from the CT scans to make the data patient specific. The first step to process patient specific data is loading the patient data onto the template subject. Then we were able to load the template subject that contains all the necessary muscle attachment sites, ligament attachment sites, and all the bone landmarks (Figure 4-3). These bone landmarks and attachment sites are then defined as template points for the next processing step.

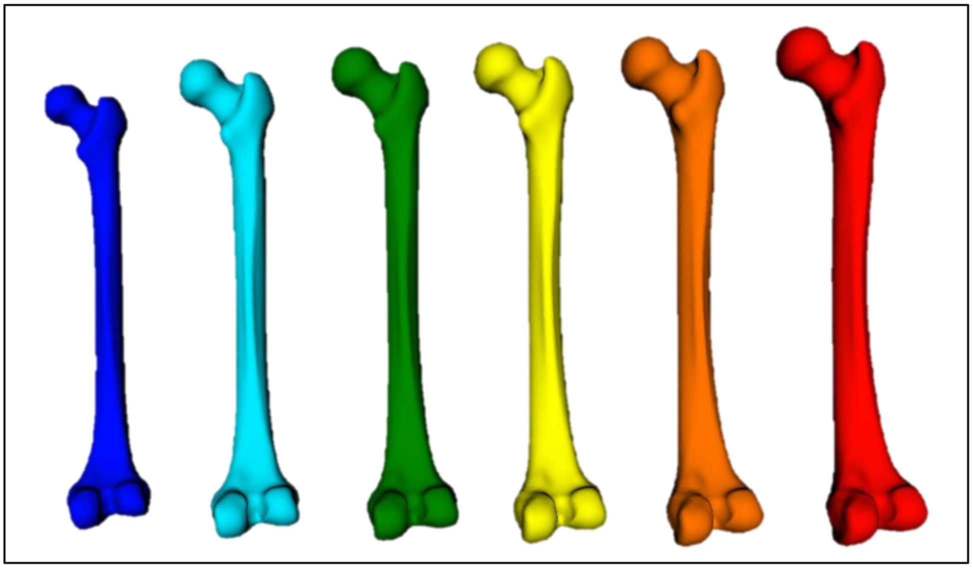

Figure 4-1: Statistical shape models.

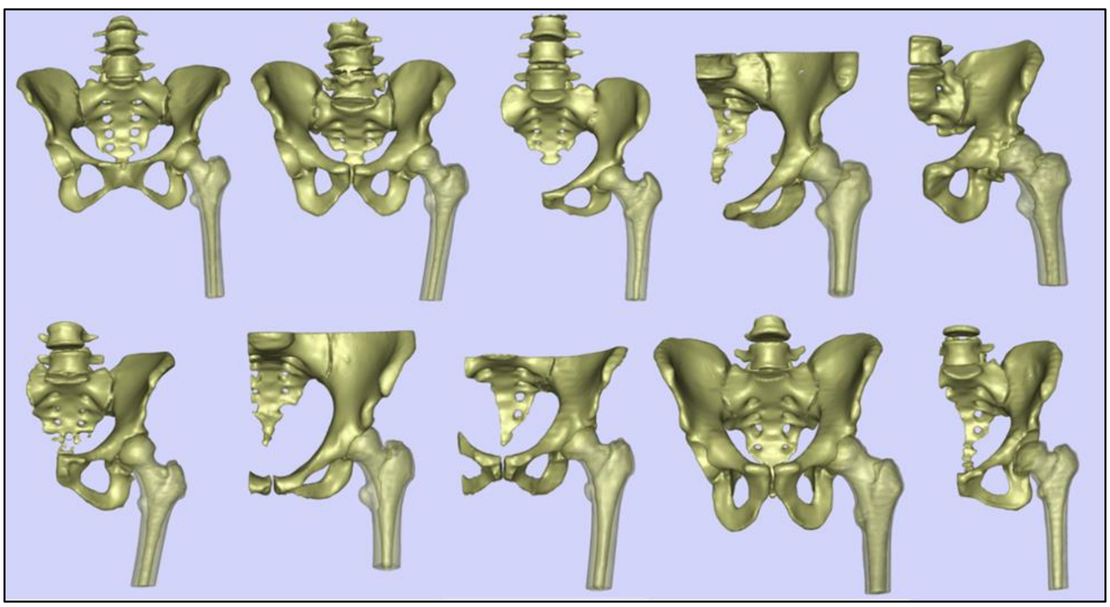

Figure 4-2: Ten "simulation" subjects.

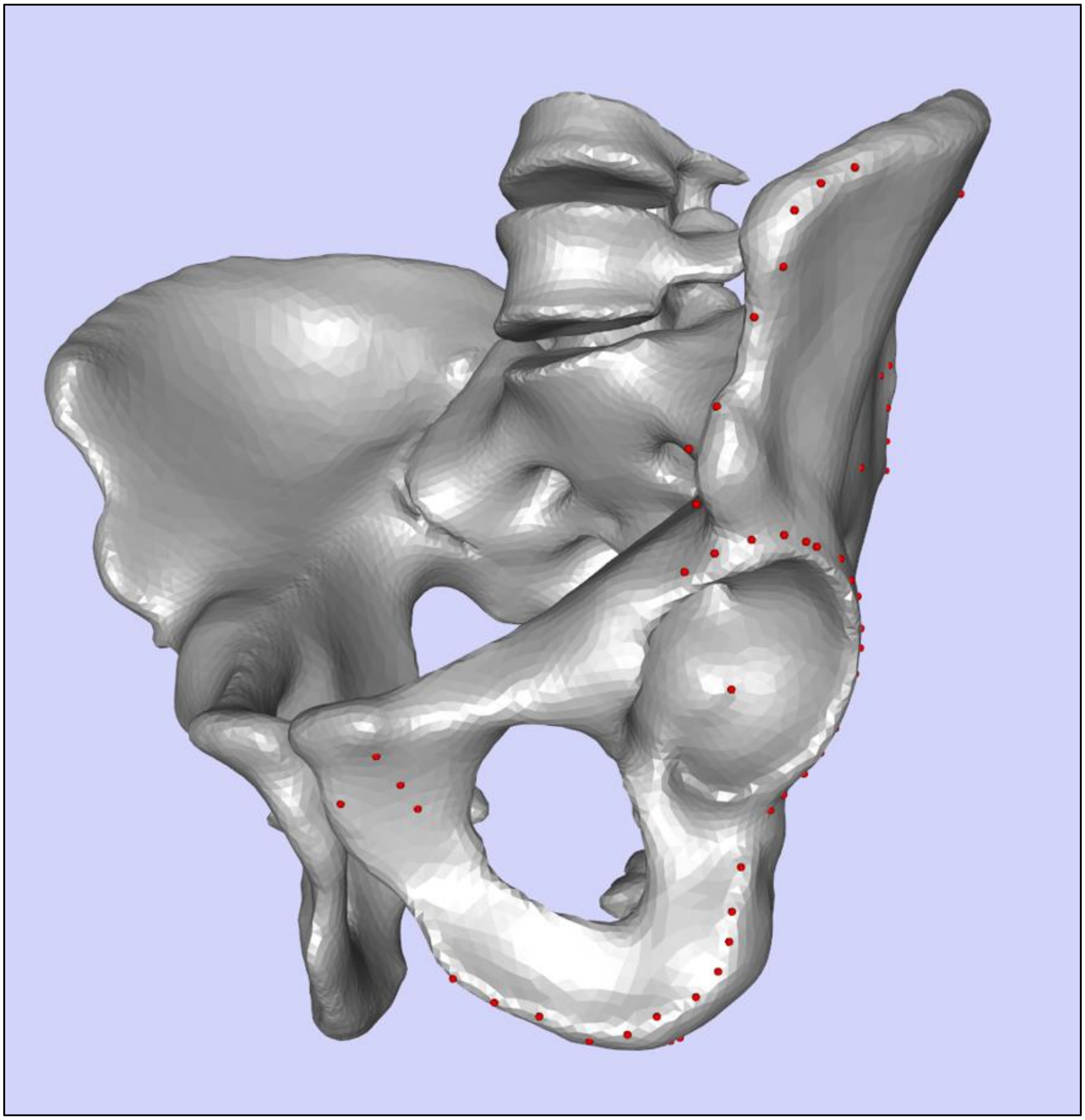

Figure 4-3: Template pelvis with muscle attachment sites, ligament attachment sites, and pelvis landmarks.

Although the program will automatically match the position between the subject bone and the template bone, the templating process still requires the User to check the relative position between two bones and making adjustment if needed (Figure 4-4). The program will then relocate each template point to the subject bone model so that it matches the anatomy of the specific patient (Figure 4-5). Then the position of that points will be displayed as the patient specific point data. After processing all the template points, the patient specific points will be exported to a HSIM file as the patient specific data. The HSIM file now contains all the muscle and ligament attachment sites as well as all the landmark points that are specifically for the corresponding subject. The User can also be able to reload and review the patient specific data in the VTK window to see if there is any point that needs to be adjusted, and they can make any changes if it is necessary.

With each patient, 2 bone model from segmented data were received, both the femoral and pelvis bone models. The pelvis is represented by 130 points, and the femur 215 points. We also reviewed the position of all the points carefully to make sure they all match with the anatomical shape of the subject. Thus, 10 patient specific subjects in total are included, which can be used in the forward solution model and implant analysis module.

4.2. Implant positioning algorithm

4.2.1. Algorithm framework

The goal of the implant positioning algorithm is to automatically suggest implant position within the femoral canal based on both canal shape and implant design, and the implant

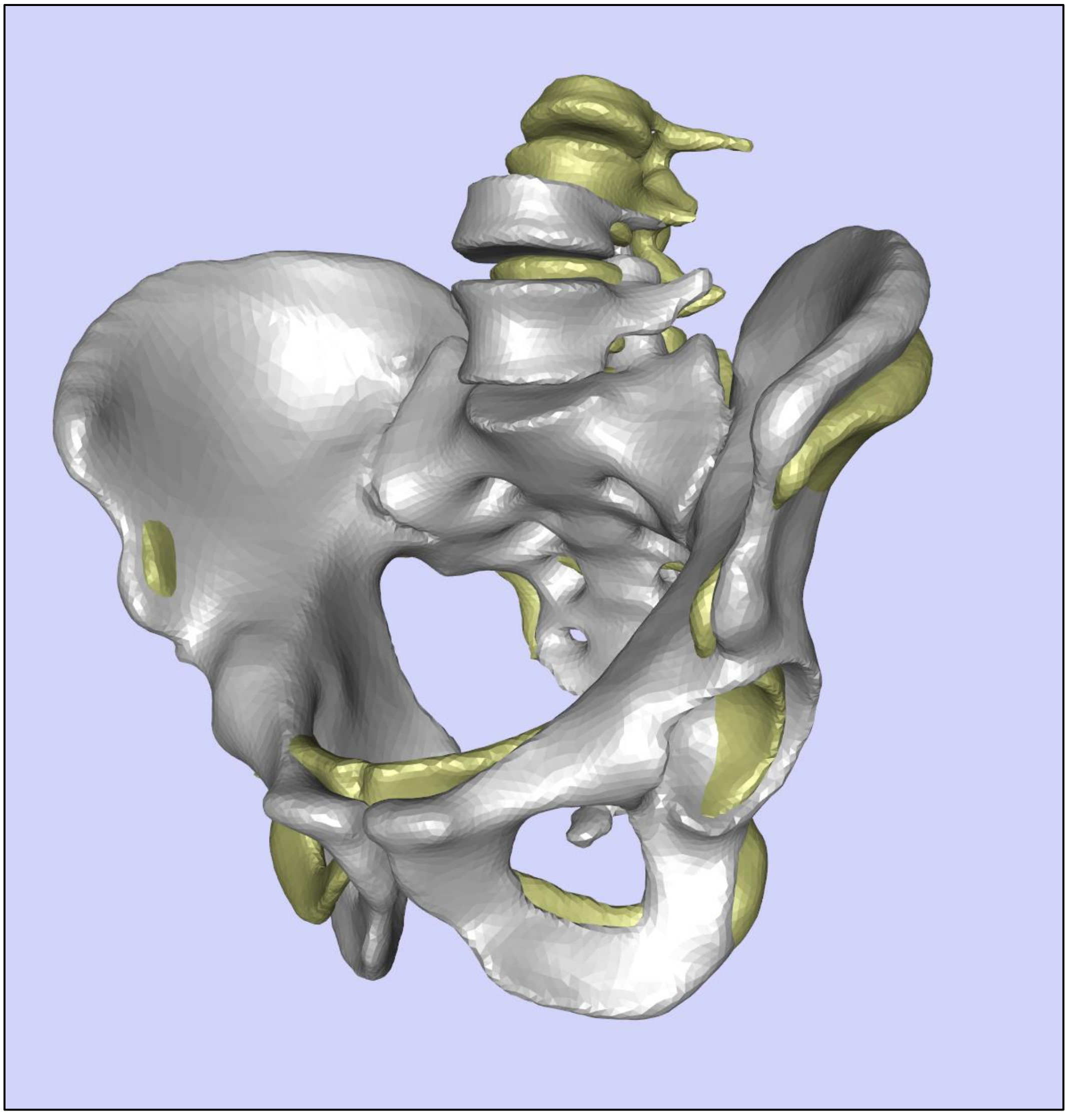

Figure 4-4: Template pelvis (white) and subject pelvis (yellow) matching in VTK window.

Figure 4-5: A patient specific pelvis with muscle attachment sites, ligament attachment sites, and pelvis landmarks.

position results are called the canal fit position. The heart of the algorithm is the mathematical forward solution model between the stem and the femoral canal. The first step of the algorithm is preparation of the input, specifically restructuring stem object and the femoral canal meshes. After making sure the input meshes are prepared properly, the second step of the algorithm is calculating the center of mass of the stem. In the third step, the initial position of the stem is defined based on both the anatomical fit position of the stem and the femoral canal shape. After the third step, the algorithm is ready to run the forward solution model to calculate the stem canal fit position (Figure 4-6).

The algorithm consists of many iterations. In each iteration, it uses the position of the stem in the previous iteration to calculate the contact map between stem and canal using mesh – mesh contact algorithm. The force and torque applied to the stem is calculated using the results of the contact map. The new position of the stem in the next iteration is updated based on the resulted force and torque. The algorithm stops when the stem is settled in the canal fit position with minimal contact area and optimal contact pattern with femoral cortical bone.

4.2.2. Restructured input meshes

In computer graphics, a mesh is a collection of vertices, edges, and faces that defines the shape of a 3D object. A mesh is made up of many small triangular or quadrilateral surfaces that cover the surface of the object. When creating a 3D model, it's important to have a well-structured mesh with consistent triangle sizes. This is because rendering algorithms, such as those used in mathematical modeling or movies, rely on the

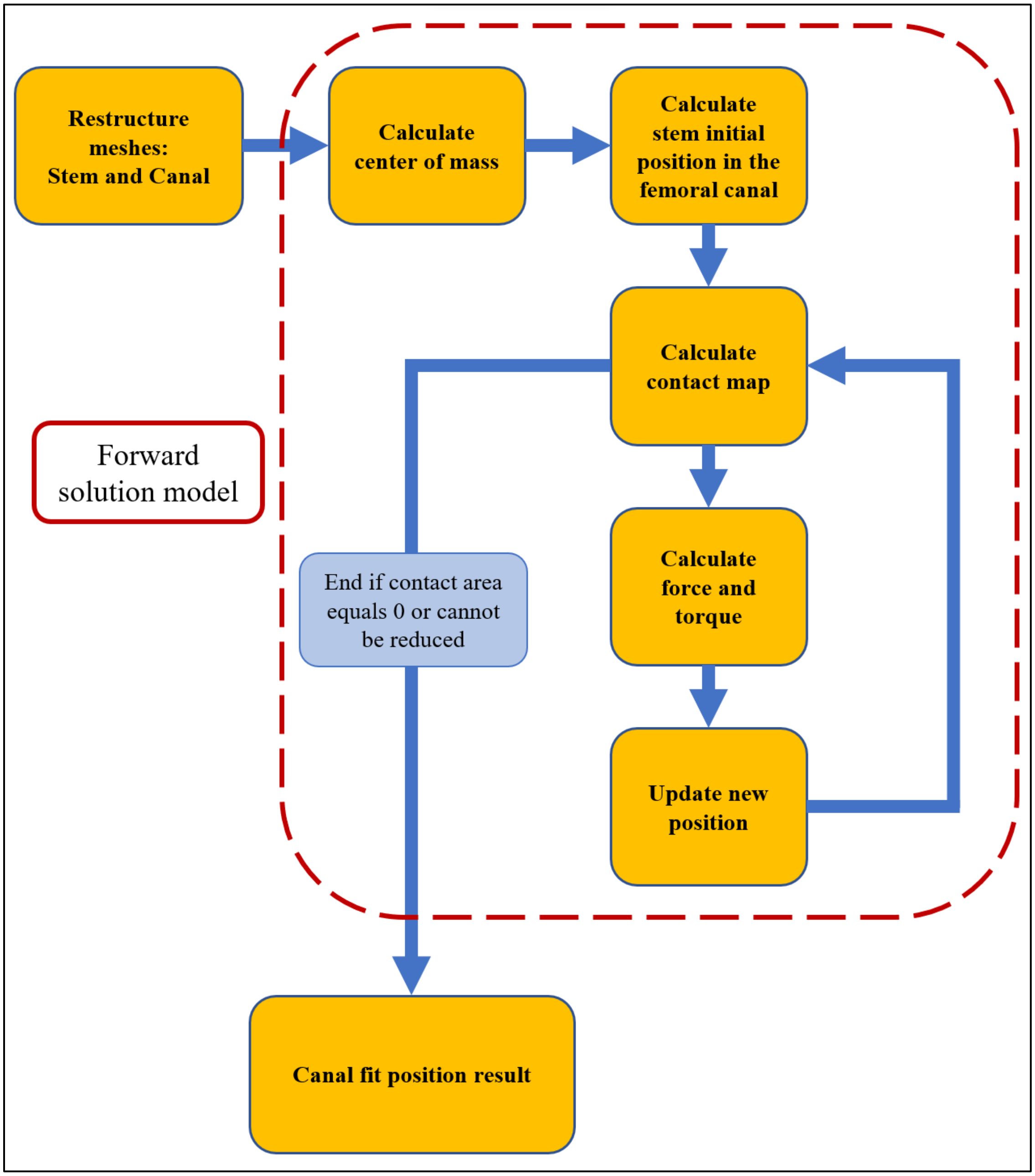

Figure 4-6: Implant positioning algorithm framework.

mesh to accurately represent the shape of the object. If the triangles in a mesh are too large or too small, it can result in visual artifacts such as jagged edges, or cause problems with lighting and texture mapping. Additionally, having inconsistent triangle sizes can also make it difficult to apply smooth shading or other visual effects to the model. To address this issue, mesh restructuring techniques such as mesh smoothing, or subdivision can be used to create a more evenly sized mesh. This involves altering the positions of the vertices in the mesh to create more regular triangles and can be done manually or with the help of specialized software tools.

The stem object meshes we received from the company usually do not have consistent triangle sizes (Figure 4-7). Thus, we used Meshmixer to restructure the mesh triangles, resulting a more evenly sized meshes (Figure 4-8). Meshmixer is a free, 3D modeling software tool created by Autodesk that allows Users to edit, sculpt, and repair 3D meshes. It is often used for tasks such as creating custom 3D designs, modifying existing models, or preparing 3D prints for 3D printing. To ensure the accuracy of the implant positioning algorithm, meshes are used as the input for all calculations, which includes the center of mass and stem contact map calculation. Therefore, it is important to process all stem objects to ensure consistency in the triangle sizes of all meshes as much as possible. This step is crucial as it can impact the final result of the algorithm, and inconsistencies in mesh triangle sizes can lead to errors and inaccuracies in the implant positioning process.

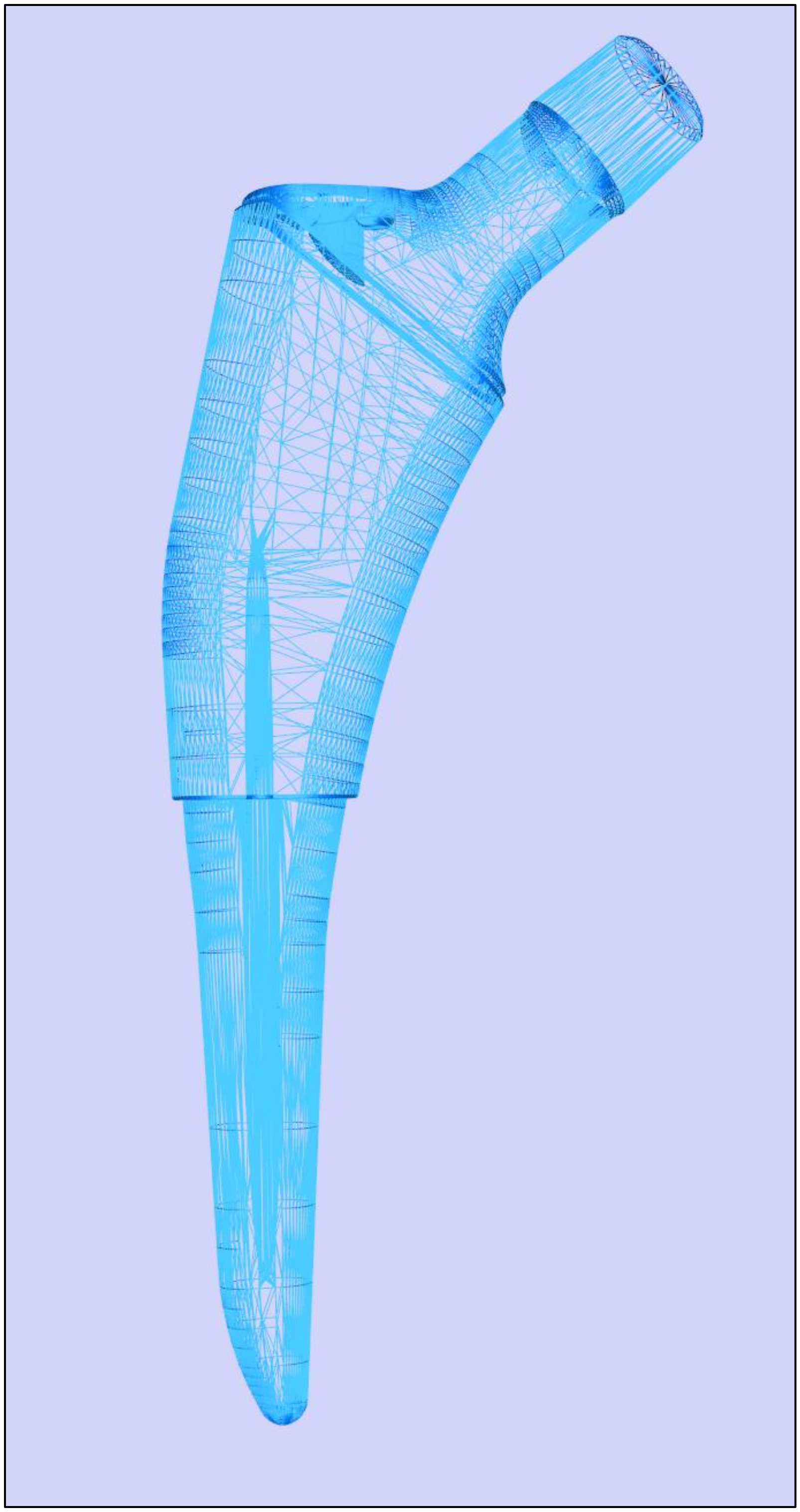

Figure 4-7: An example of original stem mesh with inconsistent triangle sizes.

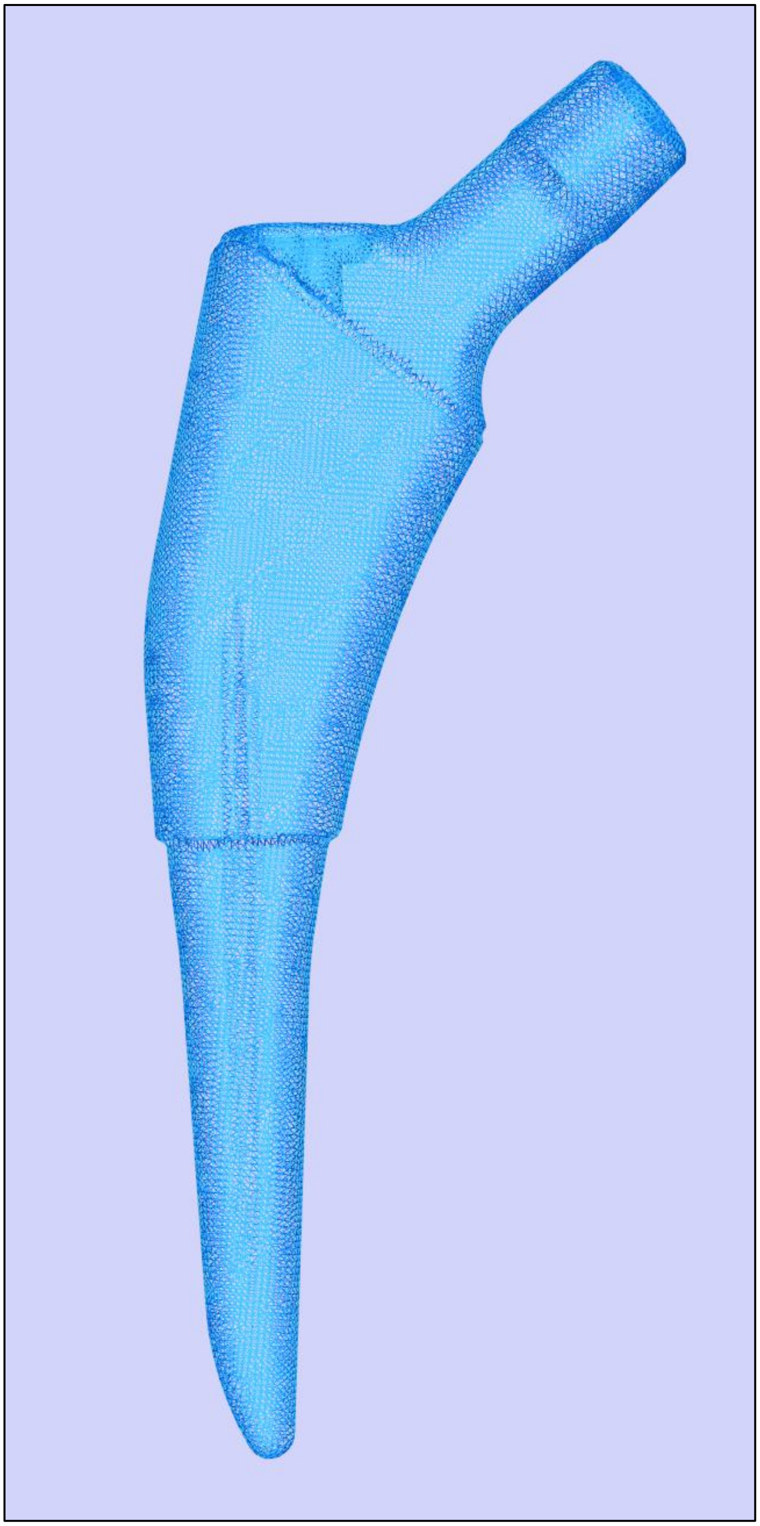

Figure 4-8: The mesh result after being processed. The triangle sizes are evenly distributed and consistent.

4.2.3. Forward solution model of stem and canal

Newton's second law of motion, also known as the law of acceleration, states that the rate of change of the momentum of a body is directly proportional to the net force acting on it, and the direction of the change in momentum takes place in the direction of the net force. This means that if a force is applied to an object, the object will accelerate in the direction of that force, and the greater the force, the greater the acceleration. In angular motion, this law can be expressed in terms of the moment of inertia and the angular acceleration of the object. This law states that the torque acting on an object is proportional to the moment of inertia of the object and the angular acceleration it undergoes. In other words, the greater the torque applied to an object, the greater the angular acceleration it will experience, and the greater the moment of inertia of the object, the less the angular acceleration it will experience for a given torque. The Newton's second law of motion is commonly written as the following equations:

Force equation:

$$\boldsymbol{F} = \frac{\Delta \boldsymbol{P}}{\Delta t} = m * \frac{\Delta \boldsymbol{v}}{\Delta t} = m * \boldsymbol{a}$$

Torque equation:

$$\boldsymbol{T} = \frac{\Delta \mathbf{L}}{\Delta t} = I * \frac{\Delta \boldsymbol{\omega}}{\Delta t} = I * \boldsymbol{\gamma}$$

Where:

- $\boldsymbol{F}$ is the force vector acting on an object.

- $\boldsymbol{T}$ is the torque vector acting on an object.

- $\Delta\boldsymbol{P}$ is the change of the momentum of an object.

- $\Delta\mathbf{L}$ is the change of the angular momentum of an object.

- m is the mass of an object.

- I is the moment of inertia of an object.

- $\Delta\boldsymbol{v}$ is the change of the velocity.

- $\Delta\boldsymbol{\omega}$ is the change of the angular velocity.

- **a** is the acceleration.

- $\boldsymbol{\gamma}$ is the angular acceleration.

- Δt is the time duration of the change.

The Newton's second law of motion equations are very common in research. However, using Newton's equations in computer languages is not convenient because computer usually expresses problems in the matrix form. The forward solution model uses Kane's dynamics method as an alternative way to express the dynamics of a mechanical system in terms of generalized coordinates and generalized forces. The equations consider the effect of all forces acting on a system, including inertial forces, gravitational forces, and external forces, as well as constraints and the geometry of the system. The Kane's dynamics equations can be written in general form as:

$$\boldsymbol{F_r} + \boldsymbol{F_r^*} = 0$$

Where $\boldsymbol{F_r}$ are the external applied forces acting on the system, and $\boldsymbol{F_r^*}$ are the internal generalized forces resulting from the system's motion. The equation states that the sum of the external forces and the internal generalized forces must equal zero, as required by Newton's second law. In our forward solution model of the stem and femoral canal, our system only has one body which is stem, and the femoral canal is modeled as a stationary frame in the Newtonian space (Figure 4-9). The following AutoLev code define the system of one body (stem) in Newtonian space:

```
NEWTONIAN N
BODIES D %STEM

%% CONSTANTS INPUT
CONSTANTS M,I{3}
CONSTANTS G
CONSTANTS DAMPINGCOEF
CONSTANTS DAMPINGCOEFW

INERTIA D,I1,I2,I3
MASS D = M
AUTOZ ON
%%%%%%%%%%%%%%%%%%%%%%%%%%%%%%%%
%%%%%%% BODY INFORMATION %%%%%%%
%%%%%%%%%%%%%%%%%%%%%%%%%%%%%%%%

VARIABLES U{6}'          % 1 BODY, 6 PER BODY
VARIABLES NO2DO{3}''     % POSITION OF STEM CoM
VARIABLES THETA{3}''     % ANGLE OF STEM

% ASSIGN VARIABLES FOR POSITION
NO2DO1' = U1
NO2DO1'' = DT(NO2DO1')
NO2DO2' = U2
NO2DO2'' = DT(NO2DO2')
NO2DO3' = U3
NO2DO3'' = DT(NO2DO3')

% ASSIGN VARIABLES FOR ANGLE
THETA1' = U4
THETA1''=DT(THETA1')
```

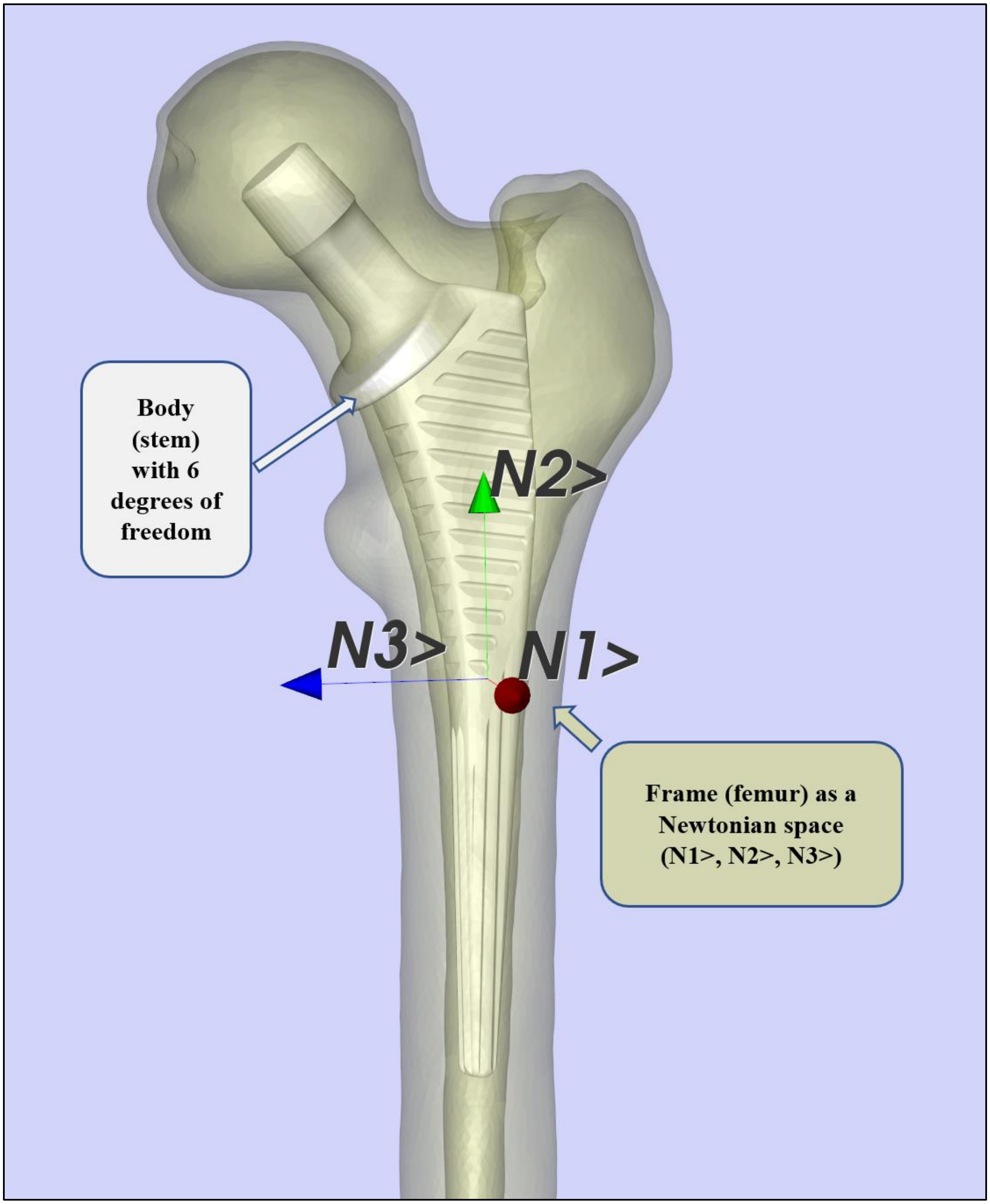

Figure 4-9: The implant positioning model: the body (stem) has 6 degrees of freedom, and the femoral canal is the Newtonian space.

```
THETA2' = U5
THETA2''=DT(THETA2')
THETA3' = U6
THETA3''=DT(THETA3')
```

The AutoLev code starts by defining the system's degrees of freedom, which in this case is the position of the stem in the Newtonian space. Specifically, the stem has six degrees of freedom, including three translational displacements (NO2DO1, NO2DO2, NO2DO3) and three rotational displacements (THETA1, THETA3, THETA3). The stem has the mas of M, moment of inertia I. There are also different important constants, such as gravity constant (G), damping coefficients for force and torque (DAMPINGCOEF and DAMPINGCOEFW). After defining body information, we define position vectors, liner velocities, and angular rotation of the system. We also introduce forces and torques to the system in the following lines of code:

```
%%%%%%%%%%%%%%%%%%%%%%%%%%%%%%%%%%%%%%%%%
%%%%% ESTABLISHING ANGULAR ROTATION %%%%%
%%%%%%%%%%%%%%%%%%%%%%%%%%%%%%%%%%%%%%%%%
% FOR STEM
DIRCOS(N,D,BODY321,THETA3,THETA2,THETA1)
ANGVEL(N,D)

%%%%%%%%%%%%%%%%%%%%%%%%%%%%%%%%%%%%
%%%% DEFINING POSITION VECTORS %%%%%
%%%%%%%%%%%%%%%%%%%%%%%%%%%%%%%%%%%%
P_NO_DO> = NO2DO1*N1>+NO2DO2*N2>+NO2DO3*N3>     % NO2DO

%%%%%%%%%%%%%%%%%%%%%%%%%%%%%%%%%%%%%%
%%%%% DEFINING LINEAR VELOCITIES %%%%%
%%%%%%%%%%%%%%%%%%%%%%%%%%%%%%%%%%%%%%
V_DO_N> = V_NO_N>+DT(P_NO_DO>,N)      % VELOCITY OF STEM CoM

%%%%%%%%%%%%%%%%%%%%%%%%%%%%
%%%%% INTRODUCE FORCES %%%%%
%%%%%%%%%%%%%%%%%%%%%%%%%%%%
SPECIFIED EXFORCE{3}                  % CONTACT FORCES
GRAVITY(-G*N2>)
```

```
FORCE(DO,EXFORCE1*N1>+EXFORCE2*N2>+EXFORCE3*N3>)% CONTACT FORCES
FORCE(DO,-DAMPINGCOEF*V_DO_N>)

%%%%%%%%%%%%%%%%%%%%%%%%%%%%
%%%%% INTRODUCE TORQUES %%%%%
%%%%%%%%%%%%%%%%%%%%%%%%%%%%
SPECIFIED EXTRATORQUE{3}
TORQUE(D,EXTRATORQUE1*N1>+EXTRATORQUE2*N2>+EXTRATORQUE3*N3>)
TORQUE(D,-DAMPINGCOEFW*W_D_N>)
%%%%%%%%%%%%%%%%%%%%%%%%%%%%%%%%%%%%%%%%
ZERO = FR()+FRSTAR()
% OUTPUT FILES
OUTPUT T, THETA1, THETA2, THETA3, NO2DO1, NO2DO2, NO2DO3
OUTPUT T, THETA1', THETA2', THETA3', NO2DO1', NO2DO2', NO2DO3'
OUTPUT T, THETA1'', THETA2'', THETA3'', NO2DO1'', NO2DO2'',
NO2DO3''
OUTPUT T, EXFORCE1, EXFORCE2, EXFORCE3, EXTRATORQUE1,
EXTRATORQUE2, EXTRATORQUE3
ANIMATE(N,NO,D)
CODE DYNAMICS() calculateImplantSurgeonFit.m
```

After setup the forward solution model system, we export the dynamics model to a MATLAB file. All the forces and torques are not defined in the AutoLev code. Instead, they will be defined in the MATLAB file (`calculateImplantSurgeonFit.m`). In general, a system of one single body with six degrees of freedom without any constrain is quite simple. The difficulties of the implant positioning algorithm do not come from the process of defining the forward solution model. In fact, the real challenges come from the implementation of contact detection algorithms, force and torque calculation, center of mass calculation, damping coefficients tuning. All that details will be discussed in the following sections.

4.2.4. Center of mass calculation

The center of mass (or center of gravity) of an object is the point where the entire mass of the object can be considered to be concentrated. It is the point where the object would balance if it were suspended from that point. The position of the center of mass depends on the distribution of mass within the object. For a simple, symmetrical object like a sphere or a cube, the center of mass is at the geometric center. For more complex objects, the center of mass can be calculated by considering the mass of each part of the object and its distance from a reference point. To calculate the stem center of mass, we calculate the center of all vertices of the stem mesh by using the following equation:

$$\boldsymbol{P}_{CoM} = \frac{\boldsymbol{P}_{\boldsymbol{1}} + \boldsymbol{P}_{\boldsymbol{2}} + \cdots + \boldsymbol{P}_{\boldsymbol{n}}}{n}$$

Where $\boldsymbol{P}_{CoM}$ is the position vector of the center of mass point, $\boldsymbol{P}_{\boldsymbol{i}}$ is the position vector of an element vertex, and n is the total number of vertices. However, we will adjust the center of mass of the stem by projecting the $\boldsymbol{P}_{CoM}$ point to the stem shaft axis. The purpose of this adjustment is to increase accuracy of the force and torque calculation in the following steps.

4.2.5. Canal analysis for initial stem position in the forward solution model

The implant positioning algorithm uses forces and torques to correct the stem position within the canal. However, if the penetration depth is too small, the algorithm will take many iterations to finish, which can largely increase the implant positioning algorithm run time. The initial position of the stem also affects how much time the algorithm will require to complete this task. Additionally, the implant positioning algorithm also needs to be sensitive enough to derive even a very small difference between various stem designs. Therefore, finding an initial position which can make the results more accurate and also potentially optimize running time is a necessary step to further improve the performance of implant positioning algorithm.

The canal analysis process starts at the anatomical fit position where the distance from the stem head center to the anatomical femoral head center is minimized, and the stem shaft axis is aligned with the canal shaft axis. Since the canal shaft axis and femoral neck axis usually do not align and/or reside in the same plane, even though the stem shaft axis and stem neck axis do align in the same plane. Thus, when the stem is at the anatomical center position with stem shaft axis and femoral shaft axis aligned, the stem body is usually in contact with the cortical bone in the medial size of the stem. An example slice where the contact area between stem and cortical bone can be seen in the proximal medial side of the stem body is shown in Figure 4-10.

To realign the stem to the more ideal initial position, the stem body and femoral canal shape must be further analyzed by detecting and viewing many slices. A plane that performs slicing process will be put in a perpendicular position with the shaft axis. Then, that plane will be moved along the shaft axis to perform the cut, each cut is 0.5 mm apart. The results of each cut will be two contours (Figure 4-11), the canal contour and stem contour are in red and yellow respectively. With each contour, the algorithm will automatically define the most medial points of the contour (blue point for canal and yellow point for stem in Figure 4-11), and this point will be used later to realign the stem. An example of the full slices analysis of the stem and canal is shown in Figure 4-12. Based on all the medial points of the canal and the stem, the stem initial position will be adjusted so that on average the medial points of the stem will align with the medial points of the canal. The stem is also translated along the shaft axis so that it minimizes the contact between the stem and canal in the proximal medial side of the stem.

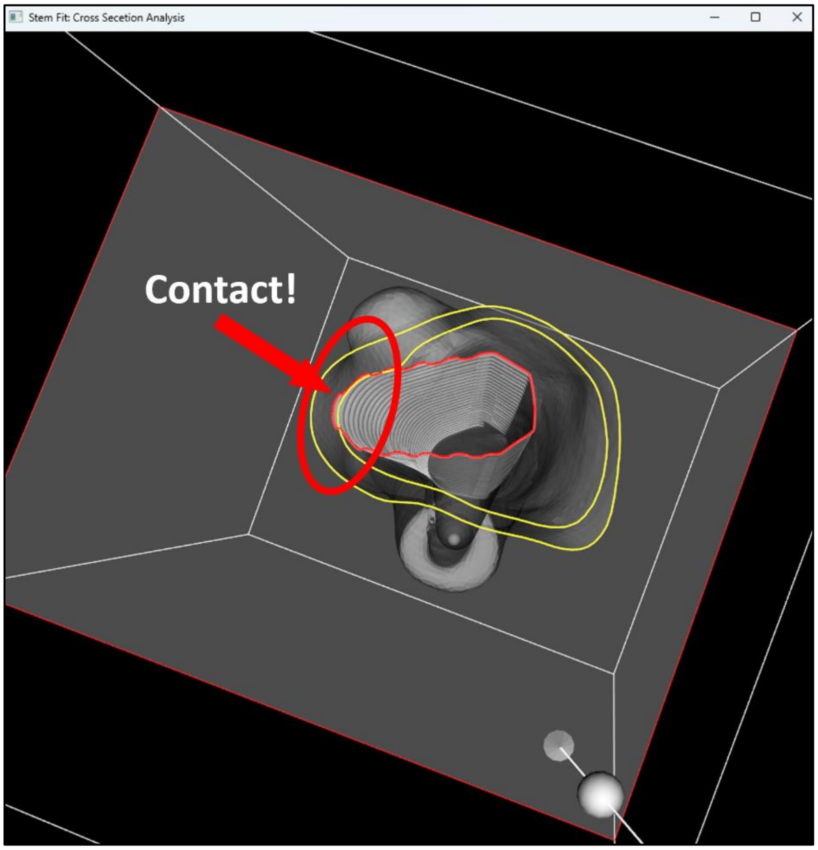

Figure 4-10: Anatomical position stem in contact with cortical bone in medial side.

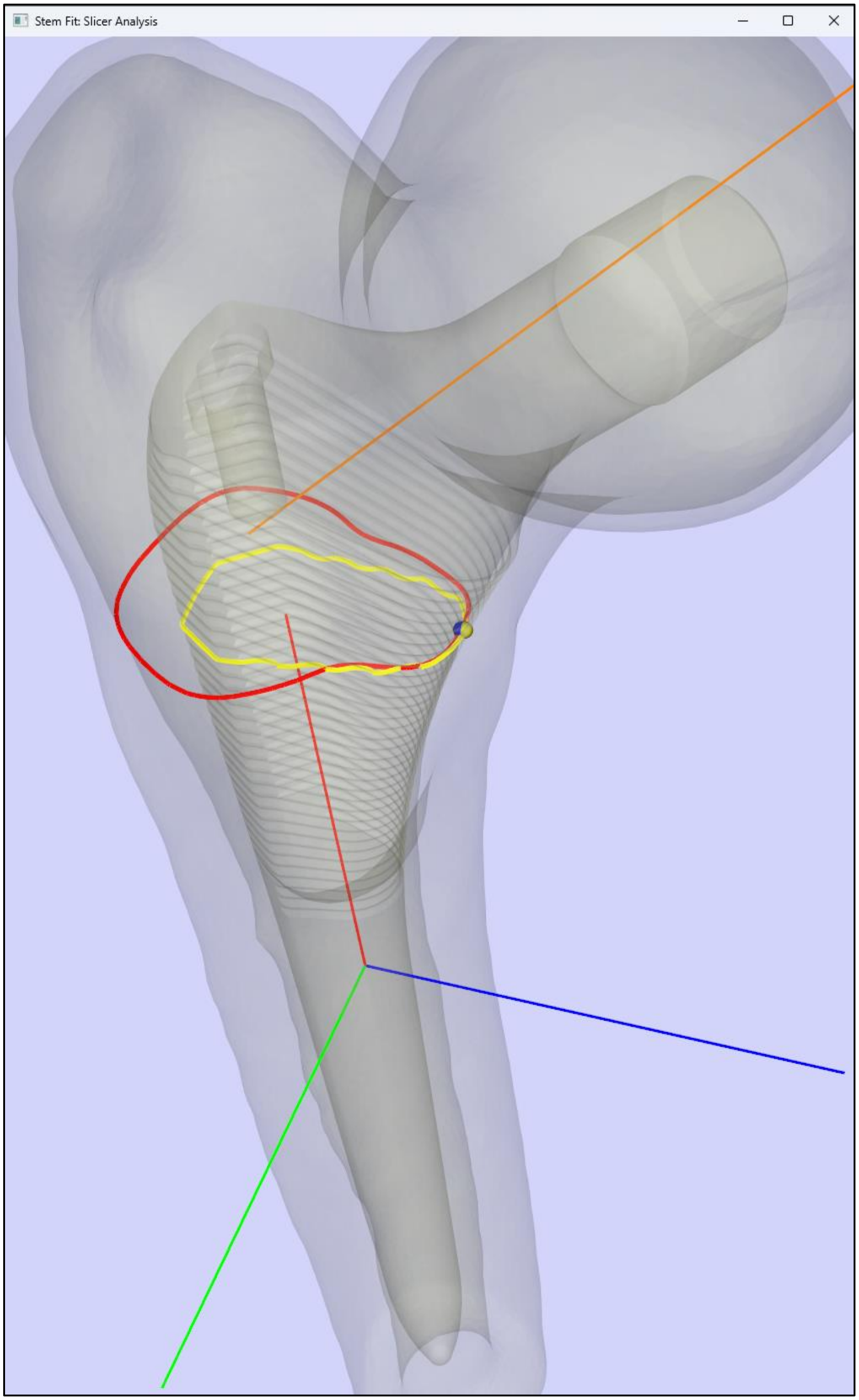

Figure 4-11: Stem and canal contours.

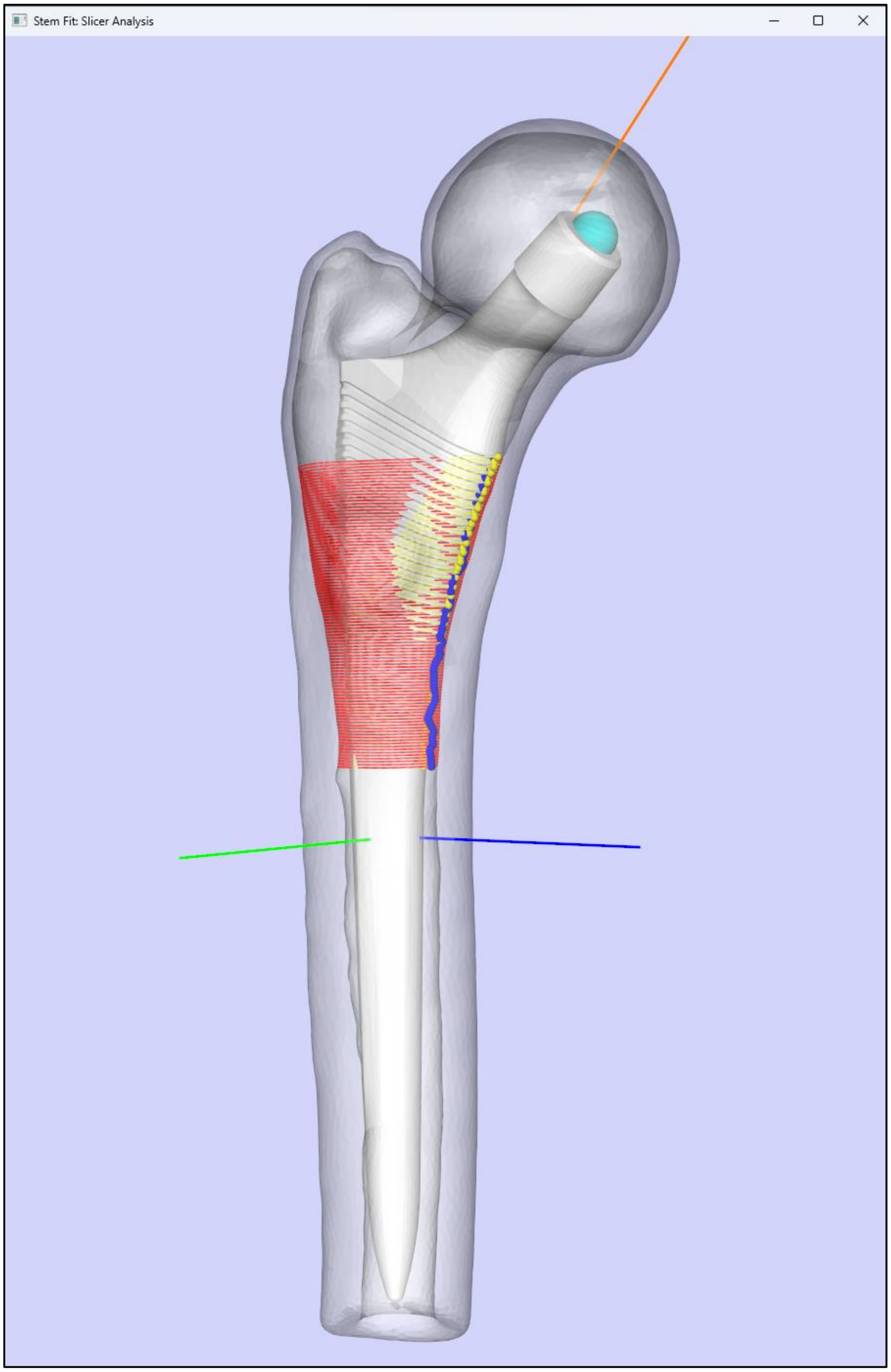

Figure 4-12: Stem and canal slices analysis.

The adjusted initial position of the stem is shown Figure 4-13. In this position, the stem is still in contact with the cortical bone mainly in the distal portion of the stem. The approach is similar to peeling an onion by doing one layer at a time. In this second development process, the contact between the stem and the femur is optimized in the proximal medial area of the stem. Thus, the forward solution model will be used to reduce any remaining contact area. The adjusted initial position also results in lower running time for the forward solution model because there will be less contact area needed to be optimized.

4.2.6. Mesh – mesh contact calculation

Traditionally, the contact map interacting between two point clouds is the distance from each point of the first point cloud to the closest point of the second point cloud for every point within each point cloud. When the word "distance" is used in mathematics, it is generally referred to the definition of metric. Let X is a point set with each element in X is a point in the 3D space. A point in 3D space is represented by 3 real numbers. A metric d is a function from set $X \times X$ to set $\mathbb{R}$ (the set of real numbers).

$$d: X \times X \rightarrow \mathbb{R}$$

For all $x,\ y,\ z$ in X. A metric must satisfy the four following conditions:

1. Non-negativity: $\mathrm{d}(\mathrm{x}, \mathrm{y}) \geq 0$.
2. Identity of indiscernible: $\mathrm{d}(\mathrm{x}, \mathrm{y}) = 0$ if and only if $\mathrm{x} = \mathrm{y}$.
3. Symmetry: $\mathrm{d}(\mathrm{x}, \mathrm{y}) = \mathrm{d}(\mathrm{y}, \mathrm{x})$.
4. Triangle inequality: $\mathrm{d}(\mathrm{x}, \mathrm{z}) \leq \mathrm{d}(\mathrm{x}, \mathrm{y}) + \mathrm{d}(\mathrm{y}, \mathrm{z})$.

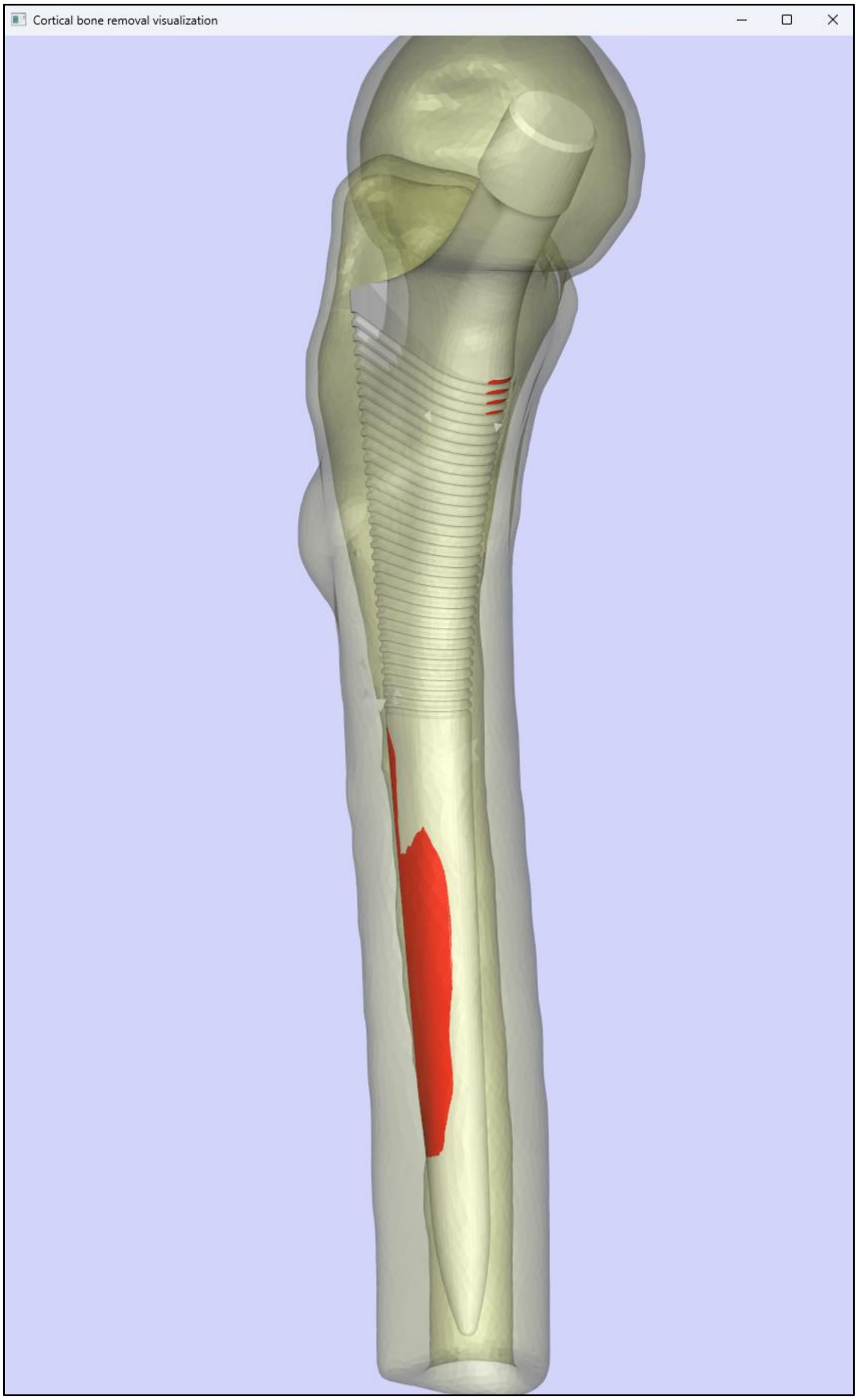

Figure 4-13: Stem initial position with contact visualization.

The implant positioning algorithm requires a signed distance calculation between two meshes, which means there are cases where the distance value is smaller than zero. The non-negativity condition, on the other hand, requires a distance that is always greater than or equal to zero. Thus, the distance between two point clouds does not provide enough information for implant positioning algorithm. Even though the distance between two point clouds was not used directly in this dissertation, its mathematical definition provides a solid background for the mesh – mesh contact map calculations.

A mesh can be described as a set that contains both face and vertex information. A vertex is a set of three real numbers that represents its coordinates in 3D space, and a face is a triangle with 3 vertices representing 3 nodes of the triangle. Each face has a normal vector that distinguishes two sides of the object, one side is inside and the other is outside the object. Since the normal vector is available, a signed distance can be applied to the mesh – mesh contact map calculations.

An example of the contact calculation from a small sphere to a big sphere where a portion of the small sphere is penetrated the bigger sphere can be seen in Figure 4-14. In this example, the small sphere has a radius of 6 mm, and the small sphere center is at $[0, 0, 0]$ mm position. The big sphere has a radius of 10 mm, and the sphere center is at $[12, 0, 5]$ mm position. The distance scalar bar shows the distance result ranges from -3.00 mm to 9.00 mm. In this case, all the vertices of the small sphere which are located inside the big sphere have distance values smaller than zero. Consequently, vertices outside the big sphere have positive distance value. The contact area is indicated from red to yellow colors, whiles the non-contact area is indicated from light green to blue.

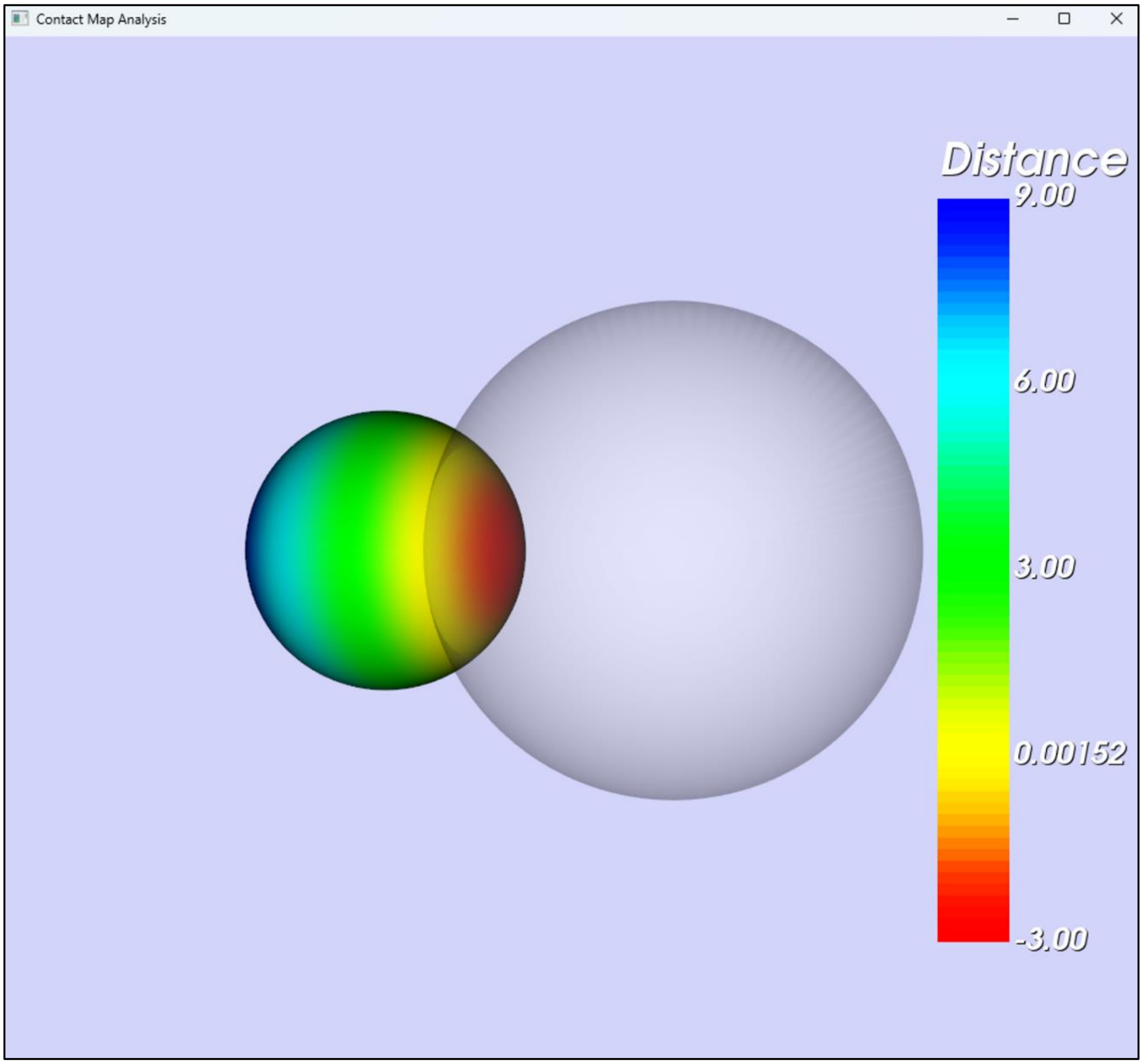

Figure 4-14: Distance between two spheres example.

4.2.7. Contact force and torque calculation using contact detection algorithm

The contact map information is very important during the implant positioning algorithm calculation because negative distance values indicate areas of contact for the implant positioning algorithm. The contact detection algorithm is responsible for finding penetration between stem and femur cortical or cancellous bone within the canal using the same principle that was discussed in the 2 spheres example previously. Furthermore, the contact detection algorithm also calculates the direction as well as magnitude of the contact force. In general, a contact force is applied to the model to reduce penetration area between stem and cortical bone. As the stem is “inserted” into the proximal aspect of the femoral canal, if the stem penetrates/contacts the cortical bone, a counterforce will be applied to that area to reduce the penetration (Figure 4-15).

The illustration for contact detection algorithm is shown in the Figure 4-15, whereas the contact force has an opposite direction to the penetration vector. The magnitude of the contact force is proportional to the depth of the penetration between stem and the cortical bone. The precise equations for contact force and torque are shown below:

Contact force equation:

$$\mathbf{F}_{\mathrm{contact}} = k * \Delta * \mathbf{N}$$

Contact torque equation:

$$\mathbf{T}_{\mathrm{Contact}} = \boldsymbol{r} \times \mathbf{F}_{\mathrm{contact}}$$

Where:

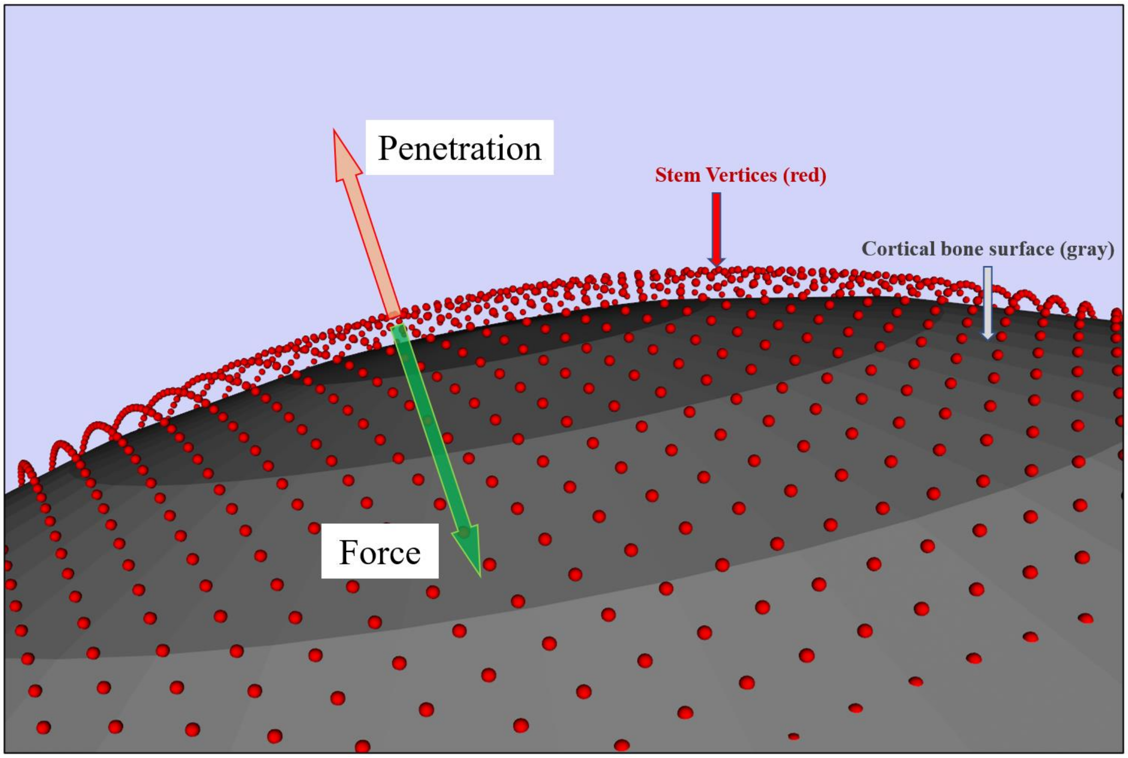

Figure 4-15: Contact force calculation based on contact map.

- k: Contact coefficient
- Δ: Penetration amount
- **N**: Normal vector
- $\boldsymbol{r}$: Moment arm

With respect to the contact force and torque equation, k is a contact coefficient with the unit is N/mm. Δ is the signed distance value from the mesh – mesh contact calculations. **N** is a unit normal vector indicating the outside surface of the stem, where each face has its own normal vector. $\boldsymbol{r}$ is a moment arm vector from the stem center of mass (CoM) to the current vertex. To calculate the total force and torque that are applied to the stem, the contact detection algorithm loops through all vertices of the stem object. Whenever the algorithm detects a vertex that has the negative distance value into the cortical/cancellous bone, it will apply a small portion of force and torque based on the equations above. After looping through all vertices, the total force and torque are recorded and applied to the stem for the next step of calculation.

4.2.8. Damping coefficient for force and torque

The law of conservation of energy is a fundamental principle in physics, stating that energy cannot be created or destroyed, only transferred, or transformed from one form to another. This means that the total amount of energy in a closed system remains constant over time. This law is based on the first law of thermodynamics, which states that the change in internal energy of a system is equal to the sum of the heat and work exchanged between the system and its surroundings. In the context of an implant positioning algorithm, this means that if the model does not have any mechanism to decrease the total energy of the system, including both kinetic and potential energy, the stem will continue to move indefinitely without settling into a final position. As a result, it becomes impossible to determine the canal fit position of the stem within the femoral canal. This highlights the importance of designing a model that can effectively manage and minimize energy within the system to achieve desired outcomes.

In order to manage the energy within our implant positioning algorithm system, we introduced the damping coefficients for both force and torque. These damping coefficients create the damping force and torques in the opposite direction of the body current velocity and angular velocity calculated in the previous step. Specifically, the total force and torque applied to the stem body in each iteration including the damping force and toque are described in the following equations:

$$\boldsymbol{F}_{Total} = \boldsymbol{F}_{Contact} - \mu_{damping} * \boldsymbol{v}$$

$$\boldsymbol{T}_{Total} = \boldsymbol{T}_{Contact} - \vartheta_{damping} * \boldsymbol{\omega}$$

Where $\boldsymbol{v}$ and $\boldsymbol{\omega}$ are the body velocity and angular velocity respectively, $\boldsymbol{\mu}_{damping}$ and $\boldsymbol{\vartheta}_{damping}$ are damping coefficients of force and torque respectively. Based on the two equations above, the following AutoLev codes are where we introduce force and torque into our system with the damping force and torque included:

```
%%%%% INTRODUCE FORCES %%%%%
SPECIFIED EXFORCE{3}                  % CONTACT FORCES
GRAVITY(-G*N2>)
FORCE(DO,EXFORCE1*N1>+EXFORCE2*N2>+EXFORCE3*N3>)% CONTACT FORCES
FORCE(DO,-DAMPINGCOEF*V_DO_N>)

%%%%% INTRODUCE TORQUES %%%%%
```

```
SPECIFIED EXTRATORQUE{3}
TORQUE(D,EXTRATORQUE1*N1>+EXTRATORQUE2*N2>+EXTRATORQUE3*N3>)
TORQUE(D,-DAMPINGCOEFW*W_D_N>)
%%%%%%%%%%%%%%%%%%%%%%%%%%%%%%%%%%%%%%%%
```

The damping force are introduced to the system by the command: `FORCE(DO,-DAMPINGCOEF*V_DO_N>)`, and the damping torque are introduced to the system by the command: `TORQUE(D,-DAMPINGCOEFW*W_D_N>)`. In both commands, the damping force and torque act opposite to the direction of the velocity vector and angular velocity vector of the stem body (D), with the magnitude of the damping force and torque being proportional to the magnitude of the stem body's velocity and angular velocity. This results in a gradual reduction in the total energy of the system. By adjusting the damping coefficients, the rate of energy dissipation can be controlled, thereby controlling the algorithm's convergence rate. However, excessively high damping coefficients can lead to premature termination of the algorithm, preventing the stem from reaching a stable position. Conversely, very low damping coefficients can result in a longer running time of the algorithm. Thus, extensive testing is necessary to determine the optimal damping coefficients for the system.

After discussing all the steps necessary for the implementation of the implant positioning algorithm, the following section will summarize the algorithm and provide the overall view of the algorithm in the hip analysis software.

4.2.9. Implant positioning algorithm implementation to hip analysis GUI

4.2.9.1. Implant positioning algorithm summarize

The first step of GUI development pertaining to the implant positioning algorithm is implementing a dynamic mathematical model that automatically places the stem in the “Path of Least Resistance” (PLR) position by assessing the shape of the canal. To summarize the algorithm, the implant positioning algorithm model consists of two bodies, one is the stem and the other is the femur. This method of aligning the stem is also called the “canal fit” method in the model, and the alignment is calculated automatically using a “miniature” forward solution model subroutine that incorporates similar contact detection algorithms to determine contact between the stem and cortical bone as the stem is pushed into the canal. As the stem translation occurs, the stem is repositioned accordingly to eliminate contact. By “advancing” the stem in the distal direction and iteratively monitoring and adjusting the component position, the algorithm also adjusts stem version to avoid contact with cortical bone.

The algorithm consists of many iterations. In each iteration, it uses the current position of the stem o calculate a contact map between stem and canal (Figure 4-16). Based on the contact map, it will reposition the stem to minimize contact area and recalculate the volume of bone removal. After that, the algorithm determines a new position of the stem and repeats the process again. The algorithm stops when the volume of bone removal is minimized (Figure 4-17).

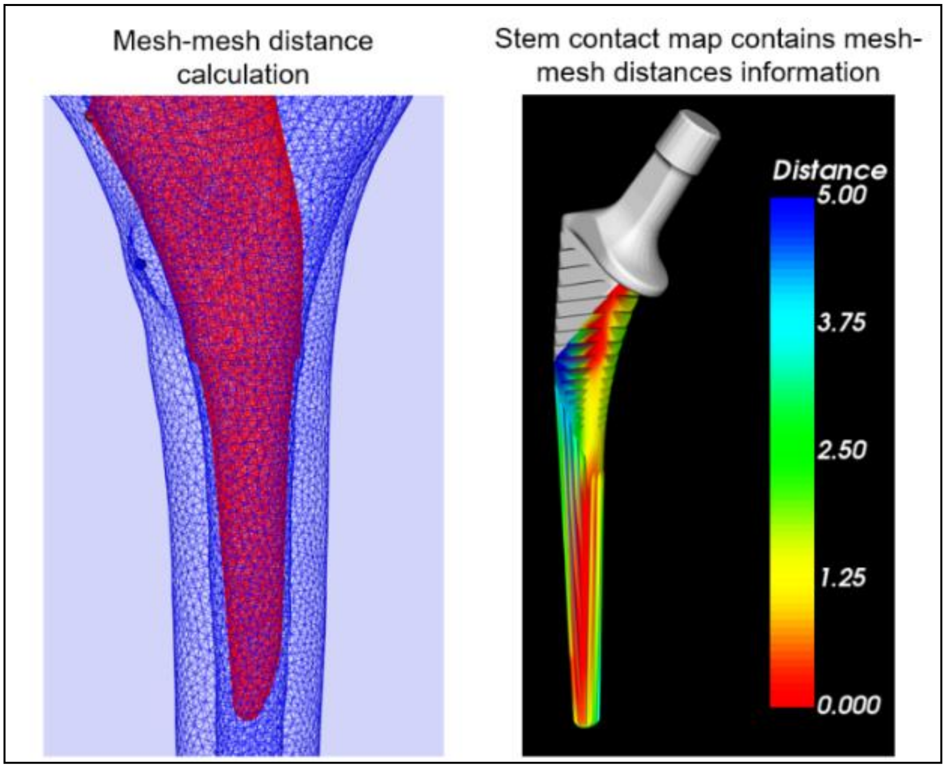

Figure 4-16: Calculation of contact map.

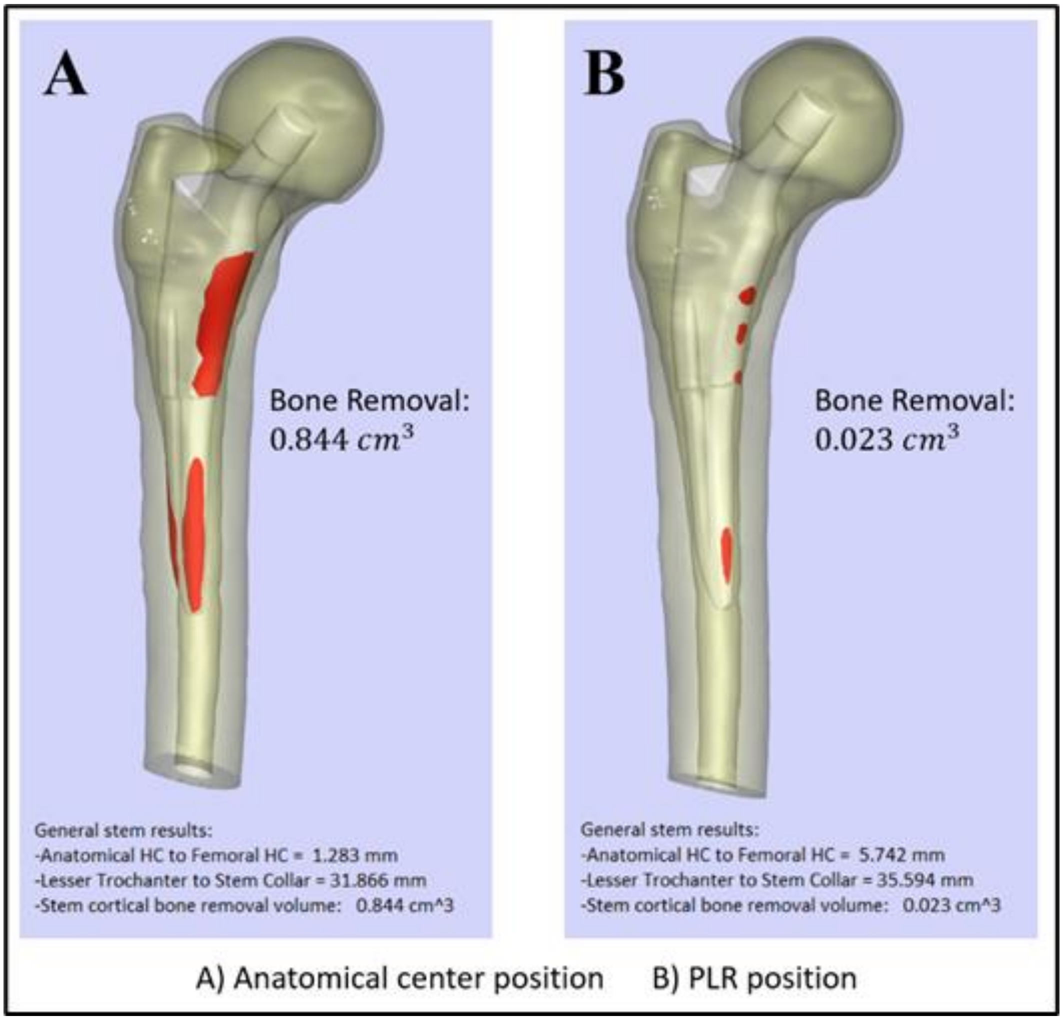

Figure 4-17: PLR position minimizes contact area and bone volume removal.

4.2.9.2. GUI implementation and results saving of the implant positioning algorithm

Since the canal fit method in the forward solution model is developed and implemented, the algorithm now has a fully functional implant positioning algorithm that can be used to calculate orientation of the stem in the canal. The calculation also takes the cancellous mantle thickness into account. After calculation, the PLR position of the stem will be defined, and that position can be used to conduct many different simulation analyses. We have included the Canal Orientation option in the GUI, so now we have two different stem positioning options – Anatomical Centers position and Canal Orientation position (Figure 4-18). With each stem, the Canal Orientation will run calculation only once. Then it will save the stem information. The next time you select the Canal Orientation option, the stem will move to the position immediately.

4.3. Hip analysis software GUI with implant positioning algorithm

The hip model has been under development since 2014, with the first version of hip model was designed by Dr. Michael LaCour [23]. His research has been the foundation of the model and a good resource for this dissertation and all the work in the future of the model. Following Dr. LaCour dissertation, Dr. Manh Ta continued to develop an implant suggestion algorithm and added the VTK visualization [4]. Since 2019, there are many new features and tools were added to the hip model. These features helped to improve the User experience and the overall capabilities of the hip model even when some features are just small changes. A German philosopher Georg Wilhelm Friedrich Hegel once said: “Quantity changes lead to quality changes” and Professor Komistek has encouraged me

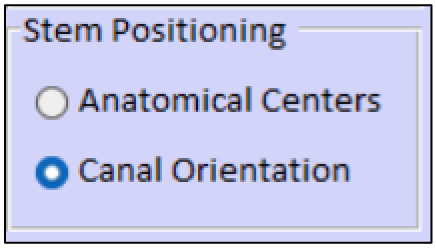

Figure 4-18: Stem Positioning options.

by telling me I made quantity changes are very much quality changes as well. For me, I am thankful for his support, and I believe quality changes only happen when there are enough small improvements were made, just like these small improvements which were made during this dissertation progress. The overview of the hip analysis software GUI is shown in Figure 4-19.

This section is dedicated to discussing all the advancements which were added to the hip model since Dr. Manh Ta's dissertation in 2019.

4.3.1. Implant sizing suggestion algorithm advancements

4.3.1.1. Stem size suggestion

The program has been improved such that it can now calculate and predict stem sizes more precisely. Previously, the hip model determined stem size using only the Superior/Inferior directions as a guiding parameter. In this dissertation, we have modified the sizing suggestion algorithms to incorporate Anterior/Posterior, Superior/Inferior, and Medial/Lateral distances together. Specifically, our algorithm functions by calculating the distance between the stem head center and the femoral head center in the 3D space (Figure 4-20). The algorithm loops through the list of all stem sizes for each stem type in our database and gets all the stem head distances. After that, it will select the stem size that has the lowest stem head distances and suggest that stem size for each stem types (Figure 4-20).

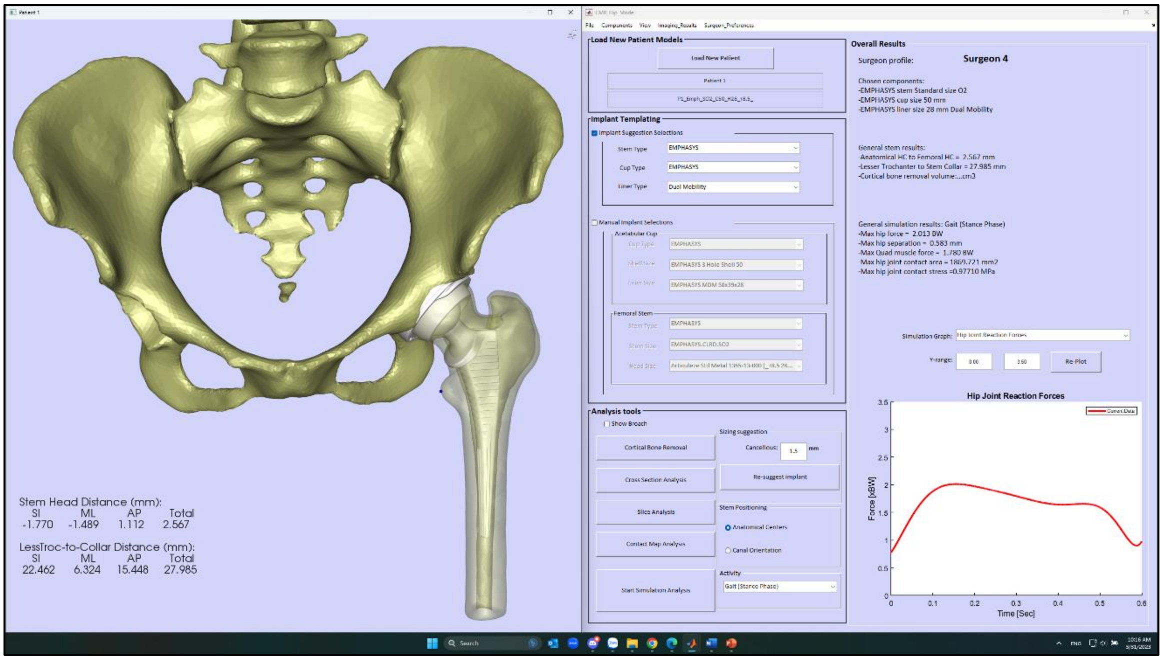

Figure 4-19: Hip analysis software GUI.

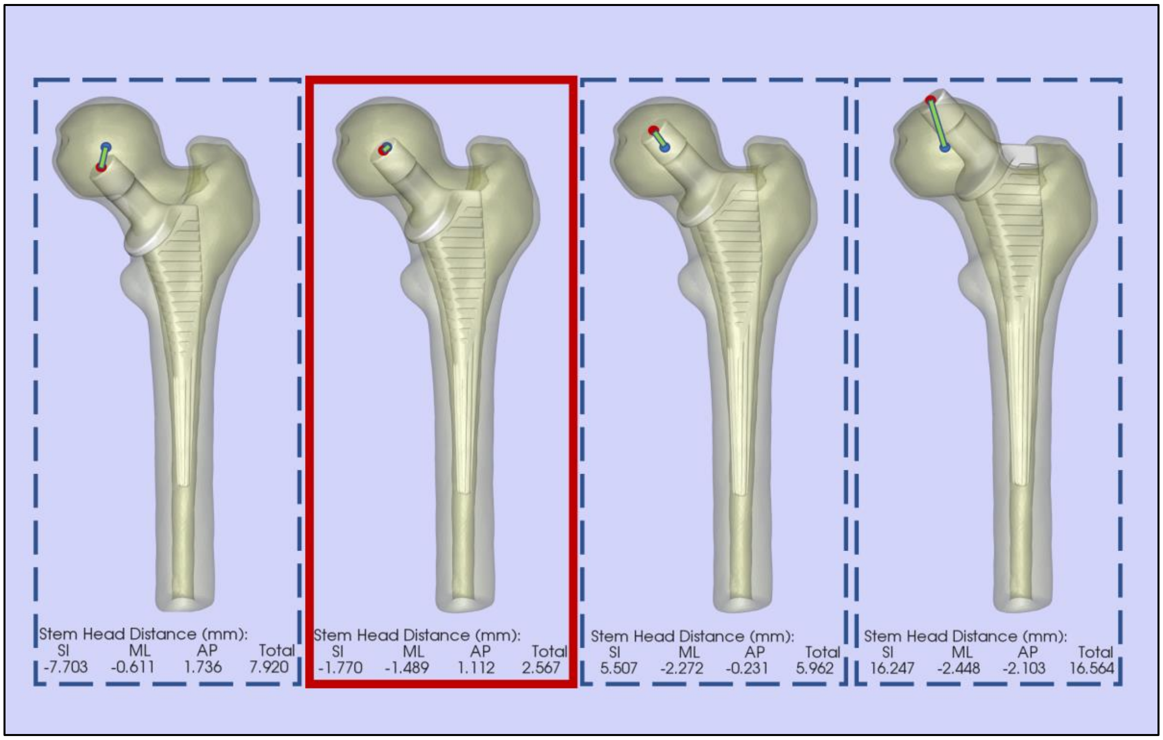

Figure 4-20: Implant sizing suggestion calculating stem head distances and choosing the stem size that has the lowest total head distance - The stem size indicated in read box.

In general, these improvements allow the User a much more robust stem selection module. Specifically, by considering the medial/lateral direction, these improvements allow the User, during a simulation, to accurately determine if the proper choice is a high-offset stem. Similarly, by considering the anterior/posterior direction, these improvements allow us to account for femoral component version changes. A visualization as well as numerical outputs of the distance from the stem head center to the anatomical femoral head center in 3-dimensions is shown in Figure 4-21.

4.3.1.2. Liner size suggestion

The liner suggestion algorithm allows the User to choose the liner size with the inner-diameter as high as possible. This choice can be done manually or by using the automated feature in the model. This change in the liner suggestion algorithm is based on the surgeon's preference when they choose stem size. Specifically, from our internal conversations with surgeons, surgeons usually choose the liner size that maximizes the contact area between liner and stem head. Therefore, it could lower the wear rate of components and lengthen the stem life cycle. Two different liner sizes that fit same shell size (shell size 50) can be seen in Figure 4-22. It can be clearly seen that the liner with the larger inner diameter will have a higher inner contact area. Thus, our algorithm will now automatically choose the liner on the right instead of on the left.

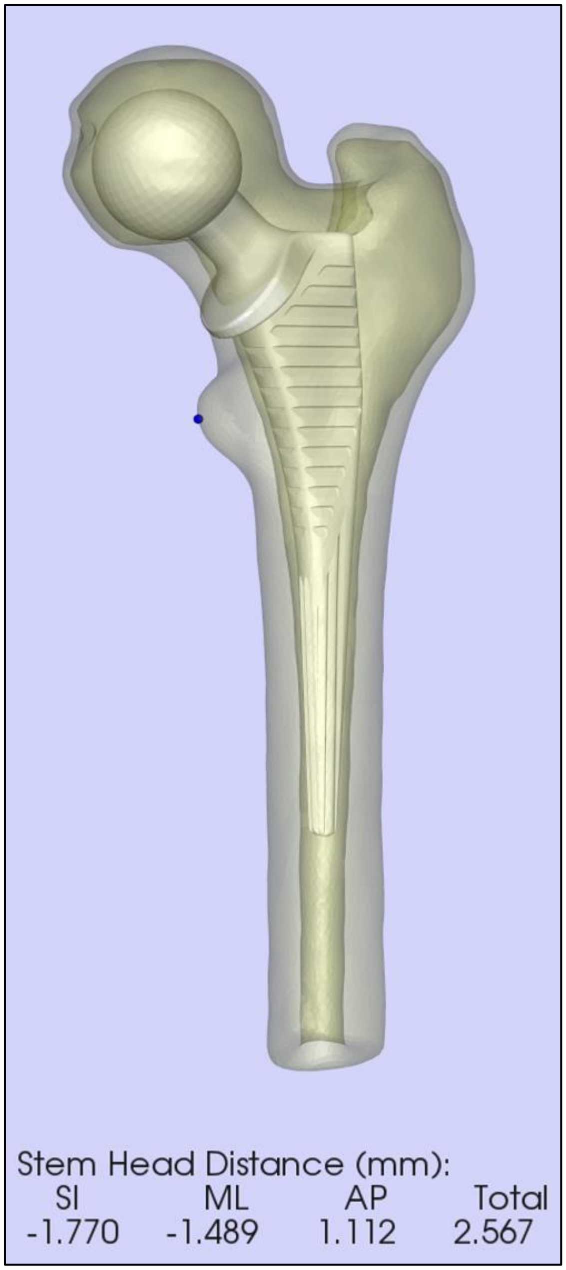

Figure 4-21: Distance from stem head center to anatomical head center (mm).

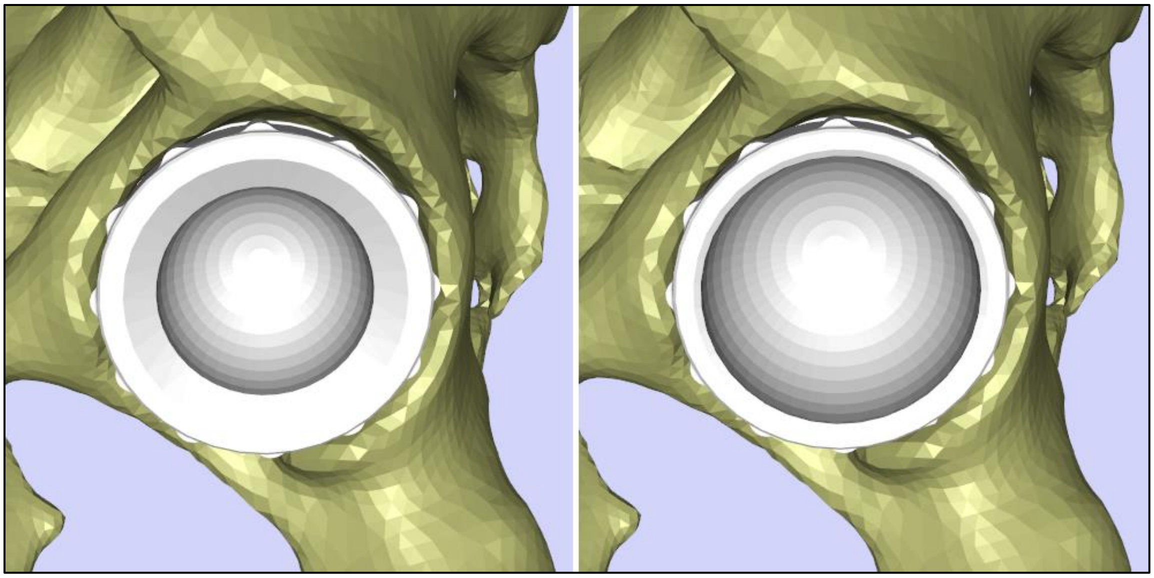

Figure 4-22: Liner size 50×28 (left) and 50×36 (right).

4.3.1.3. Head size suggestion

Since the algorithm can now choose the liner size that has the biggest inner diameter, the algorithm must correspondingly increase the stem head diameter (head size). This feature has been updated appropriately. Furthermore, each head size has many different offsets (neck increment), and the algorithm used to choose the highest offset as a default. This selection can also be manually modified by the User, and this is a feature that will further be improved in the future by incorporating an algorithm that will choose more appropriate head offsets such that stem head center is as close to anatomical femoral head center as possible. A stem head size 36 with different offsets can be clearly visualized in Figure 4-23.

In the latest version of the hip analysis software, we have implemented an algorithm to automate the head offsets suggestion process. The algorithm will loop through all the stem head offset available in the database. With each head offset, it calculates the distance between that head offset center to the femoral head center. Consequently, the algorithm will suggest the head offset that has the lowest distance between the stem head center and the femoral head center (Figure 4-23 and Figure 4-24). This feature is already included in the hip analysis software and will automatically process in the background whenever User select a different stem size.

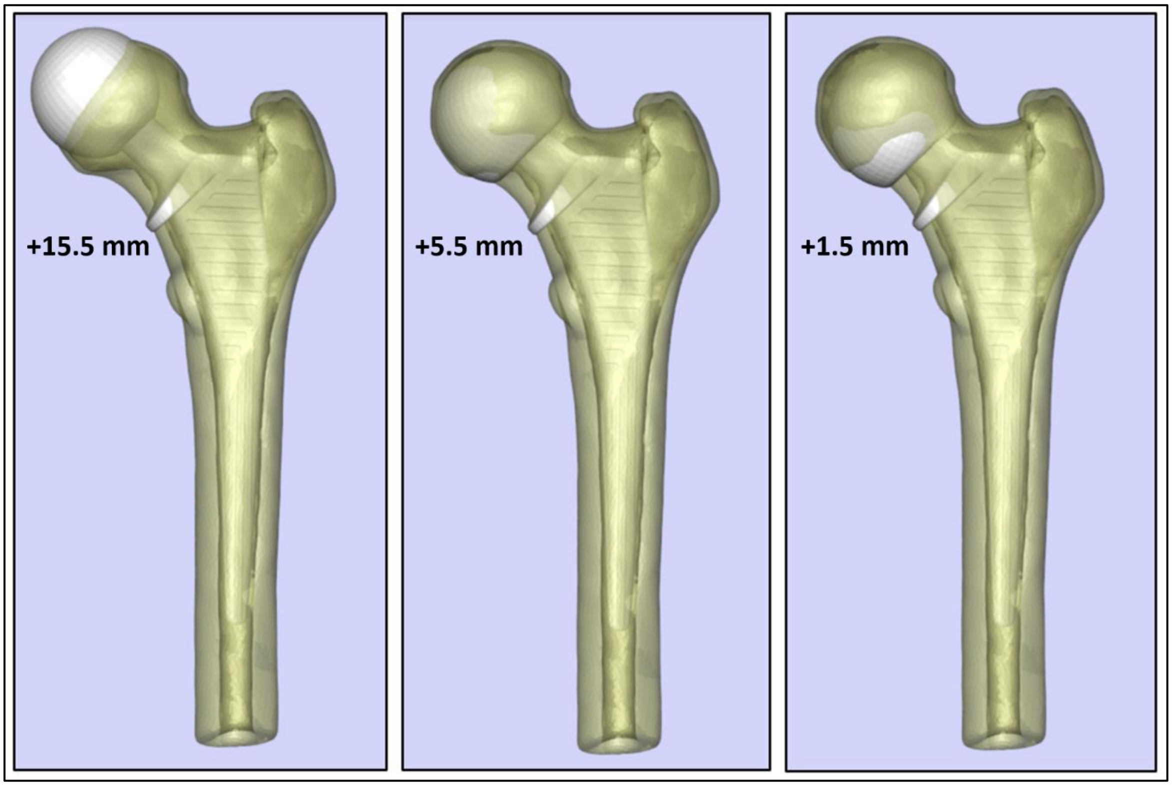

Figure 4-23: Head size 36 with different offsets (right to left: +15.5mm, +5mm, +1.5mm).

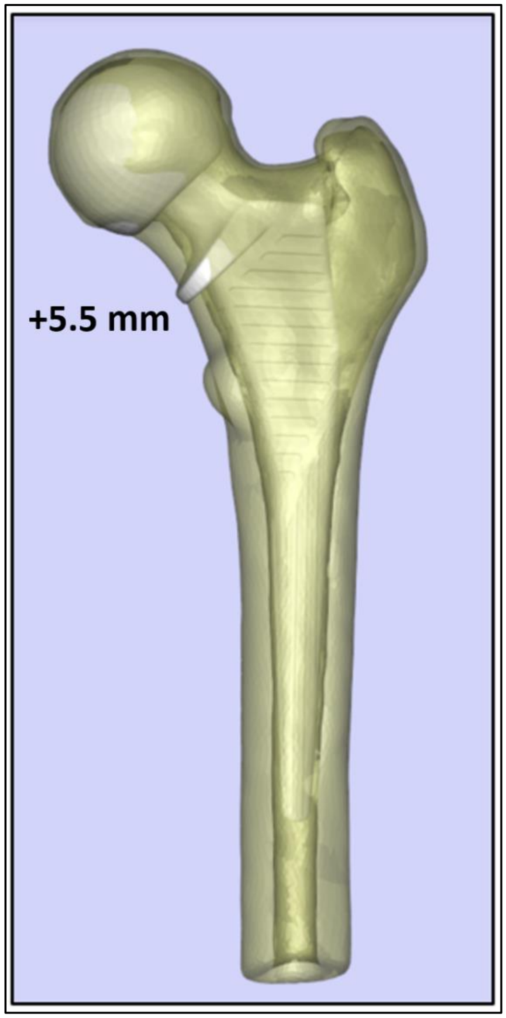

Figure 4-24: Stem head offset with the lowest distance to the femoral head center is chosen (+5.5 mm).

4.3.2. Cup position suggestion

Cup position is also a big factor that affects the quality of a THA. Therefore, it is necessary to accurately predict the cup position in the acetabulum, so having a better cup fitting algorithm in the model can lead to improvements with regard to hip kinematics and reduce stress on hip ligaments. We have implemented an algorithm to fit the cup in acetabulum. Specifically, the algorithm finds the cup position where the cup center aligns with the anatomical acetabular center. As shown in Figure 4-25, the cup on the right side (updated algorithm) is fitting in the suggested position and more accurately mimicking the shape of acetabulum, while the cup on the left side (old algorithm) is clearly misaligned.

4.3.3. Data transferring between implant sizing suggestion algorithm and mathematical hip model

After choosing an implant using the improved algorithm, the GUI allows the User to modify the alignment of the components, including the stem and cup positions. The GUI has been improved, such that it can more efficiently obtain information from the “implant suggestion” tools and feed patient-specific data directly to the theoretical model. These improvements include:

1. Direct communication of bone CAD models/anatomical landmarks to the model input files,
2. Direct communication of variations in implant size suggestions through separate input files, and
3. Robust algorithms for component positioning changes through relative transformation matrices.

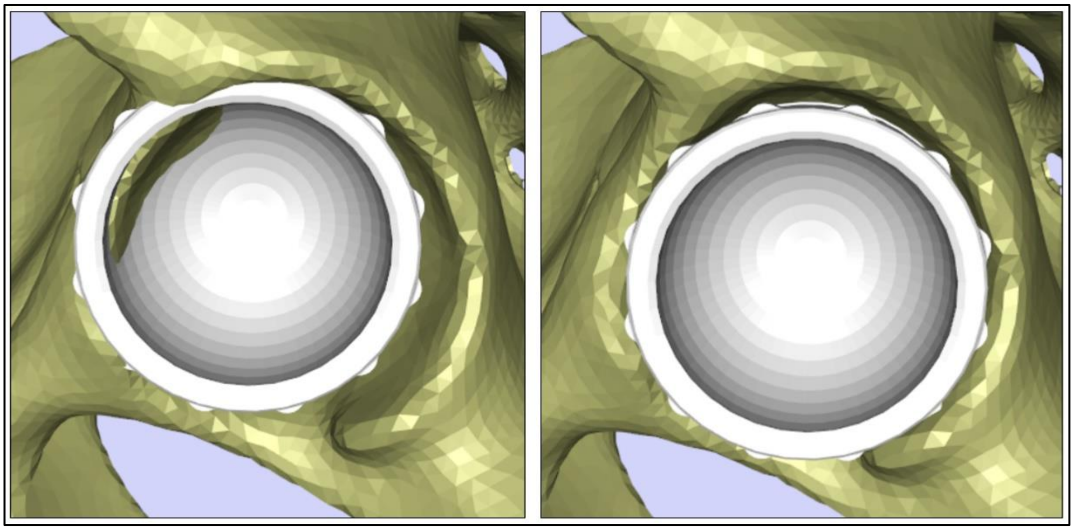

Figure 4-25: The cup in the arbitrary (left) and suggested (right) position.

The User can choose the “Load New Patient” button in the panel (Figure 4-26), then selecting the desired patient, the GUI will use data from the implant suggestion algorithms and conduct an analysis. After the analysis is completed, the implant suggestion results are available in the “Overall Results” area. After the analysis is completed, the implant suggestion results are available in the “Overall Results” area.

4.3.4. Cancellous mantle thickness inclusion

The cancellous mantle thickness is now processed when the User runs the implant suggestion algorithm. By default, cancellous thickness is set to 1.5 mm (Figure 4-27) based on the surgeon preferences profile currently in used for compaction broaching stems. The User can change the mantle thickness based surgeon preference for a particular stem or a desired evaluation using the model. Increasing this value will decrease the space within the canal where the stem sits, typically resulting in a decreased stem size.

4.3.5. Surgeon preferences feature

A surgeon preferences menu has been included in the GUI (Figure 4-28). Selecting this menu will open the Surgeon preferences options in the GUI (Figure 4-29). Within these options, individual surgeon profiles are displayed with different saved preferences, such as the stem type, cup type, component positioning, cancellous mantle thickness, etc. Each of these parameters are directly linked to the specific algorithms discussed above. After selecting a specific surgeon profile, the hip analysis software will automatically apply the preferences to the simulation window, including changing component type, modifying desired surgical method, updating specific component orientations, etc. Specific position

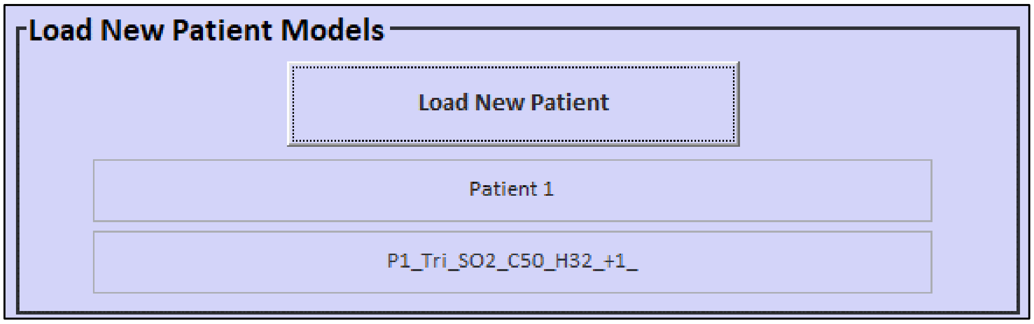

Figure 4-26: Load New Patient option.

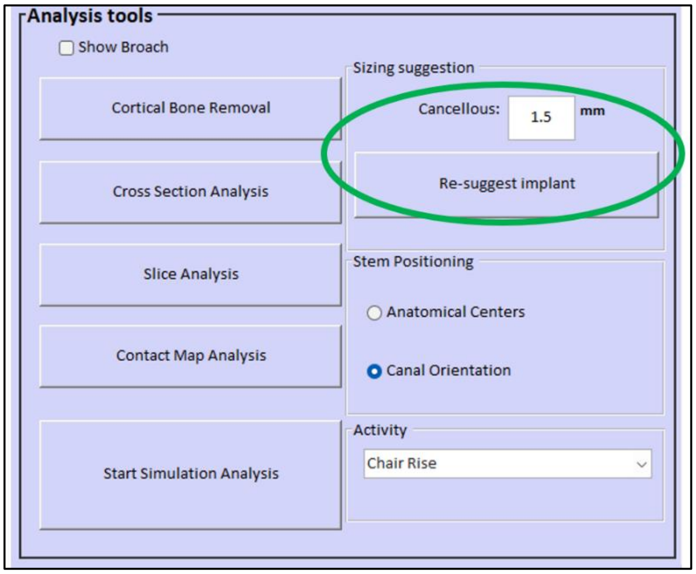

Figure 4-27: Cancellous mantle option.

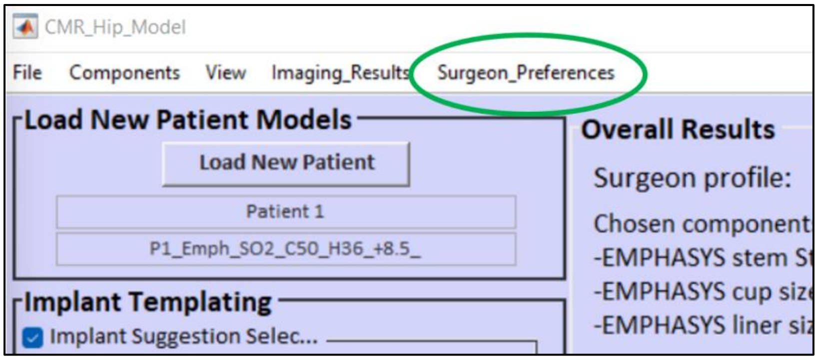

Figure 4-28: Surgeon Preferences menu.

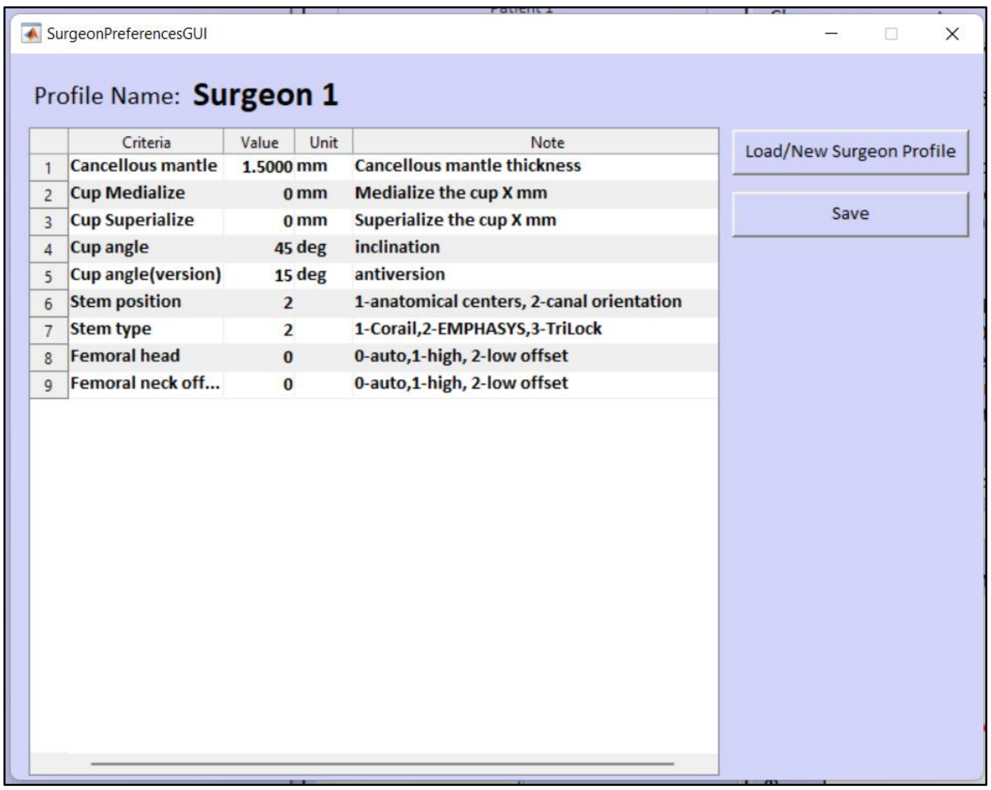

	Criteria	Value	Unit	Note
1	Cancellous mantle	1.5000	mm	Cancellous mantle thickness
2	Cup Medialize	0	mm	Medialize the cup X mm
3	Cup Superialize	0	mm	Superialize the cup X mm
4	Cup angle	45	deg	inclination
5	Cup angle(version)	15	deg	antiversion
6	Stem position	2		1-anatomical centers, 2-canal orientation
7	Stem type	2		1-Corail,2-EMPHASYS,3-TriLock
8	Femoral head	0		0-auto,1-high, 2-low offset
9	Femoral neck off...	0		0-auto,1-high, 2-low offset

Figure 4-29: Surgeon Preferences GUI.

calculations, such as femoral head distances and bone removal volumes, are also re-calculated. Multiple surgeon profiles can be created as desired, and automatically applying these preferences to the model's updated algorithms can save time and also reduce human variability.

4.3.6. Automated femoral head point cloud creation

An advanced algorithm has been derived that accurately and fully automates a point cloud on the surface of the femoral head. This is a major improvement that increases the accuracy of the femoral head point clouds while simultaneously reducing processing time and User-required time, to ultimately improve the overall efficiency of the hip model. Since this feature automatically reads the CAD model data, one can easily incorporate any femoral head shape that can be imagined, including non-spherical shapes (as seen in Figure 4-30).

4.3.7. Settling algorithms

A settling algorithm has been implemented to improve the initial stability of the simulations. In order for the settling algorithm to function properly, the dynamic model is run twice: the first run is a "test" run that includes the "ideal" position for the cup and the stem where no separation will occur. This process will allow the model to determine the "stable" or "settled" positions of the femoral head within the cup, which will allow the model to automatically adjust the initial position of the femoral component. While these adjustments are minor, they can dramatically improve the initial stability of the simulations, especially in more complex scenarios or cases with larger hip separation. By

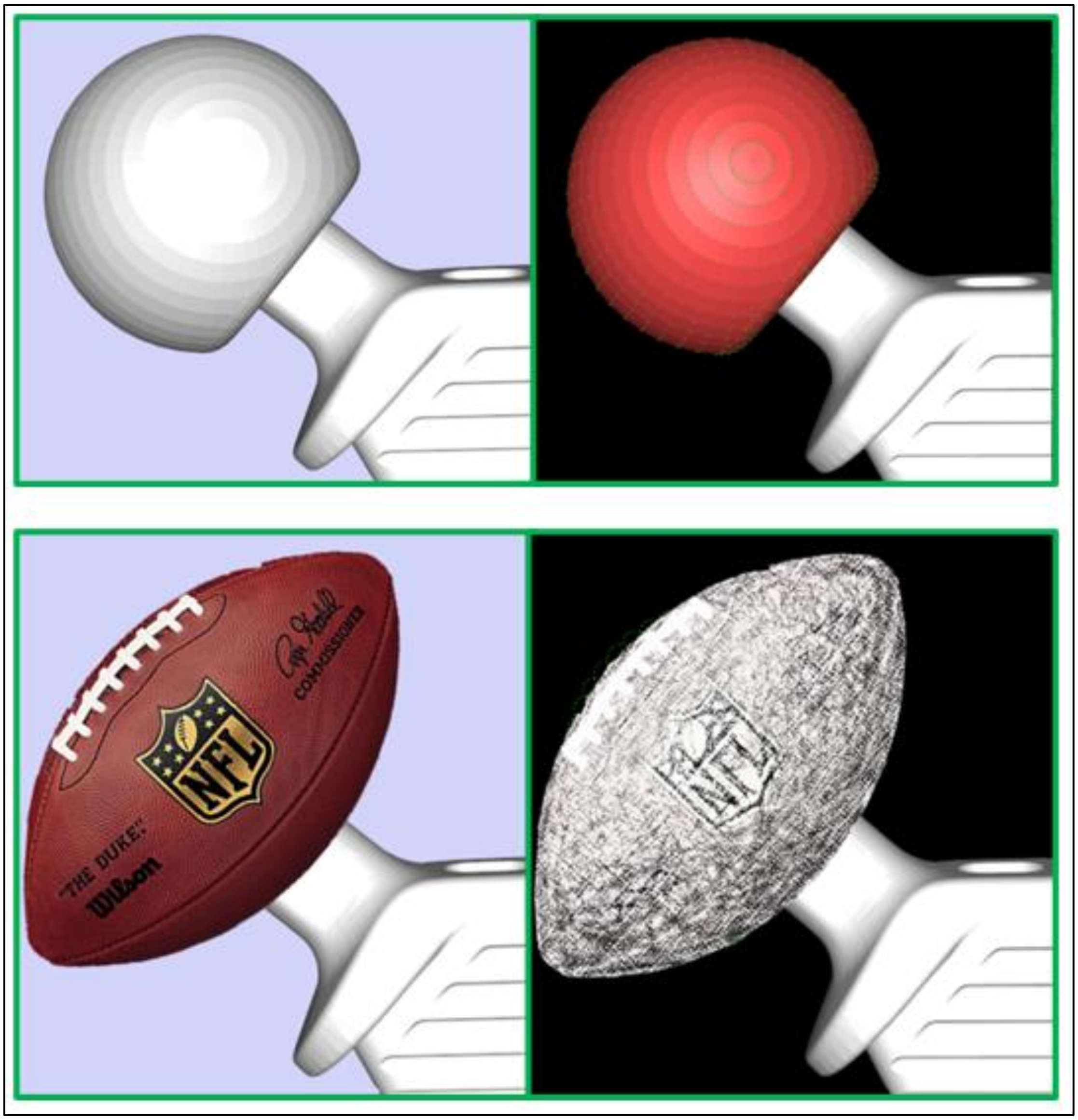

Figure 4-30: Automatic femoral point cloud that will work with any shape.

updating the initial position to determine stable femoral positioning within the acetabular cup, the second run of hip model (which is the actual simulation) will yield more stable results of hip separation (Figure 4-31).

4.3.8. Adding new activities to the model

The Chair Rise activity has also been added into the hip model. The new activity allows for simulations to be conducted using Neutral, Lipped, and Dual Mobility liners. Thus, there are now two different activities available in the model that be utilized for simulations: (1) Gait and (2) Chair Rise. Changing the activity can be done by selecting the Activity panel and then choosing the activity that User wants to analyzing in the simulation. An example results of Chair Rise activity with EMPHASYS stem is shown in Figure 4-32.

4.3.9. Hip analysis tool developments

4.3.9.1. Mesh – mesh Boolean operations

A bone cutting algorithm was developed that uses the mesh–mesh Boolean operations to perform cutting process. In this dissertation, we assume that each mesh creates a closed boundary area that encloses a region in 3D space. Mathematically speaking, a 3D space is represented by an $\mathbb{R}^3$ space where $\mathbb{R}$ is the set of real number. A and B are two meshes in the 3D space, whereas the mesh-mesh Boolean operations consist of three types of operations:

1. Intersection operation: $A \cap B$
2. Union operation: $A \cup B$

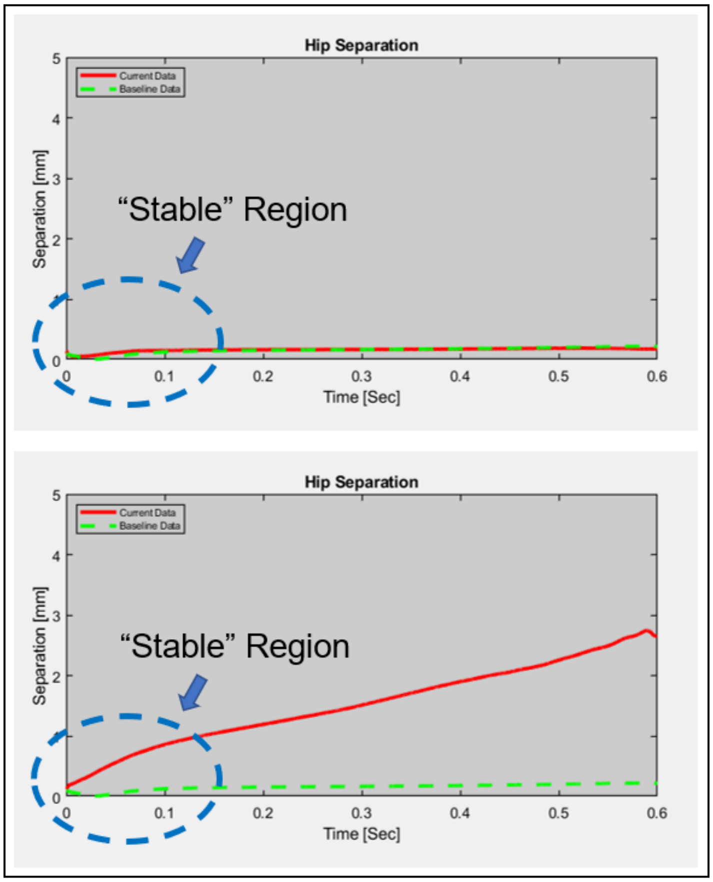

Figure 4-31: Hip separation results with settling algorithm.

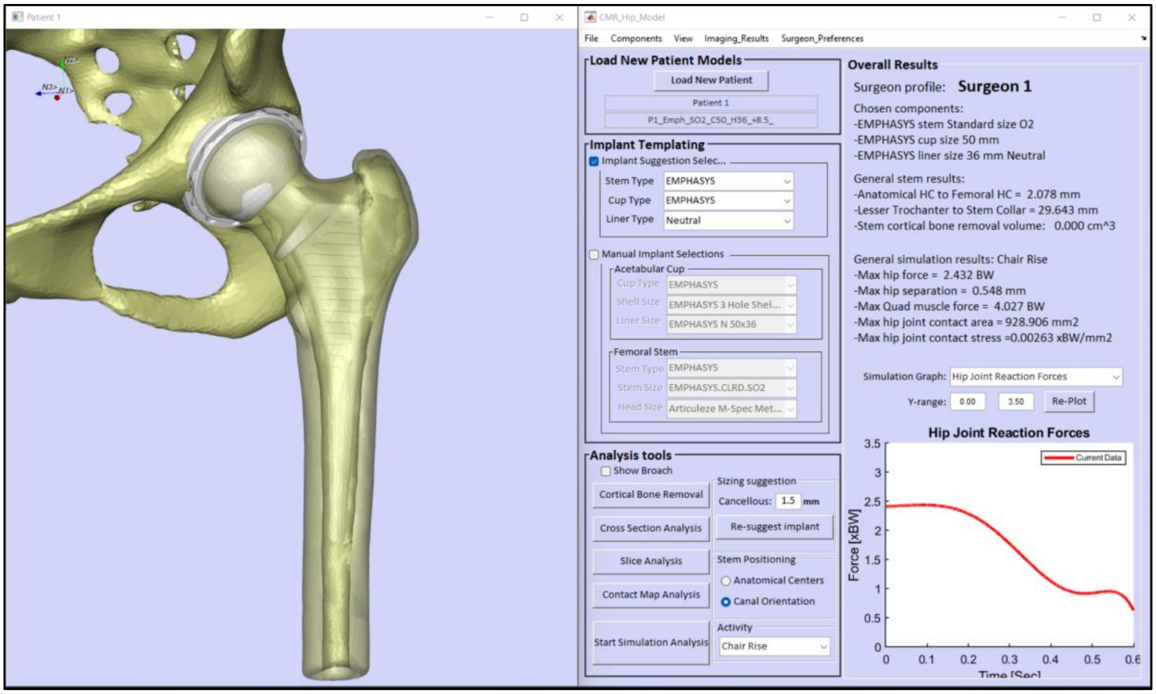

Figure 4-32: Chair Rise activity.

3. Difference operation: $A \backslash B$

The intersection operation ($C = A \cap B$) results an area that is an intersection between the two meshes. The union operation ($C = A \cup B$) creates a new mesh that contains both two original meshes. The difference operation ($C = A \backslash B$) creates a mesh C that is in mesh A and not in mesh B. Each type of operations is illustrated in the Figure 4-33 below.

Mesh – mesh Boolean operations are available in many libraries and software such as PyMesh, Autodesk and VTK. An example of stem cutting tool using Boolean operation on a stem body to get a medial side of stem is shown in Figure 4-34. The mesh – mesh Boolean operations are used in many tools in the hip model from stem cutting tool, acetabular cut reaming tool, broaching canal tool to bone removal tool and bone removal volume calculation.

4.3.9.2. Pelvis acetabular cup reaming

A bone cutting algorithm was also implemented in the hip model to ream the acetabulum once the cup has been placed using mesh–mesh Boolean operations. The algorithm uses the shape of the exterior surface of the cup's CAD model to remove the faces and vertices of the pelvis acetabulum it intersects with. This will ultimately lead to a much cleaner joint space and give a better idea of how the component placement would look after surgery (Figure 4-35).

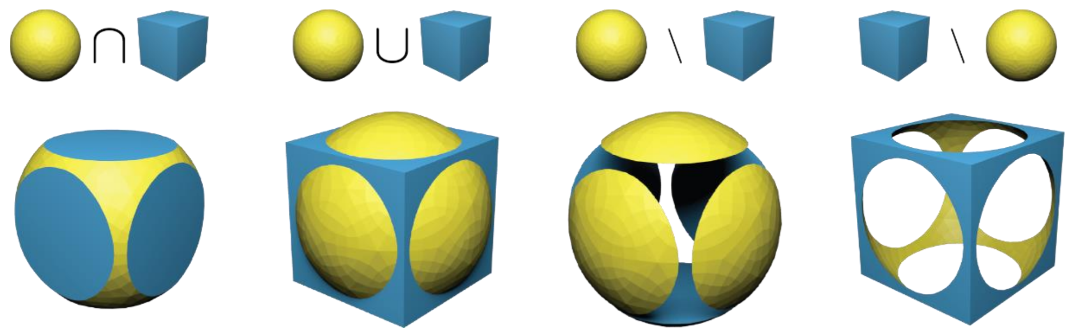

Figure 4-33: Mesh – mesh Boolean operations (image from: pymesh.readthedocs.io)

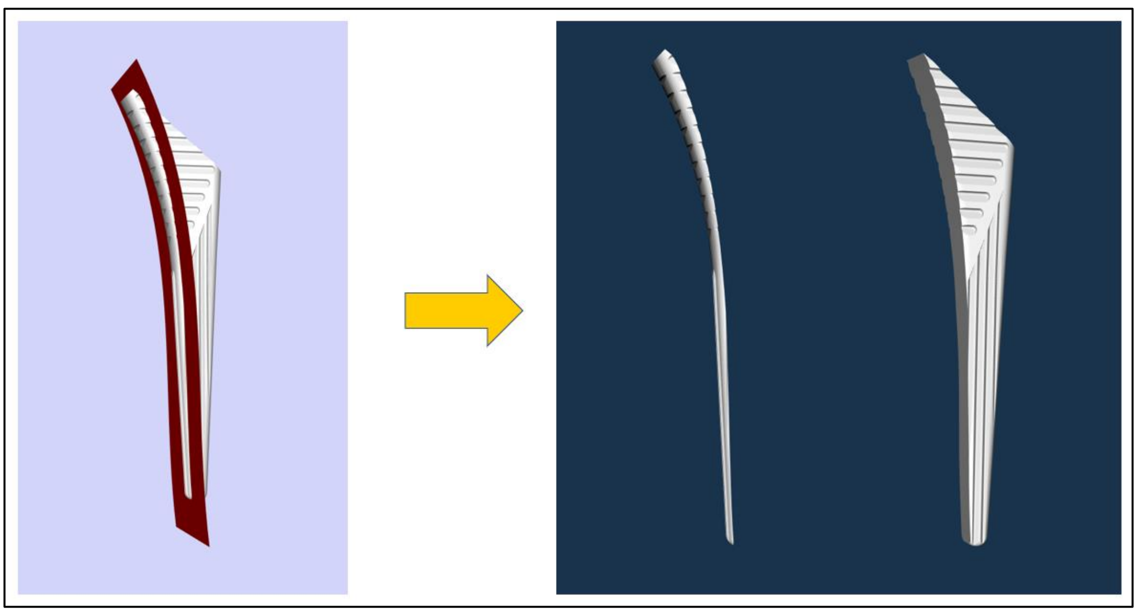

Figure 4-34: Example result of stem cutting for medial side using mesh – mesh Boolean operation.

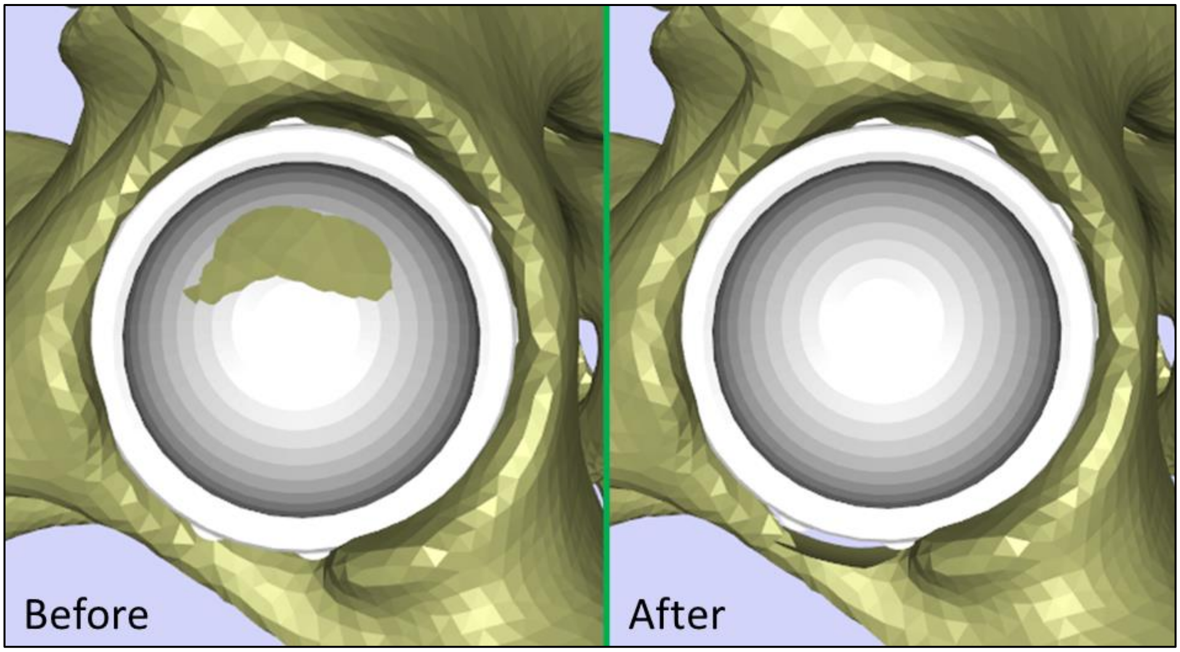

Figure 4-35: Before and after of cup reaming to remove bone.

4.3.9.3. Cortical bone removal analysis with stem and broach

The cortical bone removal analysis is an advanced too that was developed during the scope of this dissertation. The tool provides a quantitative method for evaluating the stem position within the canal by comparing bone removal volume between different stem positions. In the cortical bone removal analysis, the program can perform the bone removal analysis for ether stems or broaches. Including the broaches in this algorithm offers a new option in the hip analysis software package, which now included 3D CAD models of the broaches. The broach can be utilized by selecting the “Show Broach” option (Figure 4-36). The broach is shown in the gray as opposed to the stem is displayed in white (Figure 4-37).

The broach size is selected corresponding to the stem size. For example, an EMPHASYS stem standard size 04 will have a broach size 04. This allows the User to visualize the teeth of the broach within the canal and how the cortical and cancellous bone will be affected by the chosen stem.

Clicking on “Cortical bone removal” button (Figure 4-38) allows for the cortical bone removal analysis to be run. After the analysis is completed, the cortical bone removal volume results will be updated automatically (Figure 4-39) and the bone removal visualization will appear. In the visualization window, the amount of bone removal is indicated in red on the femur. This bone removal visualization allows the User to more clearly visualize the areas of the femur that would need reaming in order to achieve the specified fit (Figure 4-39).

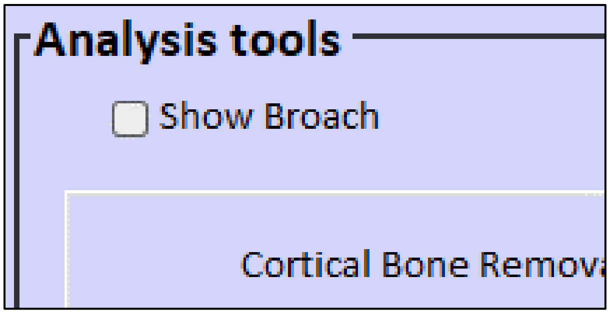

Figure 4-36: Show Broach option.

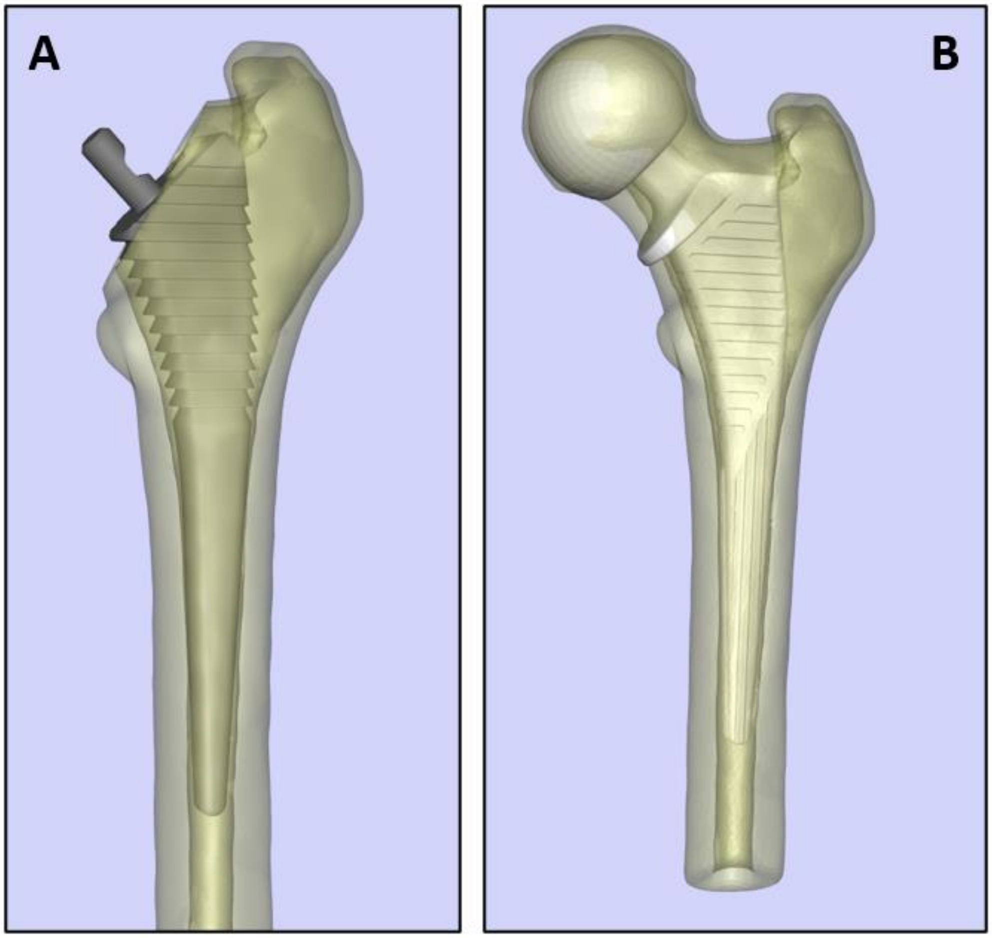

Figure 4-37: Broach (A) and Stem (B) in the canal.

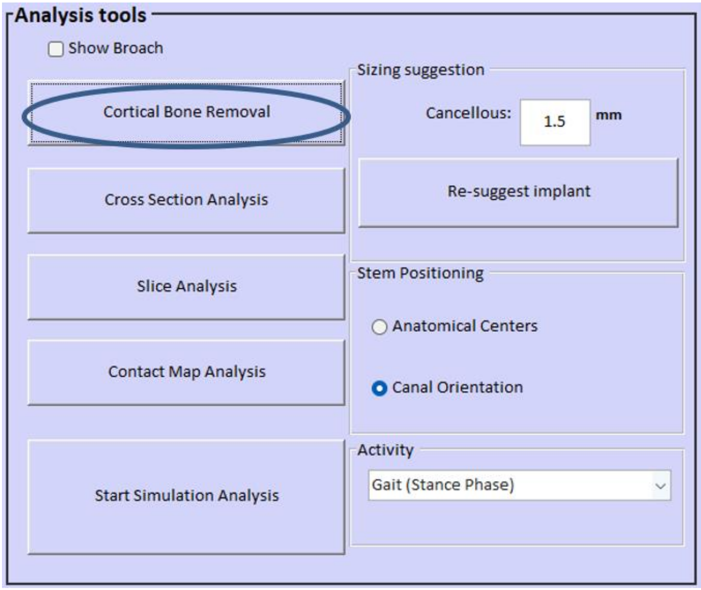

Figure 4-38: Cortical Bone Removal button.

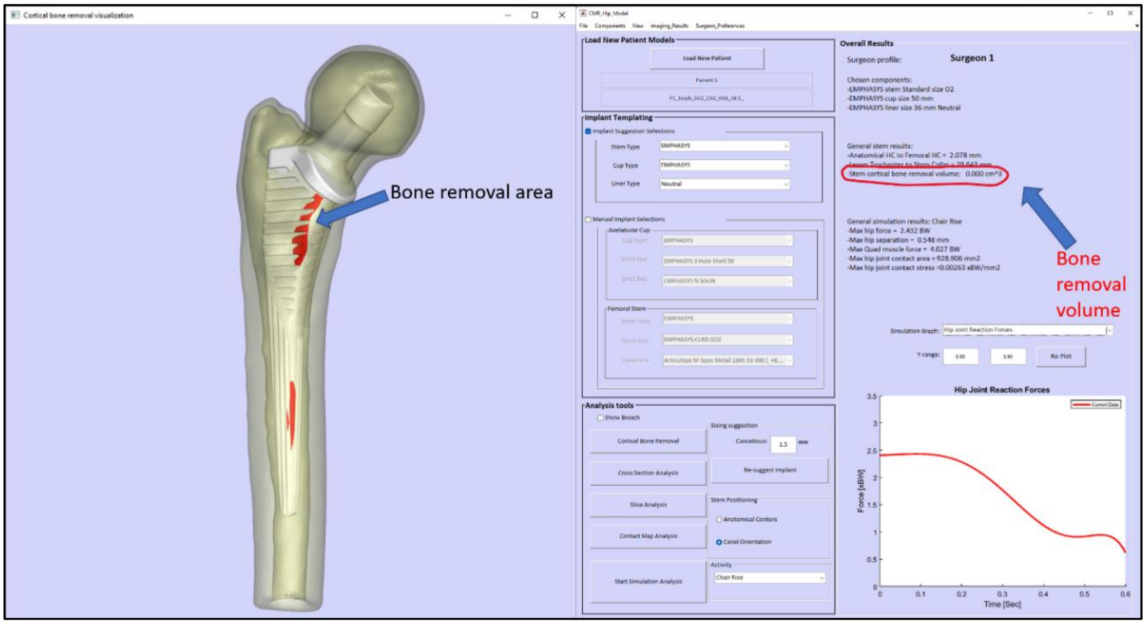

Figure 4-39: Cortical bone removal volume results in the main GUI.

4.3.9.4. Stem contact map analysis

Evaluation of stem position has always been one of the most important tasks in hip analysis software. Previously, an optimal fit is when the distance between femoral head center and stem head center is minimized. However, achieving optimal fit sometimes requires more bone removal. Therefore, it does increase the risk of bone fracture so there is a trade-off that surgeons have to make. In an attempt to incorporate stem contact area and bone volume removal into analysis, two quantitative tools have been developed. The first tool is cortical bone removal analysis tool, and the second tool is stem contact map analysis tool. These tools can calculate how well the stem sits in the canal and how much bone needs to be removed to make the stem fit in the canal.

The stem contact map analysis has been designed so that it not only can display the full stem contact map (Figure 4-40), but also displays contact maps for either the medial or lateral side of the stem (Figure 4-41). The stem contact map is the result of mesh–mesh contact calculation, this calculation was explained in depth in the implant positioning algorithm section. The medial and lateral faces are detected automatically and are displayed separately. This tool can also quantitatively analyze stem contact area based on how much the stem penetrates the femoral bone. The application of the stem contact map analysis tools can be illustrated briefly by reviewing the following example. In this example, shown in Figure 4-42. the full stem area contact analysis is shown, whereas in Figure 4-43 and Figure 4-44 only the medial or lateral face contact analysis is shown. These evaluations show, by default, the total amount and normalized amount of contact area within a certain threshold. In other words, this tool determines how much of the stem is within a 1.0 mm

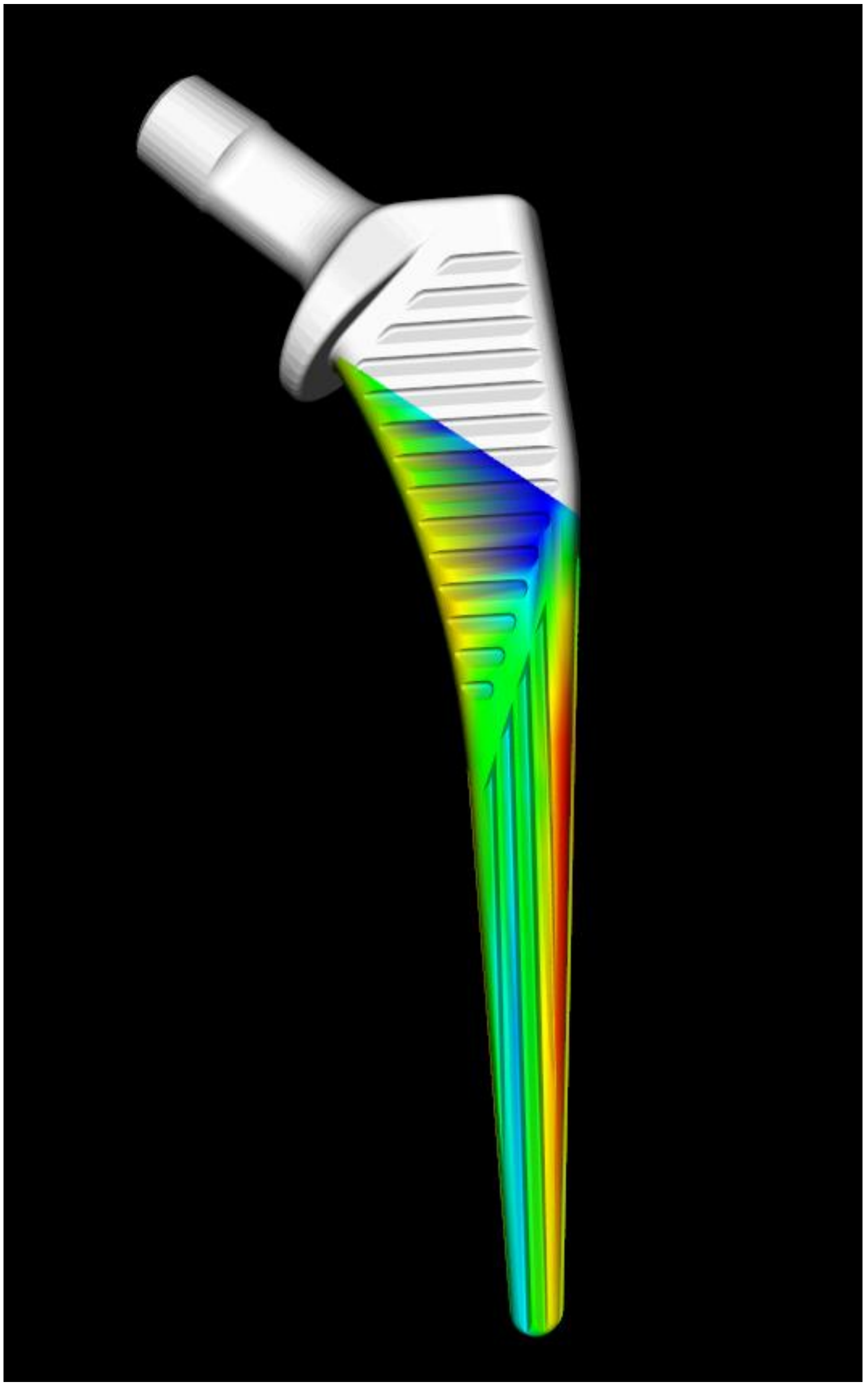

Figure 4-40: Full stem contact map.

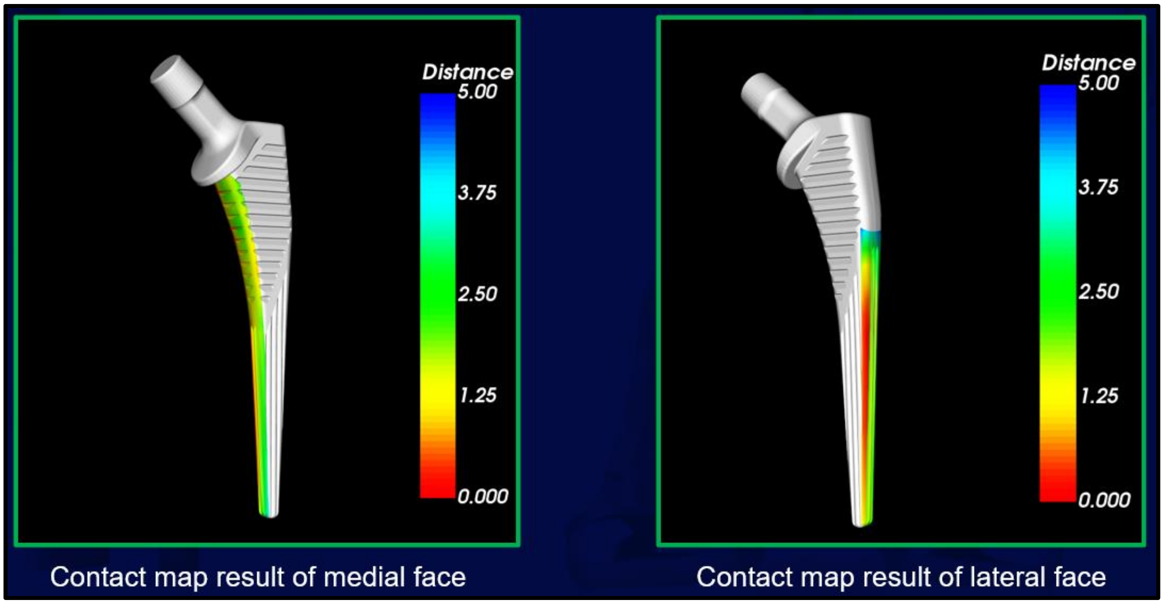

Figure 4-41: Stem contact map in medial and lateral faces.

Threshold	Stem Area	Contact Area	Contact Percentage
< 0.0	4497.12	0125.81	02.80%
< 1.0	4497.12	0853.94	18.99%
< 2.0	4497.12	2348.61	52.22%
< 3.0	4497.12	3519.19	78.25%
< 4.0	4497.12	4184.73	93.05%
< 5.0	4497.12	4357.56	96.90%

Figure 4-42: Total stem area analysis from Figure 4-40 example.

Threshold	Stem Area	Contact Area	Contact Percentage
< 0.0	1187.39	0091.07	07.67%
< 1.0	1187.39	0372.20	31.35%
< 2.0	1187.39	0939.88	79.15%
< 3.0	1187.39	1134.41	95.54%
< 4.0	1187.39	1168.80	98.43%
< 5.0	1187.39	1183.39	99.66%

Figure 4-43: Stem medial face area analysis from Figure 4-41 example.

Threshold	Stem Area	Contact Area	Contact Percentage
< 0.0	0965.44	0000.00	00.00%
< 1.0	0965.44	0243.35	25.21%
< 2.0	0965.44	0661.01	68.47%
< 3.0	0965.44	0895.94	92.80%
< 4.0	0965.44	0942.73	97.65%
< 5.0	0965.44	0956.84	99.11%

Figure 4-44: Stem lateral face area analysis from Figure 4-41 example.

threshold from the cortical bone, a 2.0 mm threshold from the cortical bone, etc., up to 5.0 mm based on User selection. From these figures, it can be seen that in this particular example, contact area in medial side is larger than contact area in lateral side.

4.3.9.5. Cup contact map 3D visualization and activity simulation

Contact map visualization is an important part of the GUI. The contact map is available to conduct both stem and cup analyses. The 2D and 3D cup contact map visualization and animations have been incorporated in the result section of the hip analysis software. With respect to the contact map visualization, the User could access the synced animation. Specifically, the contact map visualization of the cup has been moved to the result drop down menu (Figure 4-45). We have implemented the contact map visualization, such that, it allows the User to visualize the animation of the model next to the contact map. The contact map GUI has 3 viewing options: “Hip View”, “Body View” and “Free View”. The “Hip View” option pertains to the model animation close-up of the hip, and it visualizes the hip from the anterior direction (Figure 4-46). The “Body View” option visualizes the full body animation from the medial-lateral direction (Figure 4-47). The “Free View” option allows User to view the animation from any angle. The contact map visualization and the animation run simultaneously when User hits the “Animate Cup” button.

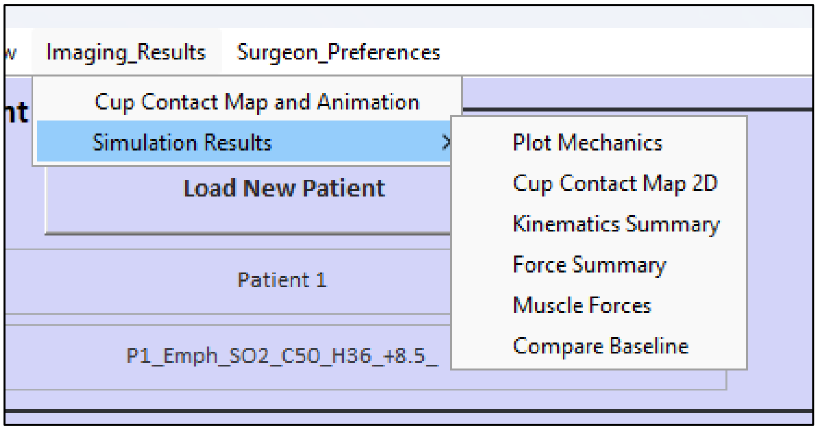

Figure 4-45: 3D and 2D cup contact map features in the main GUI.

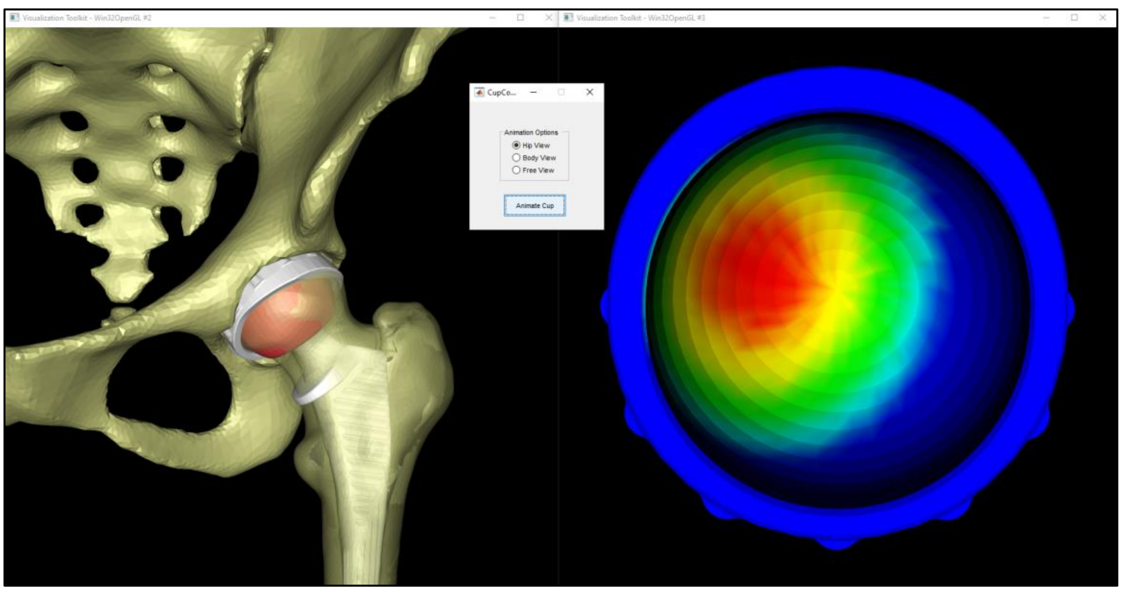

Figure 4-46: Cup contact map - Hip View option.

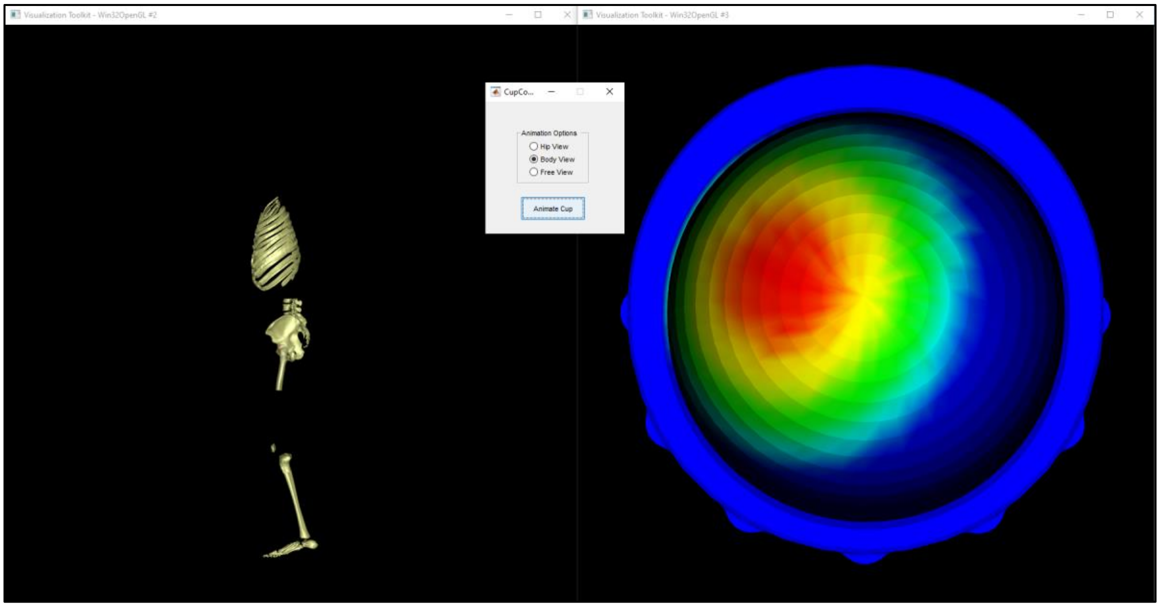

Figure 4-47: Cup contact map - Body View option.

4.3.9.6. Cup contact map 2D visualization

A 3D view of cup contact map, shown on the left in Figure 4-48, is very useful when User is conducting simulations using the model. However, fully visualizing and comprehending 3D maps can be difficult, as 3D objects are best viewed interactively on a computer or other display devices. Therefore, we have come up with a different way to demonstrate the contact map of the cup by essentially "flatting" the cup into 2D plane, then applying the contact map from the 3D map to the 2D map (shown on the right in Figure 4-48). This 2D contact map offers a new and more consistent method to analyze the cup, and it also helps User export information that can be more easily used in publications.

Figure 4-49 depicts the 2D contact map GUI, with the ability to display the animation of contact map in 2D in the same way we already have in 3D. The 2D contact map GUI was developed recently with the second version of 2D contact map, discussed below. The "Update Sigma" button will get the sigma value from the edit box and then use that value to calculate a new 2D contact map. Sigma is defined as the standard deviation of a normal distribution, and thus we use a normal distribution to calculate the point penetration information for the 2D grid from 3D contact map.

The limits panel controls the limits of penetration displayed on the color bar. The "Auto Limits" option sets the limits automatically, the "Manual Limits" option sets the limits based on User preference. Each activity encompasses 60 frames that make up the animation. The User can choose to display entire animation by setting the frame value from 1 to 60, or they can choose to display any specific frame by setting the frame value to that specific frame number. Hitting the "Display" button will run the 2D contact map animation.

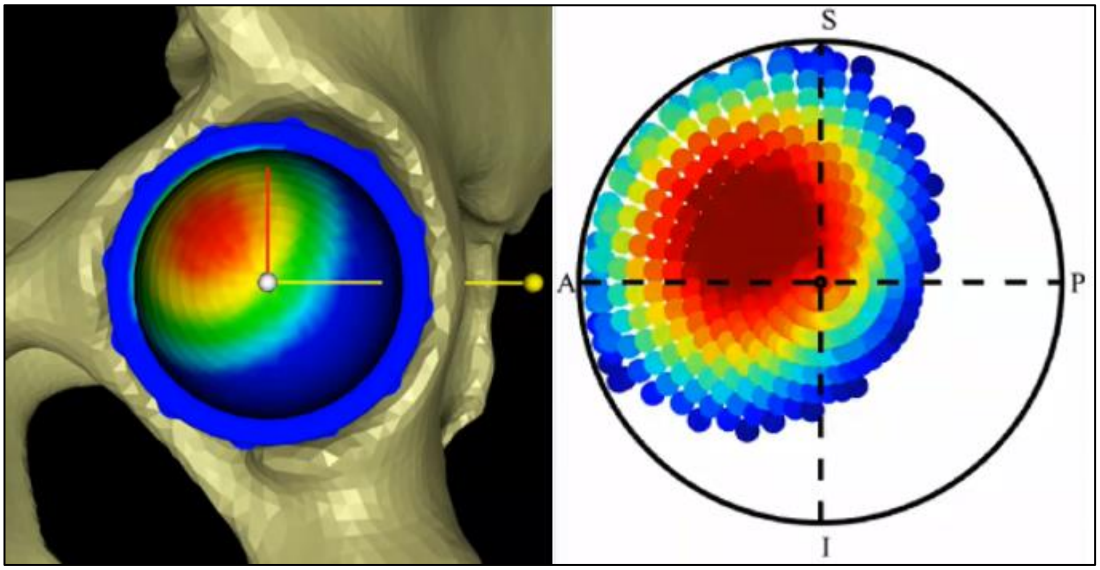

Figure 4-48: 3D (left) and 2D (right) Contact Maps.

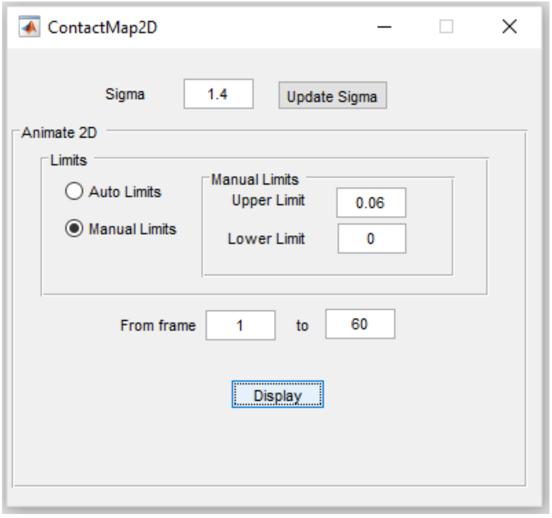

Figure 4-49: 2D Contact Map GUI.

There are two versions of 2D contact map, and this feature is still continuing to be improved and optimized. The first 2D contact map version is shown in Figure 4-50 and Figure 4-51. The second 2D contact map version is shown in Figure 4-52 and Figure 4-53. The first version of contact map also includes calculations of contact area and the contact path (shown by the grey line in Figure 4-50), as well as a penetration color bar and SI/AP directions of the cup. The contact area is illustrated using many small color circles that together form a representation of the contact area. Furthermore, a black circle is used to illustrate the cup area. Using a circle to describe the neutral cup is acceptable, since the neutral cup has a perfect half sphere shape. However, the lipped liner is not a perfect half sphere, and therefore using a circle to describe a lipped liner in 2D would not suffice, and this is accounted for in the second map version.

After developing and using the first version of 2D contact map, we wanted to develop a second version to offer improved resolution of contact area, corrected lipped liner boundaries, more accurate penetration representations, and more accurate contact area boundaries. All the features that are currently available in the first 2D contact map version are also included in the second version, such as the SI and AP direction markers and the contact path displayed over the entire activity. In this version, improvements such as a more accurate cup boundary and automatic 2D-Contact area boundary have been developed.

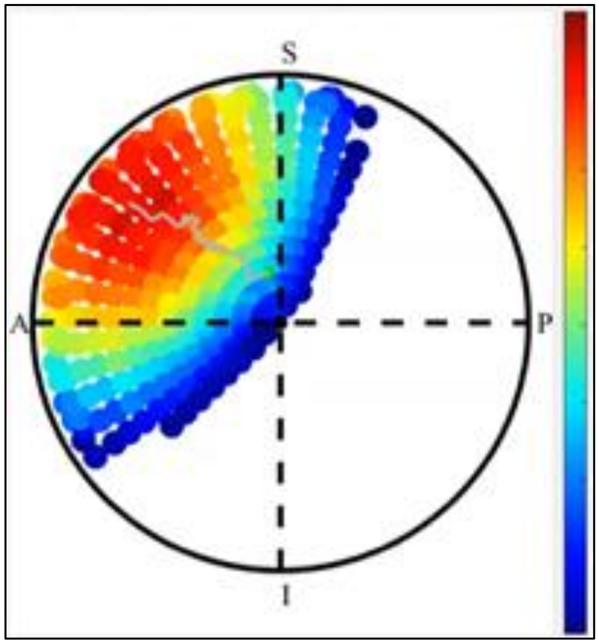

Figure 4-50: First version of 2D contact map for a neutral liner.

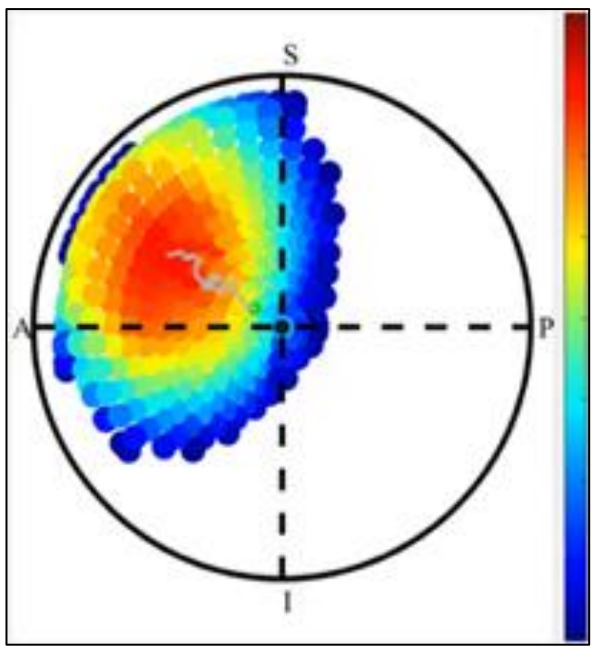

Figure 4-51: First version of 2D contact map for a lipped liner.

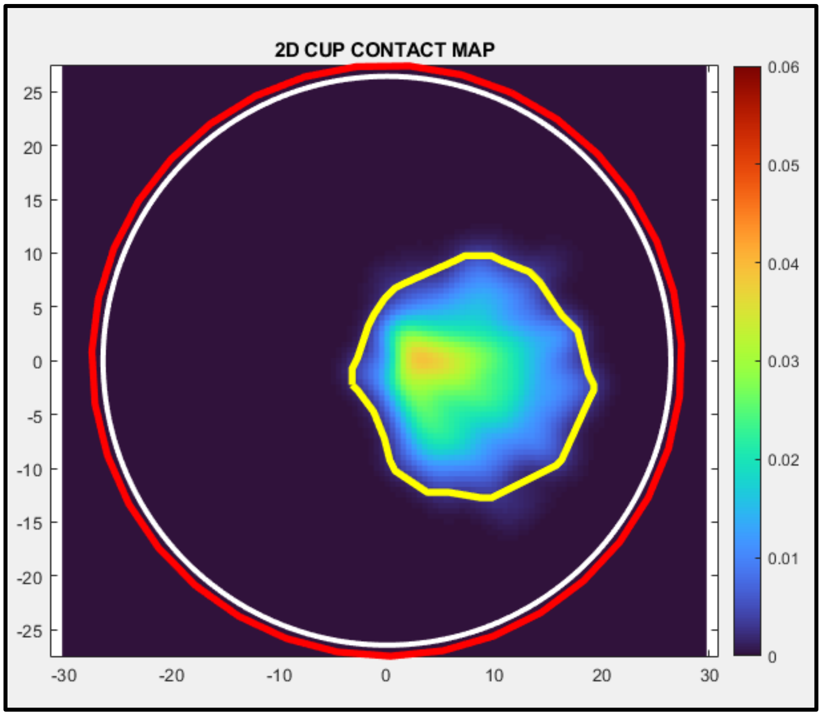

Figure 4-52: Second version of 2D Neutral cup contact map.

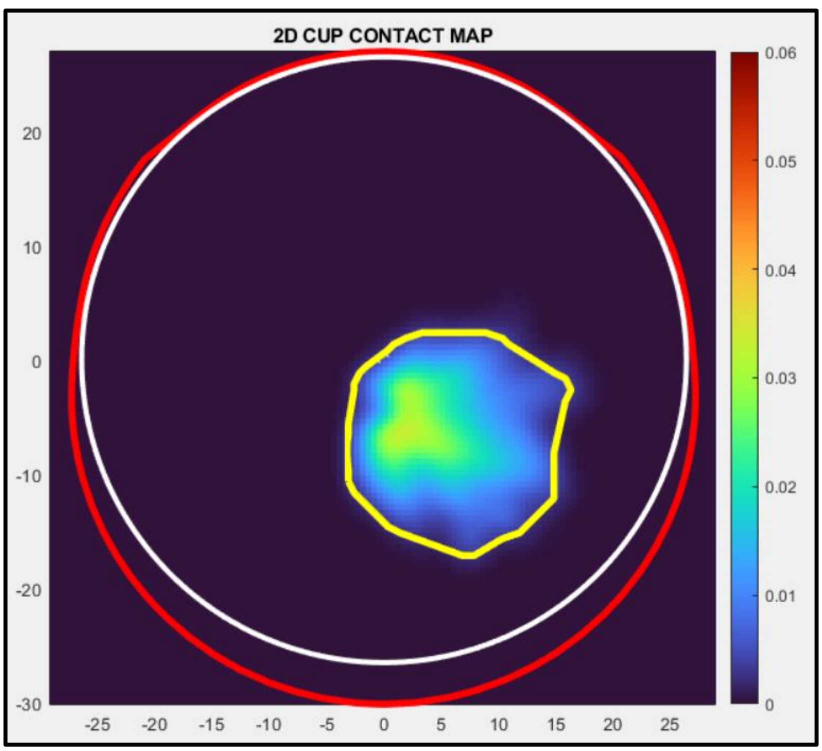

Figure 4-53: Second version of 2D Lipped cup contact map.

The second version can be found in Figure 4-52 and Figure 4-53. The 2D contact map of a neutral liner in the optimal stem position is shown in Figure 4-52 and the 2D contact map of a lipped liner in the optimal stem position is shown in Figure 4-53. The red circle indicates the area of the cup. In the lipped liner, the outer liner boundary is not a perfect circle due to the lip portion. Thus, when projecting the lipped liner into 2D, the lip of the liner can be clearly seen at the bottom of Figure 4-53. The surface area of the inner portion of the liner (the articulating surface) is calculated automatically from the 2D projection.

Finally, the contact area in the 2D contact map is also highlighted by a yellow boundary (Figure 4-52, Figure 4-53). By using a boundary algorithm, we can dynamically track the contact area throughout the entire activity. The actual area of the contact patch is calculated from the 3D contact map, but in 2D we can more easily compare the areas by looking at the yellow boundary. The color bar shows the penetration of the steam head within the liner from our contact detection algorithm.

4.3.9.7. Cup and stem alignment tools

The new Stem Alignment tool and Cup Alignment tool (Figure 4-54) have been developed using more information about the alignment of the stem and cup. The two alignment tools keep track the amount of translation (mm) and rotation (radian) of the stem and cup during the alignment process. Therefore, if a User wants to recreate the stem and cup position from the previous study, they can use that translational and rotational information to do so.

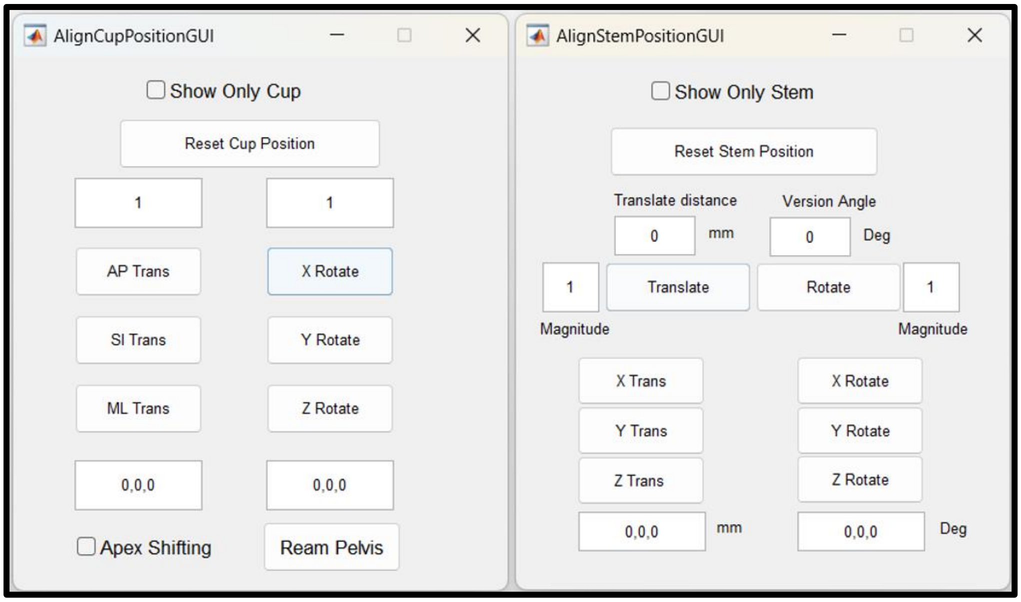

Figure 4-54: Cup and stem alignment tools.

The GUI has been improved such that User can now modify the position of the components, if desired, more easily. These improvements to the Cup Alignment tools include rotations in the X, Y, and Z directions about the cup's body-fixed axis, and translation along AP, SI, and ML direction in the pelvis's reference frame. The "Reset cup position" button will reset the cup to the initial suggested position. Improvements to the Stem Alignment tools include translation along the canal axis and rotation around canal axis. As discussed earlier, after aligning the components, the User can proceed with he "Start Analysis" or "Save Simulation" options. The Save Simulation feature allows User to save the cup and stem alignment for future investigation. Figure 4-54 shows the "Cup Alignment" and "Stem Alignment" tools side by side.

4.3.9.8. Anatomical distances calculations

Collar distance to lesser trochanter

The distance from the lesser trochanter to the lowest point on the collar was added as a metric so that comparisons between different stem systems can be conducted. All measurements are done in the global reference frame from the lesser trochanter point to the collar point. For a patient-specific bone, the lesser trochanter position (blue point in Figure 4-55) is calculated automatically using the bone templating algorithm. The collar point (red point in Figure 4-55) is loaded from the stem database. Therefore, the program calculates the distance from lesser trochanter to collar point automatically, and this distance can be computed in any reference frame (femur/stem reference frame) very easily using stem position information.

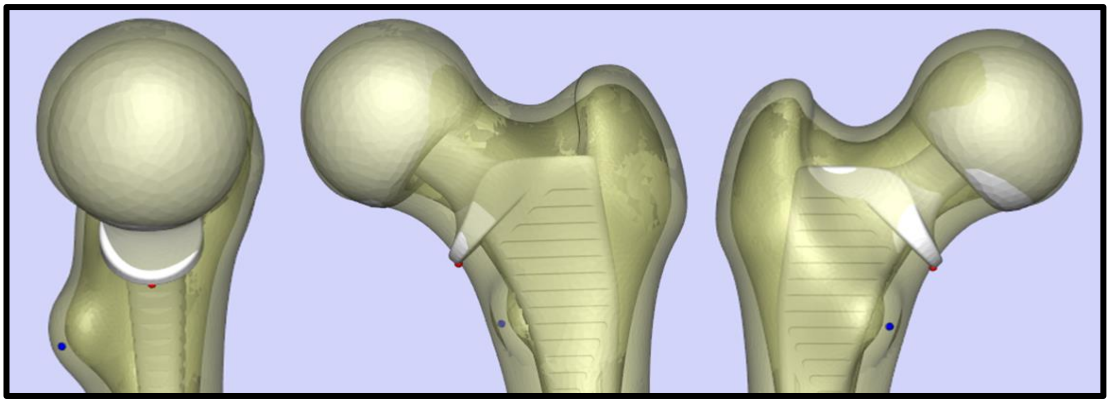

Figure 4-55: Positioning of the lesser trochanter (blue) and collar point (red).

The distance from lesser trochanter to collar point provides an extra parameter to evaluate the quality of the stem position, and the User can also use this distance to make evaluations and predictions based on maximum bone retention. With this measurement, the User can see how much more or less bone removal is needed based on the implant design, or how stem version angle reflects on this distance.

Real time distance update on the main window

Distance information is now shown directly on the main window next to the bone view (bottom left corner as shown in Figure 4-56). The User can turn on/off distance information by selecting Stem Alignment tool and checking the “Show Only Stem” option in the GUI (Figure 4-56). The distance information is updated instantly when you make any changes in stem position.

The “Total” value reveals the absolute value of the distance. The initial information that is determined is the vector from femoral head center to stem head center - “Stem Head Distance (mm)”. The second piece of information is the vector from Lessor Trochanter to Collar point - “LessTroc-to-Collar Distance”. Additionally, an axis system showing the Superior/Inferior, Anterior/Posterior, and Medial/Lateral coordinate system directions has been added to the window.

4.3.10. GUI development

As this dissertation progressed, many changes were implemented with respect to the GUI, including a totally new look of the GUI with a brighter background, adjusting the

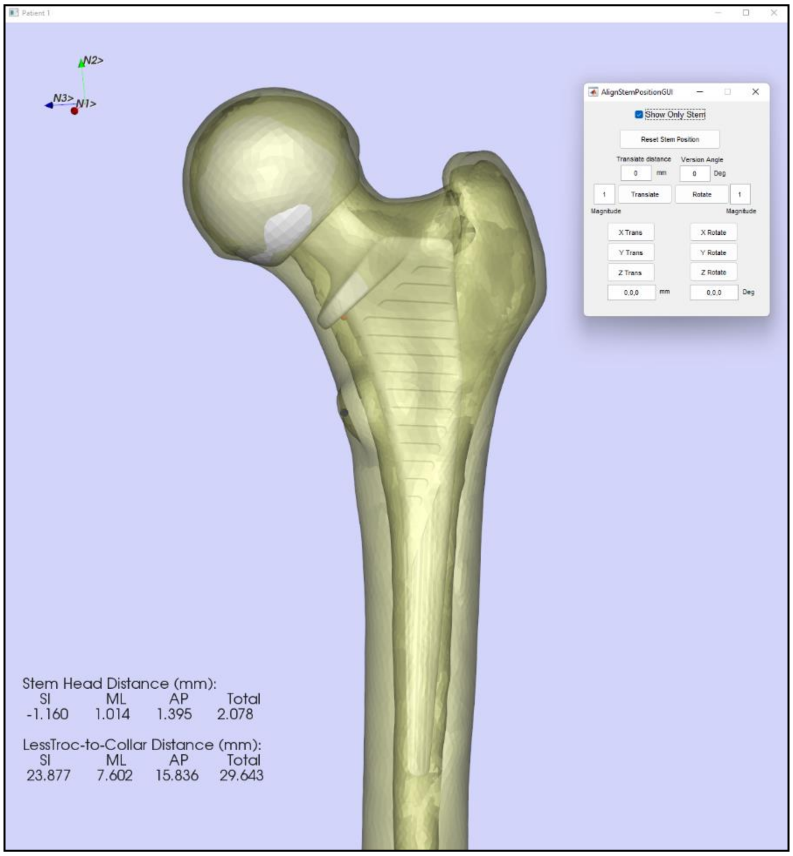

Figure 4-56: Stem alignment tool and distance information.

window sizes and layouts, and adding in real-time monitoring of the stem position, more detailed simulation information, and results that are now displayed within the GUI with real-time monitoring of component information and general stem alignment results. The GUI becomes full screen automatically after selecting a patient. The main GUI is on the right and the patient window is on the left half of the screen (Figure 4-57). The default GUI setting is currently set as full screen, but the User can still move the GUI around freely based on their preferences. Broaches for EMPHASYS and Corail stems are also added to the program. Cancellous mantle thickness can be also adjusted based on what stem type is being used. The information pertaining to the cancellous mantle thickness is used to calculate implant suggestion as well as implant position within the canal. The details about cancellous mantle thickness applications will be discussed further in the following sections as the dissertation progresses.

4.3.10.1. Menu section

The menu section (Figure 4-58) has six main options including File (Figure 4-59), Components (Figure 4-60), View (Figure 4-61), Imaging Results (Figure 4-62) and Surgeon Preferences. The Imaging Results menu has 2 main categories: “Cup Contact Map and Animation” and “Simulation Results” (Figure 4-62). With respect to the “Cup Contact Map and Animation” option (Figure 4-62), the User can access the simulation animation. The animation depicts the cup contact map and the activity simultaneously. In the Simulation Results section (Figure 4-63), there are six results options including Plot Mechanics, Cup Contact Map 2D, Kinematics Summary, Forces Summary, Muscle Forces, and Compare Baseline graphs.

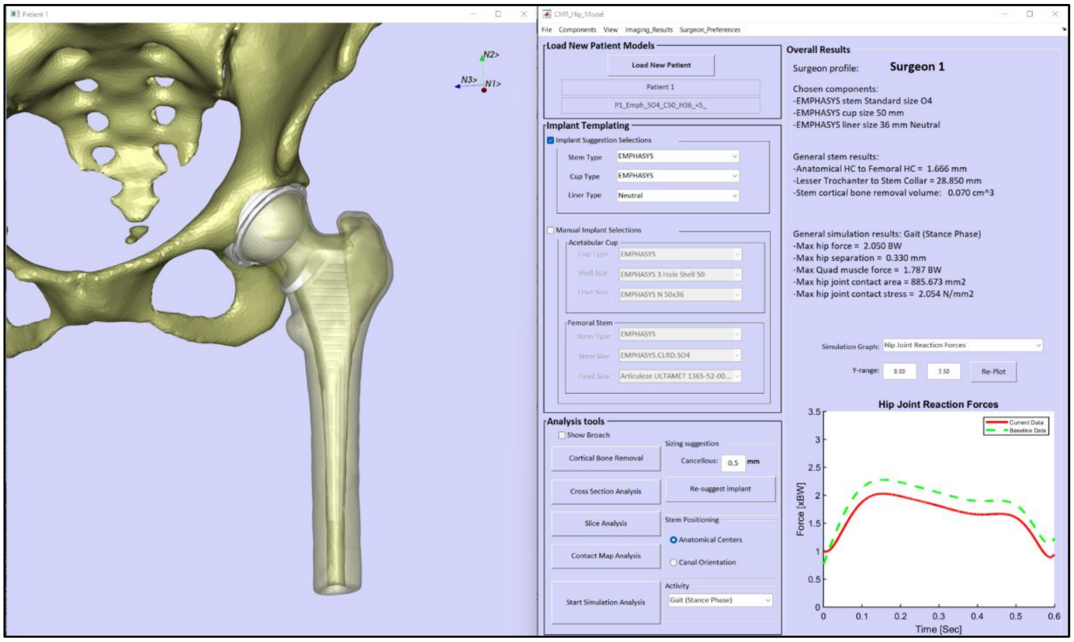

Figure 4-57: Hip model GUI.

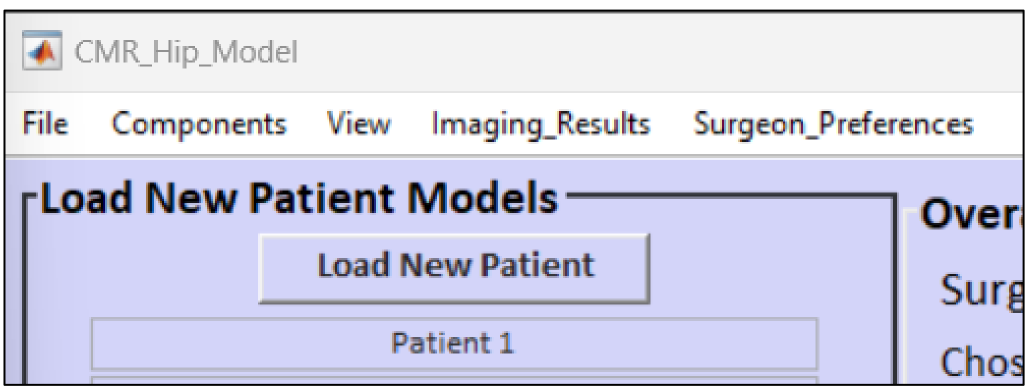

Figure 4-58: Menu options

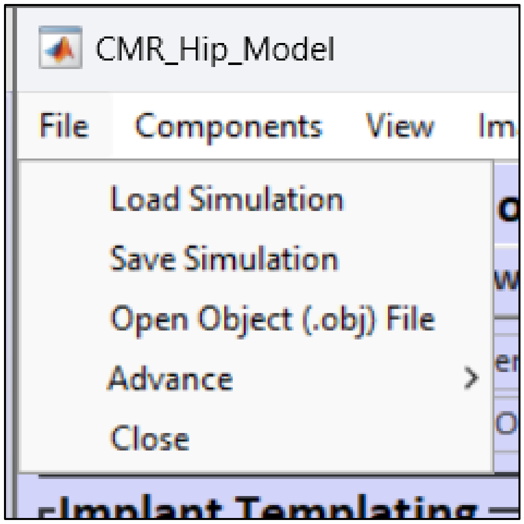

Figure 4-59: File menu

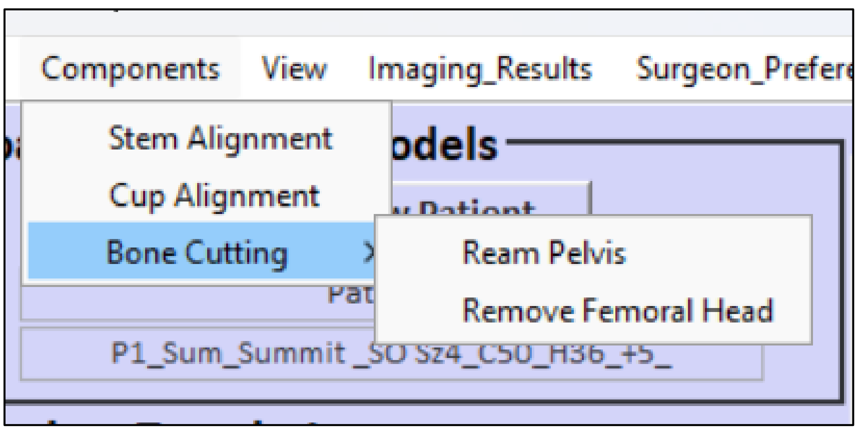

Figure 4-60: Components menu

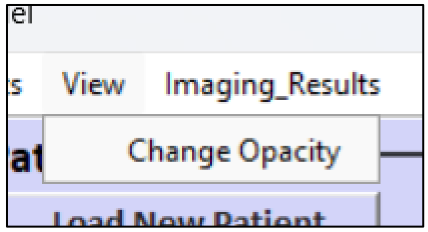

Figure 4-61: View menu

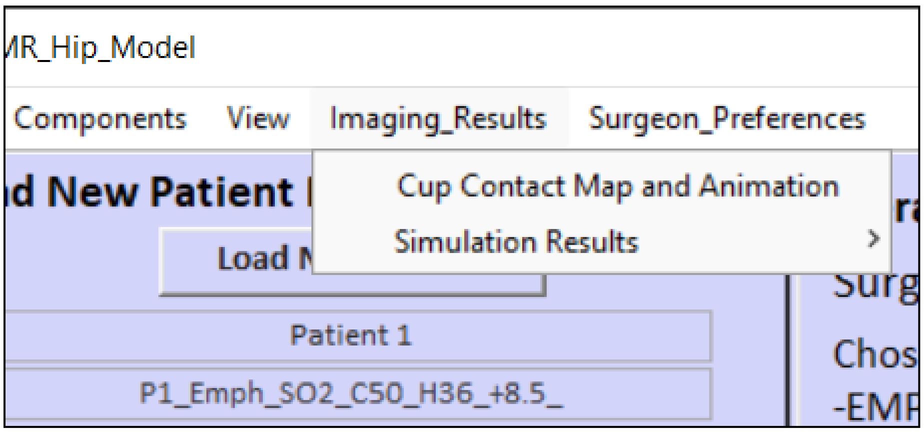

Figure 4-62: Imaging results section.

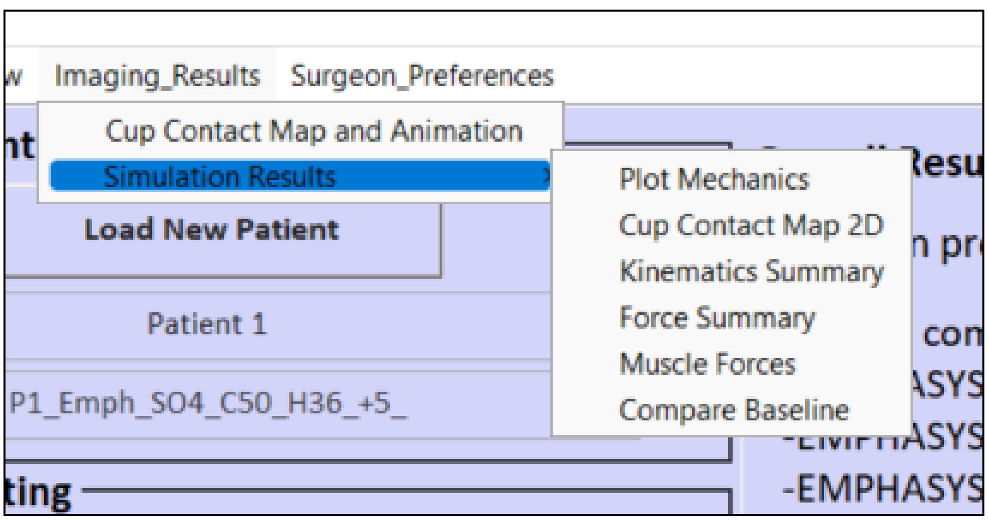

Figure 4-63: Simulation results section.

The Stem Analysis tool includes Cross Section Analysis, Slice Analysis, Contact Map Analysis, and Removal Bone Volume (Figure 4-64). The User can view Simulation Results by simply choosing the Start Simulation Analysis button, which will run the in vivo theoretical simulator. After the analysis is completed, the User can select different options such as Cup Contact Map Animation or Simulation Graph Result. Cup Contact Map Animation animates the activity of the patient. The Simulation Graph Result contains graphical results such as muscle forces, hip forces, contact stress and other parameters during stance phase of gait (Figure 4-63).

4.3.10.2. Results section

A summary of the model results is displayed in the GUI and is updated automatically (Figure 4-65). In Figure 4-65, the program is running the simulation with chair rise activity, and the result graph is displaying the hip joint reaction forces during the chair rise activity. Every time the User selects a new stem size or re-aligns a component, the information in the GUI will be updated. We will discuss the details of the "Overall Results" section below.

Chosen components information

The "Chosen components" section displays implant component information, specifically the chosen stem, cup, and liner type are being used and the sizes of each of the components. For example, in Figure 4-66, the program chose EMPHASYS standard stem size 4, EMPHASYS cup size 50 mm and EMPHASYS neutral liner size 36 mm.

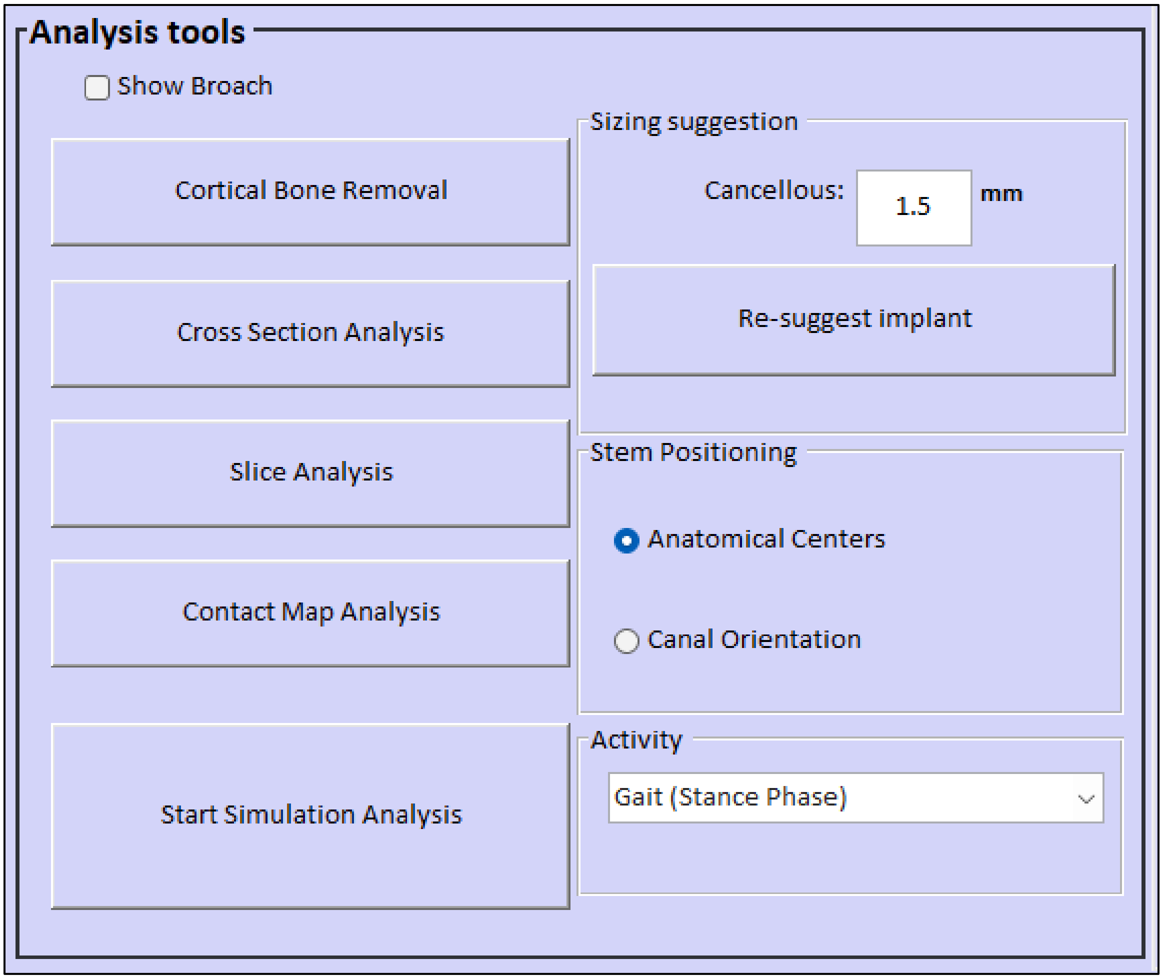

Figure 4-64: Analysis tools panel with different tools.

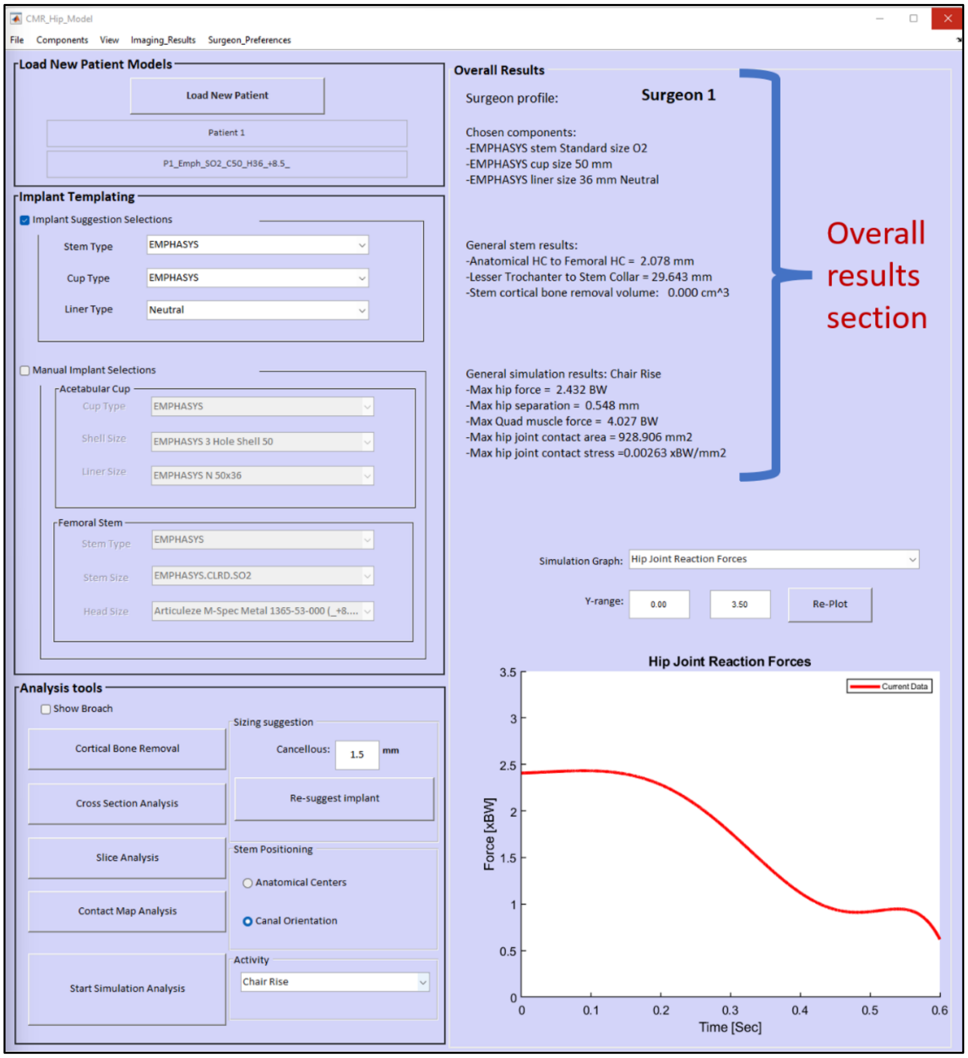

Figure 4-65: Overall Results section.

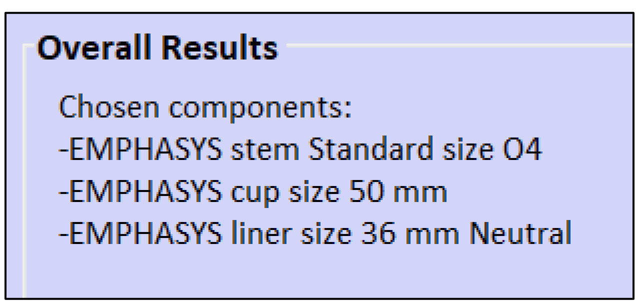

Figure 4-66: Chosen components information.

General stem fit results

The "General stem results section" reveals the alignment distances information and the cortical bone removal volume results. The distance from Anatomical Head Center (HC) to Femoral Head Center as well as the distance from Lesser Trochanter to Stem Collar are updated every time the stem or stem head is moved or reselected. For example, in Figure 4-67, Anatomical Head Center distance and Lesser Trochanter to Stem Collar distance are 1.666 mm and 27.887 mm respectively. Stem cortical bone removal volume will be updated after the "Cortical Bone Removal" button located in the Analysis Tools panel is pressed. For example, the current bone removal volume in Figure 4-67 is 0.063 cm^3.

General simulations results

After running a simulation by choosing the "Simulation Analysis" button, the simulation results section will be updated. The "General simulations results" section summarizes the simulated activity, the maximum hip force, hip separation, Quad muscle force, hip joint contact area, and hip joint contact stress (Figure 4-68). All the forces are normalized based on the subject body weight (BW), while hip separation, contact area and contact stress are in mm, mm^2 and MPa respectively.

Simulation graphs

The simulation graphs feature provides a quick access to visualization of the simulation results. There are five graphs available in this section, including Hip Joint Reaction Forces, Hip Separation, Muscle Forces, Hip Joint Contact Area, and Hip Joint

General stem results:
-Anatomical HC to Femoral HC = 1.666 mm
-Lesser Trochanter to Stem Collar = 27.887 mm
-Stem cortical bone removal volume: 0.063 cm^3

Figure 4-67: General stem results.

General simulation results: Gait (Stance Phase)
-Max hip force = 2.056 BW
-Max hip separation = 0.243 mm
-Max Quad muscle force = 1.786 BW
-Max hip joint contact area = 913.377 mm2
-Max hip joint contact stress =2.05150 MPa

Figure 4-68: General simulation results.

Contact Stress, as shown in Figure 4-69. The “Re-Plot” takes the information in the Y-limits text box and changes the range of simulation graph to the desired values (Figure 4-70).

4.3.10.3. Axes system visualization

An axis system is added to the main window to help the User track the orientation of the model. The axis is composed of three orthogonal arrows shown in red/green/blue colors with all three arrows intersect at the same origin point. The red, green, and blue arrows represent AP (anterior posterior), SI (superior inferior), and ML (medial lateral) direction respectively. For example, the red arrow in Figure 4-71 has “**N1>**” label, meaning the direction it is facing is Anterior direction. The axis system can be moved freely on the window and can be also zoomed in and out to give flexibility for the User when using the program.

4.3.10.4. Implant templating and analysis tools section

Implant templating section

The implant templating section consists of two templating options: “Implant Suggestion Selections” and “Manual Implant Selections” (Figure 4-72). The “Implant Suggestion Selections” options is where the model automatically suggests the stem size, head size, head offset, cup size and liner size depending on the types of components chosen by User. For example, if the Emphasys stem type is selected, the program will suggest the best fit Emphasys stem size for the current patient bone models. The details of the implant sizing suggestion were discussed in the section 4.3.1.

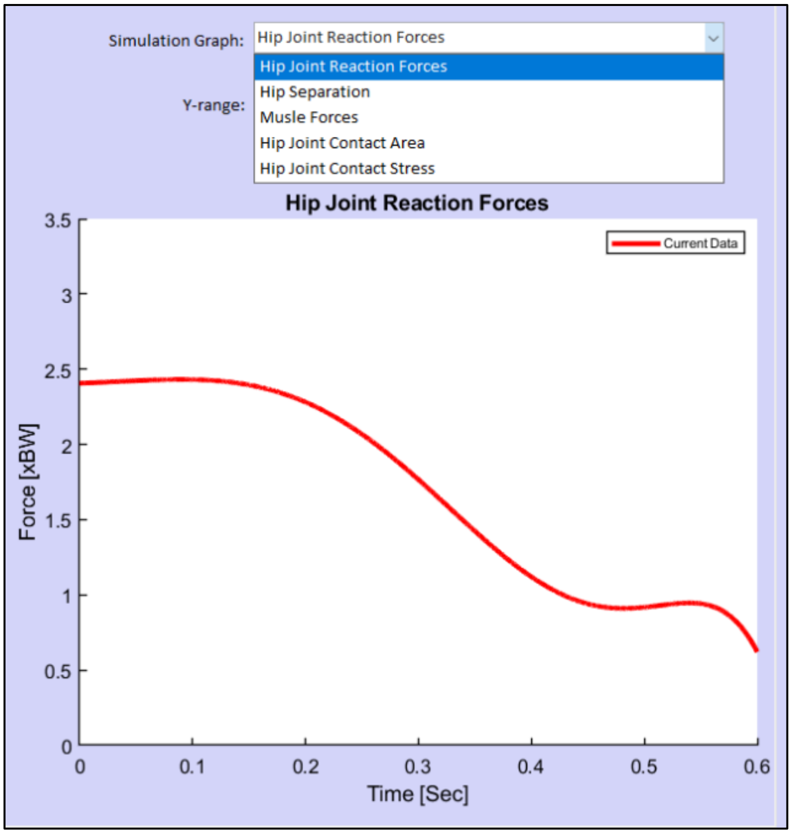

Figure 4-69: Simulation graphs.

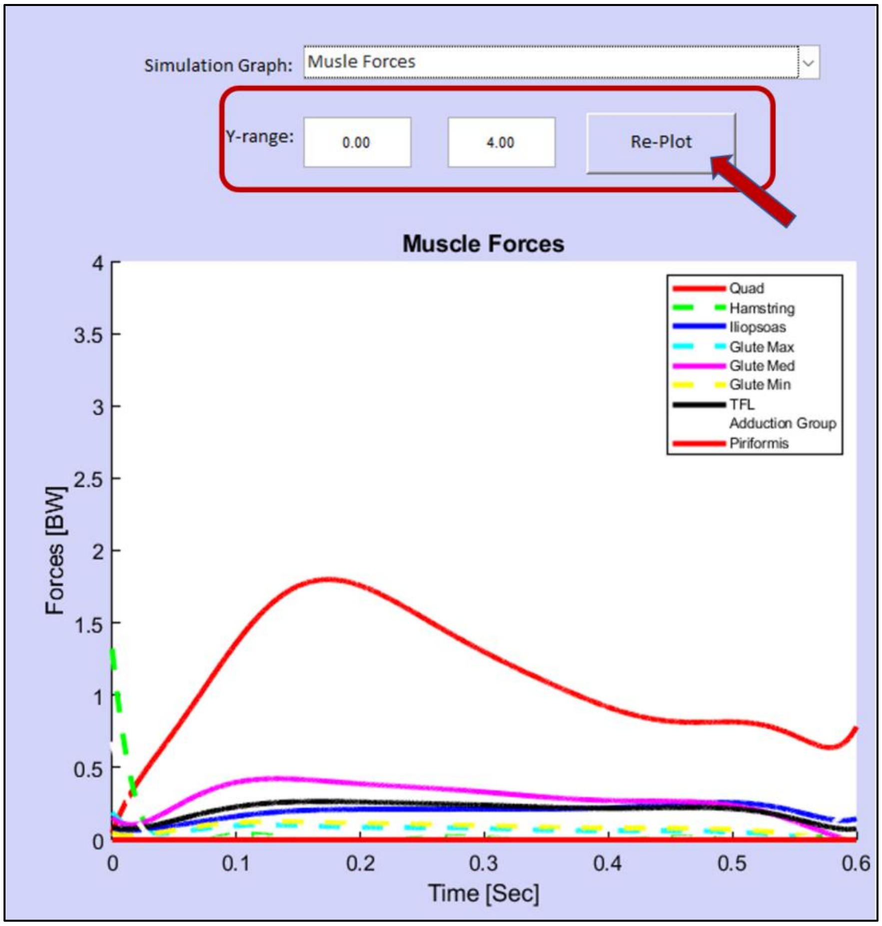

Figure 4-70: Y-range text boxes and “Re-Plot” button.

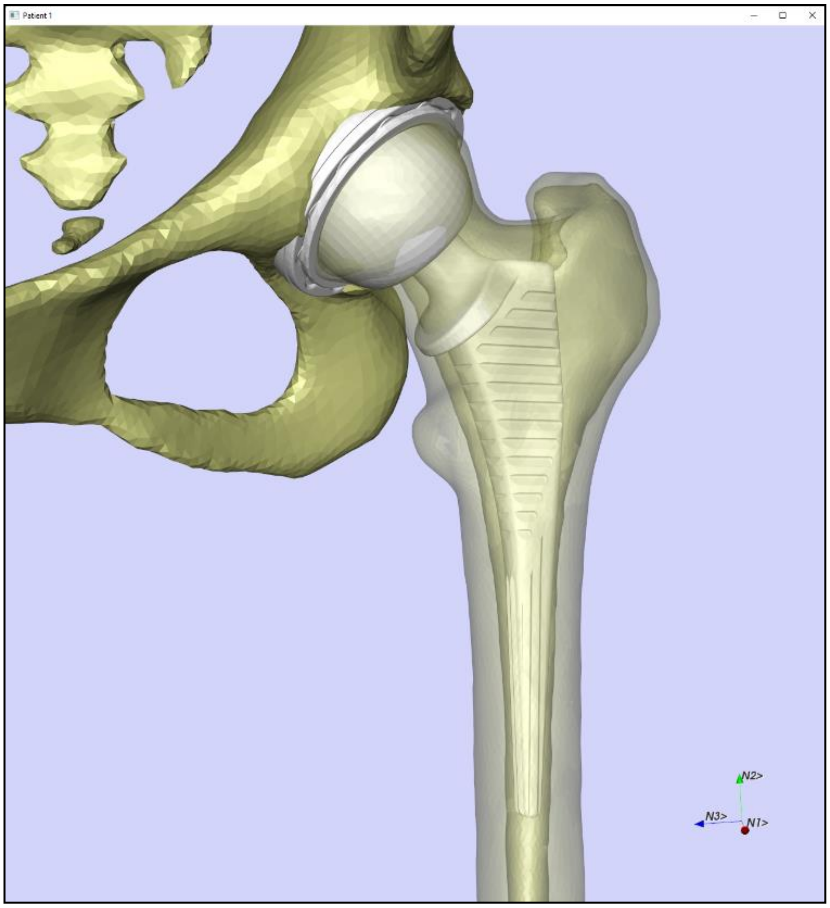

Figure 4-71: Axes system at the left right corner.

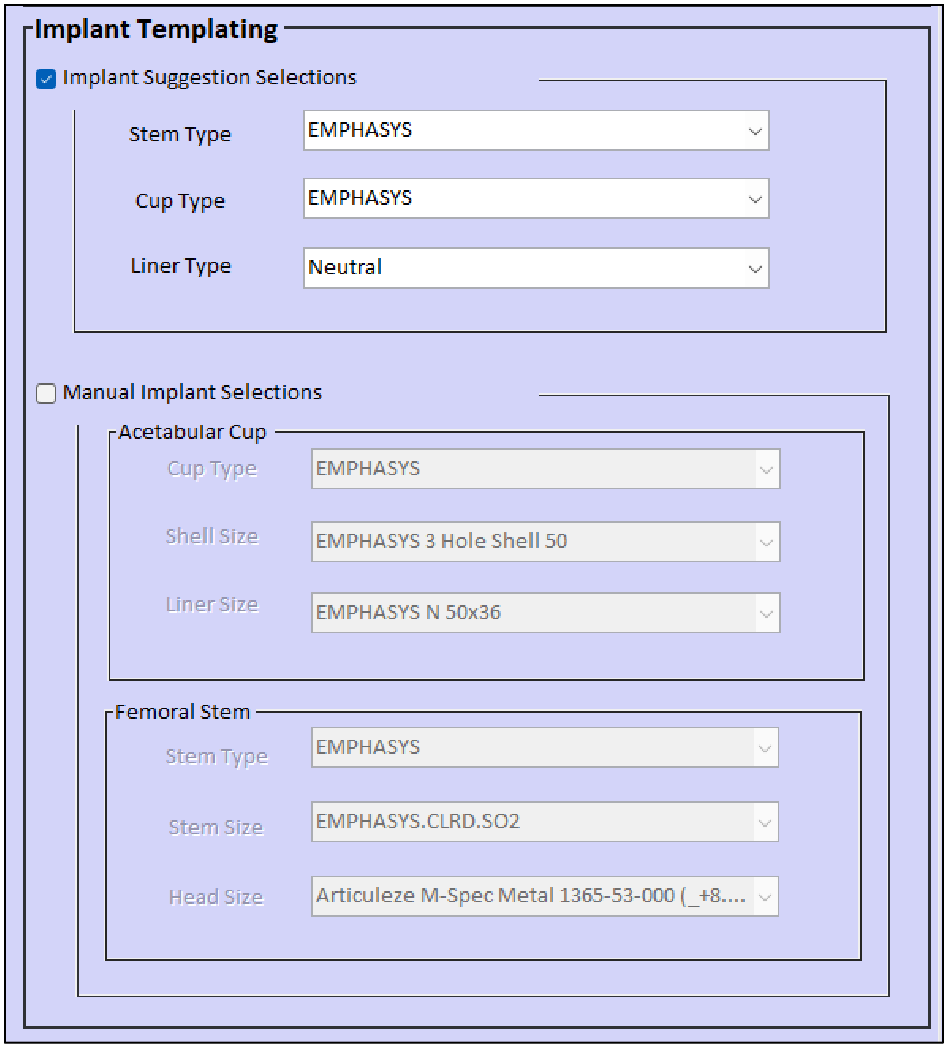

Figure 4-72: Implant templating section.

The Manual Implant Selections panel is designed to allow the User to choose implant types and sizes based on their own preferences. There is an Acetabular Cup selection and Femoral Stem selection. The Acetabular Cup selection controls cup type, shell size, and liner size. The Femoral Stem selection controls stem type, stem size, and head size. There are four stem types currently in our system: Emphasys, Corail, Tri-Lock, and Summit. These four stem types are combined with two cup options (Emphasys and Pinnacle) and three liner options (Neutral, Lipped and Dual Mobility). The combination of four stem types, two cup types and three liner types gives the model an ability to test a wide range of testing.

Analysis tools section

The analysis tools section has been developed over the past 3 years with many new tools and features added, such as cortical bone removal calculations and visualization, stem contact map analysis, implant suggestion based on cancellous mantle thickness, and changing different simulation activities (Figure 4-73). The program is also able to perform cortical bone removal calculation for both stem and broach. The simulation can simulate not only the gait activity, but it can also simulate chair rise activity. More activities such as deep knee bend or walking upstairs/downstairs are under developing process and be added to the simulation in the future.

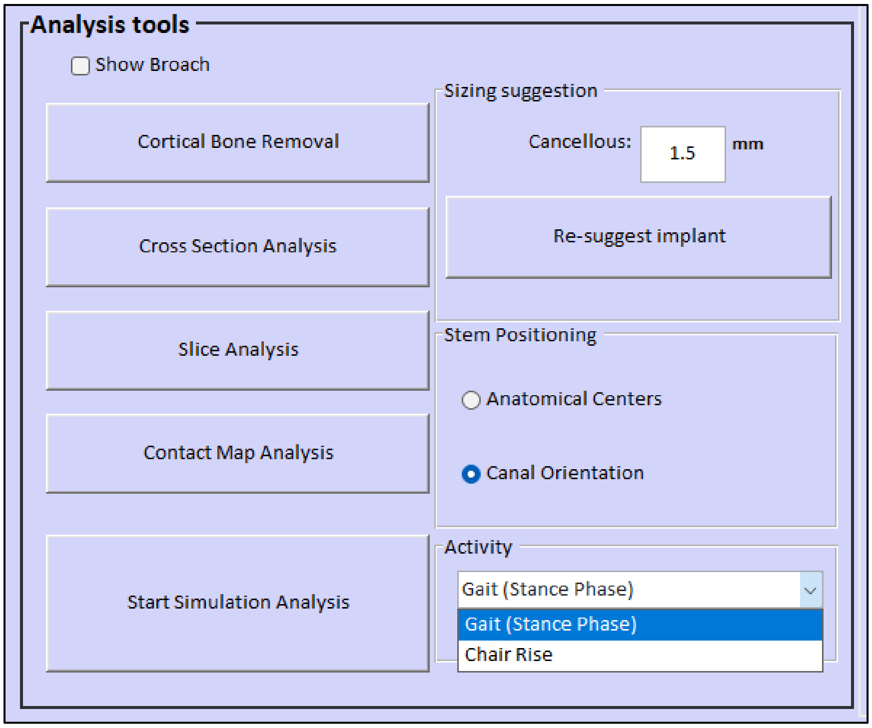

Figure 4-73: Analysis tools section.

CHAPTER 5: ASSUMPTIONS AND LIMITATIONS

5.1. Assumptions

During the process of implementation of this dissertation, there are assumptions were made. These assumptions are based on our past experience. Therefore, it is important to recognize and discuss all the assumptions in this dissertation. The assumptions are stated as follows:

1. The largest femoral head size is preferable during the liner sizing suggestion based on most of the surgeon's preferences. Previous research has often shown that larger femoral head sizes lead to more stability and a decreased risk for dislocation [67] [68], so following this logic, the implant suggestion algorithms are coded to automatically pick the largest femoral head size available. However, this does not take into consideration various surgical/clinical factors that go into this decision in the operating room, including bone quality, patient demographics, soft tissue impingement, and more. Thus, in order to test other implanted head sizes, these need to be selected manually.
2. The cancellous mantle bone layer is uniform, meaning that the thickness of the cancellous mantle layer forms a boundary that has a consistent thickness to the cortical bone border. Therefore, the implant positioning algorithm will only need to subtract the cancellous mantle thickness value during the process of mesh – mesh contact detection algorithm. The uniform cancellous mantle thickness is also used in the implant sizing suggestion.

3. Similarly, the cancellous mantle does not "compress" when a stem is inserted. Due to these 2 assumptions, bone removal volumes or implant fixation predictions based on the uniformity of fit within the canal are subject to differences compared to what may be observed postoperatively.
4. The resulting mesh after the restructuring input meshes process in the implant positioning algorithm is refined accurately so that the differences between the triangle sizes are negligible. The quality of the resulted mesh affects the accuracy of the implant positioning algorithm.
5. The femoral bone models from our database already have consistent triangle sizes. The consistent triangle sizes in the meshes are important for many algorithms in our program, such as mesh – mesh contact map calculation, mesh – mesh Boolean operations, center of mass calculation. Since all the meshes were processed, any remaining small differences between triangle sizes are negligible.
6. The stem has a uniform density. The density of the stem affects the accuracy of the center of mass calculation. Thus, we assume that the density of the stem is uniform to not over complicate the algorithm.
7. The moment of inertia of the stem body in the implant positioning algorithm can be chosen carefully by the developer and does not require to be calculated explicitly.

5.2. Limitations

During the process of implementation of this dissertation, there are limitations were made. These limitations are stated as follows:

1. The implant sizing suggestion algorithms do not include friction forces in the dynamic model, especially the static friction force. This yields limitations with regard to implant fixation predictions. In general, modeling the friction forces in the hip implants can be difficult since the surgeon can use variety of methods to fix the implant surface to the bone, including using cemented hip replacement, or coating the implant with calcium phosphate in the cementless hip prostheses.
2. The mesh – mesh contact calculation is time consuming. Even though the mesh – mesh contact calculation provides very accurate presentation of the distance map, sometime this lever of precision is not necessary. An alternative way to calculate contact map is Ray Tracing algorithm.
3. The mesh – mesh Boolean operations are time consuming and, in some cases, cannot provide accurate results because of improper mesh input. More refine meshes with closed and consistent triangles sizes could help reduce this limitation.
4. The process of adding new component types and sizes require going to MATLAB to change the source code.
5. Using MATLAB for computationally intensive tasks is generally slower than using other programing languages such as C++ or C#. Because MALTB is an interpreted language, it requires more time to execute instructions than complied languages like C++, which can result in slower performance.
6. Adding new patient specific subject to the simulation database is time consuming and still requires manual works from Users to make sure the patient specific data is accurate.

7. Currently, the program automatically fits the liner center to the acetabulum center. Therefore, this does not automatically take into consideration the effects of increased liner offsets, such as soft tissue changes or bone reaming differences that may be due to differences between the cup center and the articulating liner center.
8. Similarly, the algorithm defaults to a properly-oriented cup of 40º inclination and 15º anteversion, based on the Lewinnek safe zone [69]. This does not allow for automated patient-specific cup orientation and coverage calculations. While the cup can be reoriented manually, there is a need to have an algorithm to automatically suggest the orientation of the cup in the acetabulum.
9. When a new cup size is added to the model, the Users need to use the previous version of hip model to export the cup polynomial. The cup polynomial is needed to calculate the contact force during the simulation.
10. The implant positioning algorithm is sensitive to the changes in damping parameters. Therefore, improper damping parameters can cause the algorithm to halt prematurely before the stem can reach the canal fit position.
11. The subject in our database mostly do not have a full femur bone model. That limits the accuracy of implant positioning algorithm since the algorithm can only calculate and analyze the shape of the femoral canal in the proximal portion of the femur. To overcome this, previous distal bone models are mated to the proximal portions, which allow us access to mechanical axes of the knee when needed, but these axes are not always patient-specific.
12. The result of the implant positioning algorithm is one of many possible canal fit positions of the stem within the canal. The position of the stem within the canal not

only depends on the shape of the femoral canal, but it also depends on the surgeon factors, such as how hard the stem is pushed into the cancellous mantle. Thus, the algorithm suggests the canal fit position that is the closest to the anatomical fit position by starting at the anatomical fit position.

CHAPTER 6: RESULTS AND DISCUSSION

From all the above chapters, this dissertation has presented a hip analysis software package that allows Users to analyze a variety of interoperative and postoperative conditions, providing suggestions for component sizes and positions based on surgeon preferences, patient-specific anatomy, stability calculations, and more. The focus of this dissertation is on the development of an effective software tool for analyzing the hip joint, with potential applications for future research. Two analyses utilizing the software were conducted and will be discussed in the following sections. The first analysis involves comparing canal fit and anatomical fit positions using a standard subject from the database, while the second explores the impact of different surgeon preferences on the outcome of total hip arthroplasty, theoretically modeled using the software.

6.1. Canal fit and anatomical fit: A standard subject comparison results

This analysis was conducted on one standard subject from our patient-specific database. For this comparison, the stem was aligned using two previously-discussed alignment scenarios – anatomical fit and canal fit alignments. The anatomical fit position is where the stem shaft axis is aligned with the femoral canal shaft axis, and the stem head center is aligned with the plane formed by femoral shaft axis and femoral neck axis. The canal fit position is the result from the forward dynamics, surgical simulation portion of the implant positioning algorithm. We then used the theoretical, postoperative hip mechanics analysis tools to conduct an in-depth analysis using simulation of stance phase of gait to determine the effects of each alignment methods. For all scenarios under investigation, the specific parameters of interest include the stem cortical bone removal, the distance from the stem head center to the femoral head center, the stem contact map analysis with the cortical bone including the contact area in different threshold distances, hip separation, hip force, cup contact area, cup contact stress, and muscles forces.

6.1.1. Stem cortical bone removal and contact map analysis with the femoral canal

From the analysis results, the distance between the center of the implanted head and the center of the anatomical femoral head is lower in the anatomical fit position than in the canal fit position. Specifically, the anatomical fit successfully reduces the distance between anatomical femoral head center and implanted head center by nearly 3 mm, from 5.10 mm to 2.16 mm, occurring predominantly in the anterior/posterior and medial/lateral directions. Precisely, the distance of the head in the medial/lateral component direction reduces from 3.39 mm to 0.76 mm, and the distance in the anterior/posterior direction reduces from 3.80 mm to 0.60 mm, when the stem is in the anatomical fit position, as compared to the canal fit position (Figure 6-1). In addition, the distance from the lesser trochanter to the collar of the stem is also lower in the anatomical fit position compared to the canal fit position, with a distance of 23.647 mm and 26.734 mm, respectively. However, it is worth noting that the anatomical fit position requires the removal of more cortical bone, with 0.233 cm^2 of bone removal, while the canal fit position requires no bone removal (Figure 6-1). Having less cortical bone removal could help reduce the risk of bone fracture after the THA surgery, especially in the more elderly patients.

In both alignment scenarios, the contact maps between the stem and the femoral canal for both the anatomical fit and the canal fit demonstrate a similar pattern, with the

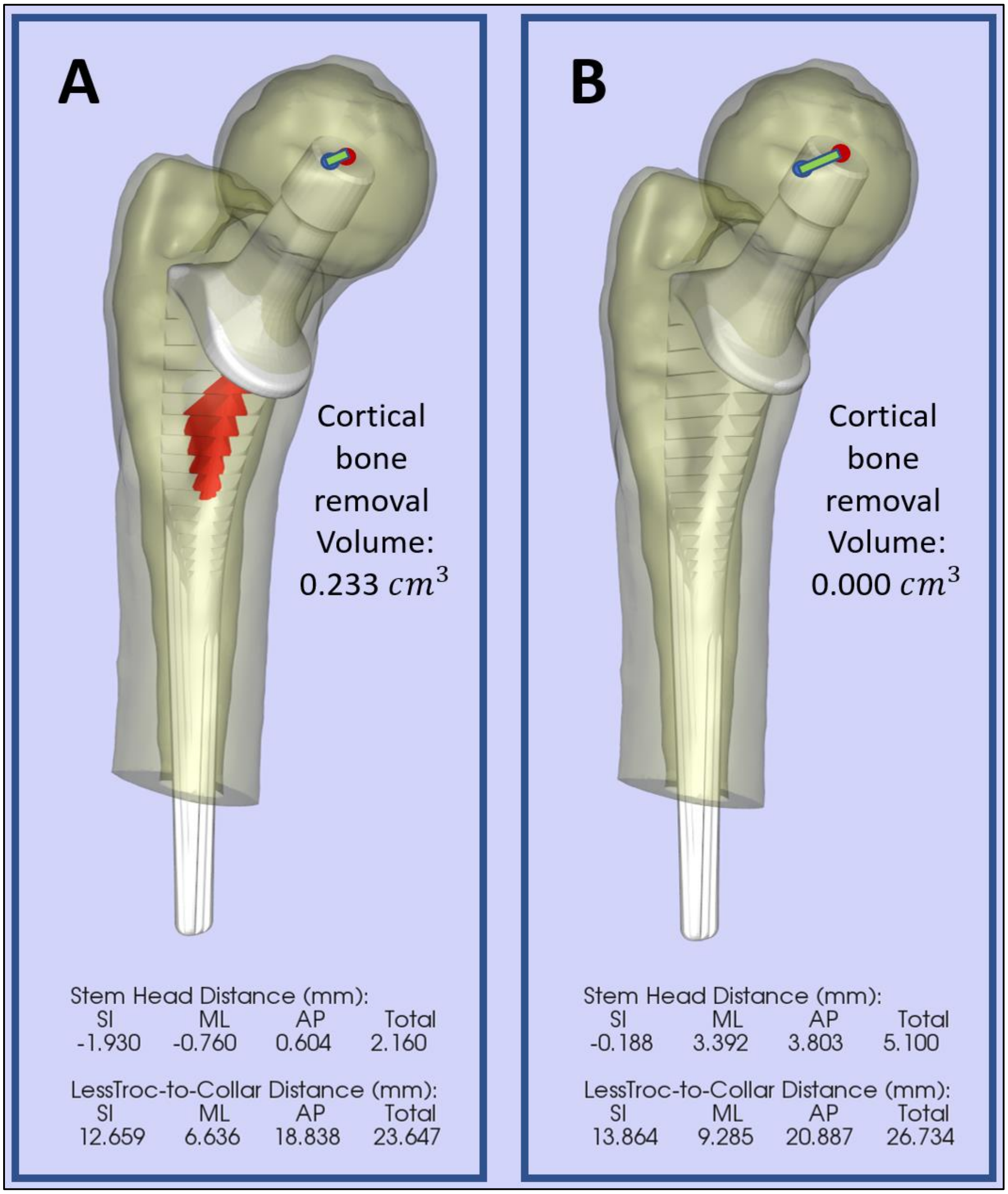

Figure 6-1: Distance between stem head center and anatomical femoral head center, and bone removal volume: (A) Anatomical fit alignment, (B) Canal fit alignment.

majority of the contact occurring on the medial and lateral sides of the stem, as illustrated in Figure 6-2 and Figure 6-3. Specifically, the contact between the stem and compressed cancellous mantle occurs primarily on the medial and lateral faces of the stem. In the anatomical fit position, more than 60% of the total contact area occurs on the medial and lateral sides within the 2 mm cancellous mantle thickness threshold (Figure 6-2). Similarly, in the canal fit position and within the 2 mm cancellous mantle thickness threshold, the total contact area on the medial and lateral sides is 785.49 mm^2, representing 64.7% of the total stem contact area (1214.13 mm^2) (Figure 6-3). However, the canal fit position shows zero contact area within the 0 mm threshold, corresponding to the bone removal results in Figure 6-1. In general, the canal fit contact map displays a more uniform contact pattern, while the anatomical fit contact map is more concentrated. A contact map that exhibits greater uniformity has the potential to enhance the stability of the stem within the canal, potentially minimizing the risk of bone fracture, as the stem applies a more symmetrical force to the cortical bone in all directions.

6.1.2. Anatomical fit and canal fit simulation results

During the stance phase of gait, hip forces can have a significant impact on implant wear and patient outcomes. In this study, we examined the effects of two different femoral stem positions, the anatomical fit and the canal fit, on hip forces, contact stress, and muscle forces using the hip analysis software. Our simulations showed that the canal fit position resulted in higher hip forces compared to the anatomical fit position. Specifically, the average hip force throughout the entire stance phase of gait for anatomical fit scenario was 3.06 times body weight (xBW), while the average hip force during the stance phase of gait

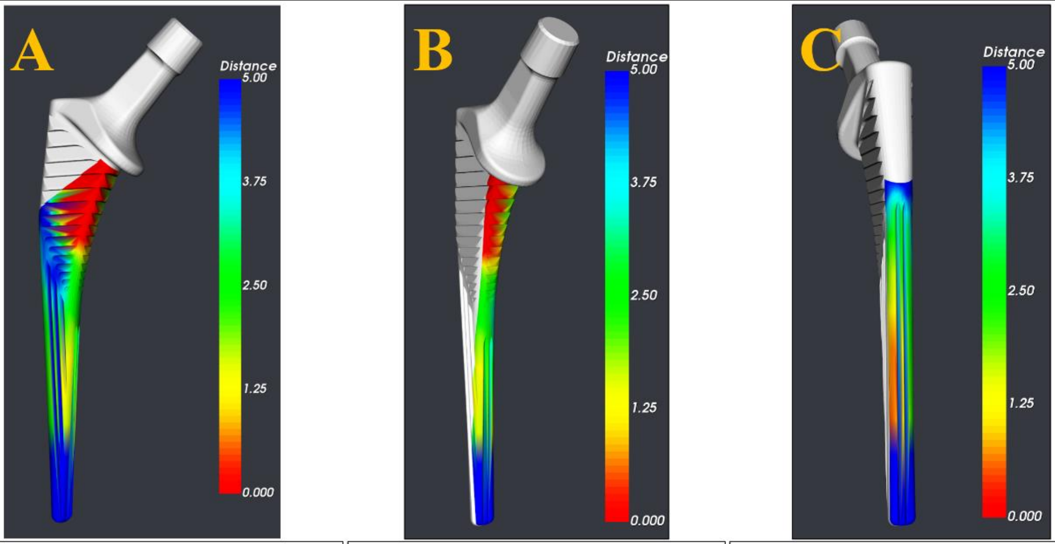

Threshold	Stem Area	Contact Area	Contact Percentage
< 0.0	4204.53	0243.22	05.78%
< 1.0	4204.53	0506.79	12.05%
< 2.0	4204.53	1256.03	29.87%
< 3.0	4204.53	2369.02	56.34%
< 4.0	4204.53	2860.29	68.03%
< 5.0	4204.53	3347.26	79.61%

Threshold	Stem Area	Contact Area	Contact Percentage
< 0.0	1256.28	0091.71	07.30%
< 1.0	1256.28	0191.77	15.27%
< 2.0	1256.28	0512.24	40.77%
< 3.0	1256.28	0887.91	70.68%
< 4.0	1256.28	0976.23	77.71%
< 5.0	1256.28	0998.46	79.48%

Threshold	Stem Area	Contact Area	Contact Percentage
< 0.0	0957.29	0000.00	00.00%
< 1.0	0957.29	0104.79	10.95%
< 2.0	0957.29	0255.98	26.74%
< 3.0	0957.29	0574.74	60.04%
< 4.0	0957.29	0665.98	69.57%
< 5.0	0957.29	0737.02	76.99%

Figure 6-2: Anatomical fit: Stem contact map with femoral canal - (A) Full stem, (B) Medial side, (C) Lateral side.

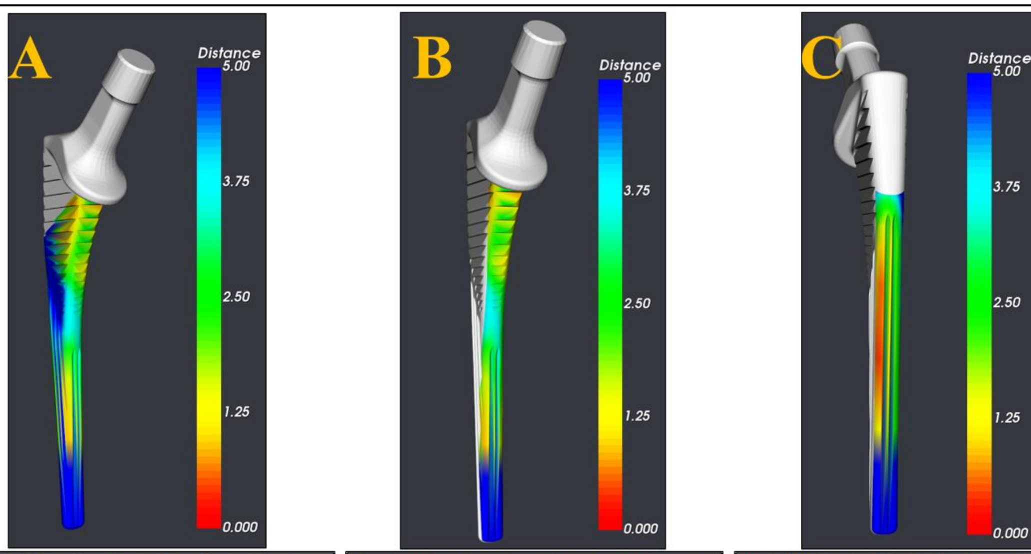

Threshold	Stem Area	Contact Area	Contact Percentage
< 0.0	4204.53	0000.00	00.00%
< 1.0	4204.53	0208.26	04.95%
< 2.0	4204.53	1214.13	28.88%
< 3.0	4204.53	2416.33	57.47%
< 4.0	4204.53	3032.14	72.12%
< 5.0	4204.53	3280.51	78.02%

Threshold	Stem Area	Contact Area	Contact Percentage
< 0.0	1256.28	0000.00	00.00%
< 1.0	1256.28	0048.98	03.90%
< 2.0	1256.28	0444.28	35.36%
< 3.0	1256.28	0746.85	59.45%
< 4.0	1256.28	0956.59	76.14%
< 5.0	1256.28	1002.80	79.82%

Threshold	Stem Area	Contact Area	Contact Percentage
< 0.0	0957.29	0000.00	00.00%
< 1.0	0957.29	0128.98	13.47%
< 2.0	0957.29	0341.21	35.64%
< 3.0	0957.29	0643.24	67.19%
< 4.0	0957.29	0718.82	75.09%
< 5.0	0957.29	0755.97	78.97%

Figure 6-3: Canal fit: Stem contact map with femoral canal - (A) Full stem, (B) Medial side, (C) Lateral side.

for the canal fit scenario was 3.51 xBW. Similarly, the maximum hip force at any single moment during stance phase was 3.41 xBW for the anatomical fit scenario and 4.30 xBW for the canal fit scenario (Table 1). In addition to resulting in lower hip force, the anatomical fit also led to lower hip separation. The simulation results indicated that the average hip separation in the canal fit position was nearly three times higher than the corresponding value in the anatomical fit position. Specifically, the maximum hip separation in the anatomical fit position was 0.2319 mm, while in the canal fit position, the value was 0.5378 mm and 0.6041 mm (Table 1 and Figure 6-4). These findings suggest that the canal fit, while possibly yielding better fixation within the canal, may also lead to more edge loading on the liner than anatomical fit. Thus, from a mechanics perspective, the anatomical fit may be associated with a more stable hip joint and reduced wear between bearing surfaces, as higher hip separation is known to increase the risk of edge loading and other complications in THA.

We also found that the average contact stress was reduced by 8.5% when the stem was aligned in the anatomical fit position compared to the canal fit position, reducing the average stresses from 9.3 MPa using canal fit to 8.5 MPa using anatomic fit (Figure 6-5). This result suggests that the anatomical fit position may distribute loads more evenly across the implant. The anatomical fit position also reduced muscle forces for all three muscles tested (Iliopsoas, Gluteus Medius, and Tensor Fasciae Latae muscle). Specifically, the Iliopsoas, Gluteus Medius, and Tensor Fasciae Latae muscle forces were 17.7%, 18.8%, and 16.7% lower, respectively, in the anatomical fit position compared to the canal fit position (Table 1 and Figure 6-6). It is very interesting to see that having the stem in the

Table 1: Simulation results of Anatomical fit and Canal fit with sample standard subject.

		Anatomical fit	Canal fit
Hip Separation (mm)	**Average**	0.18	0.54
	Max	0.23	0.60
Hip Force (xBW)	**Average**	3.06	3.51
	Max	3.41	4.30
Contact Area (mm^2)	**Average**	313.33	331.89
	Max	333.44	359.21
Contact Stress (MPa)	**Average**	8.48	9.28
	Max	9.49	11.13
Iliopsoas muscle force (xBW)	**Average**	0.62	0.76
	Max	0.72	0.91
Gluteus Medius muscle force (xBW)	**Average**	0.68	0.84
	Max	0.85	1.17
Tensor Fasciae Latae muscle force (xBW)	**Average**	0.46	0.55
	Max	0.50	0.65

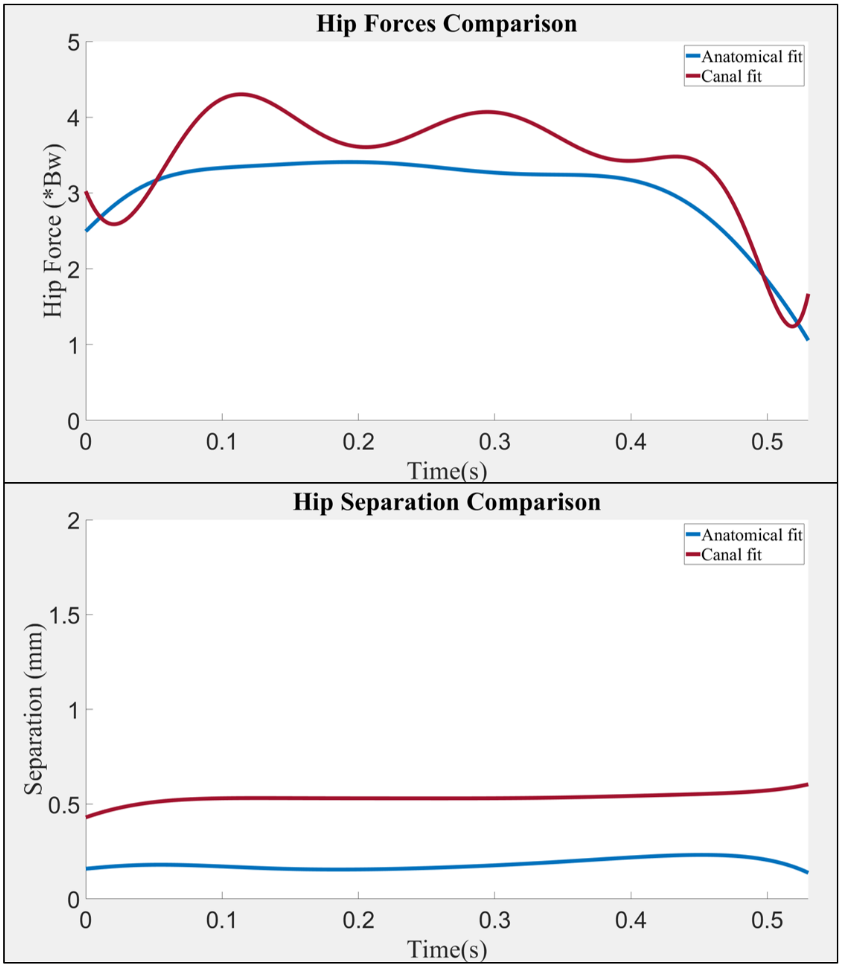

Figure 6-4: Hip joint reaction force and hip separation – Simulation results of Anatomical fit (blue) and Canal fit (red).

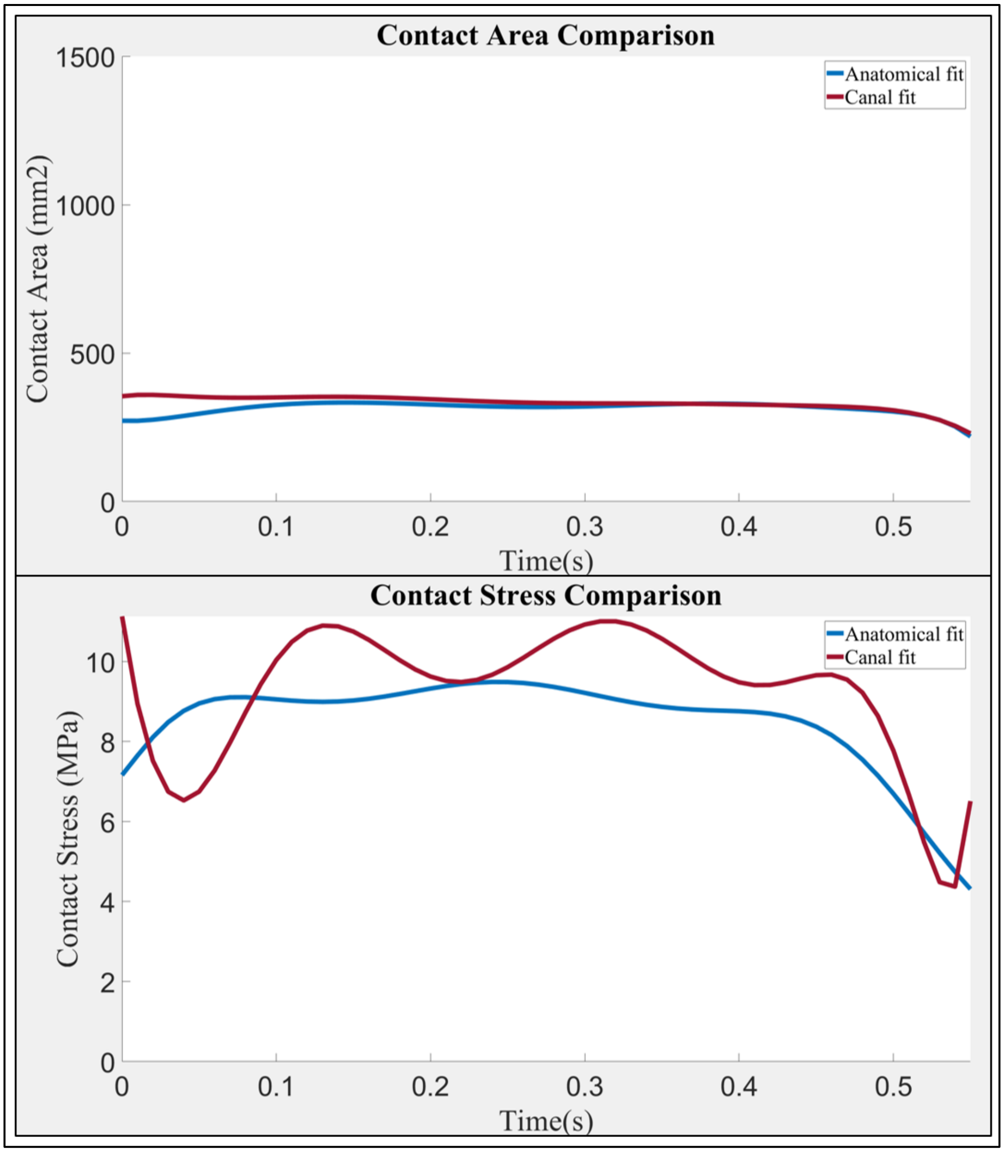

Figure 6-5: Hip joint contact area and contact stress – Simulation results of Anatomical fit (blue) and Canal fit (red).

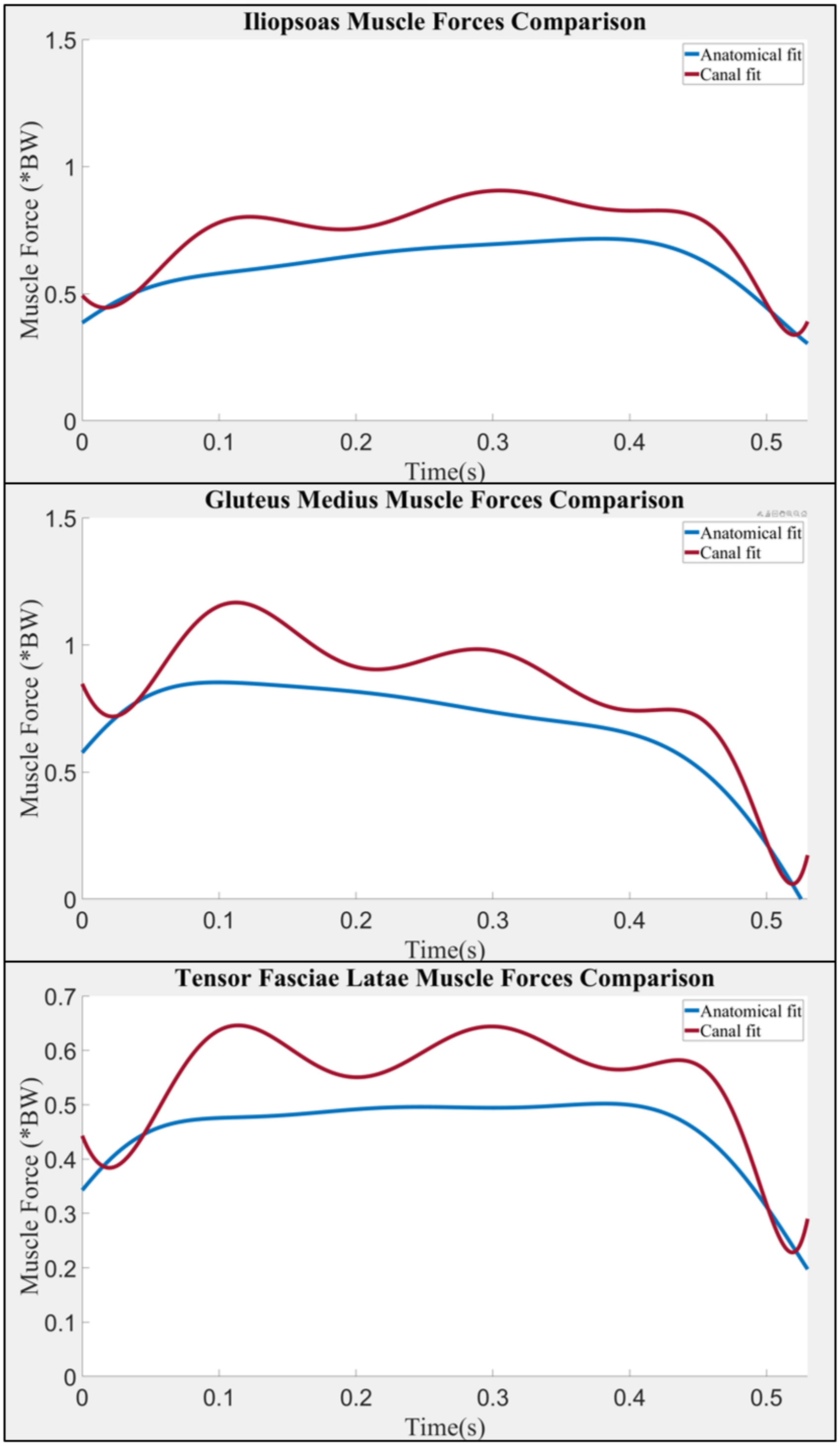

Figure 6-6: Iliopsoas, Gluteus Medius, and Tensor Faciae Latae muscle forces – Simulation results of Anatomical fit (blue) and Canal fit (red).

anatomical fit can simultaneously lower muscle forces in all three muscles. These results imply that the anatomical fit position of the stem may be associated with improved kinematic outcomes for total hip arthroplasty (THA) patients, resulting in decreased muscle forces and potentially mitigating hip muscle pain.

Importantly, our model also predicted that the canal fit position resulted in edge loading, while the anatomical fit position did not (Figure 6-7 and Figure 6-4). Edge loading can cause increased contact stress and wear on the implant, leading to a shorter implant lifespan and potentially increased risk of revision surgery. Overall, our results suggest that although the anatomical fit position requires bone removal, it may be preferable over the canal fit position for reducing hip forces and contact stress and improving muscle forces, which could ultimately improve implant longevity and patient outcomes. Although anatomical fit alignment may produce better postoperative mechanics of the hip joint, this study on one standard subject also shows that the anatomical fit alignment position might not always be feasible for surgeon, as the anatomical fit alignment position also requires more bone removal and canal preparation.

Perhaps, the “best” clinically relevant goal is to find a common middle ground between getting as close as possible to the anatomical fit while also minimizing excess canal preparation. In order to further investigate the effect of different stem alignments method (canal fit and anatomical fit alignments), the next study in the following section will be conducted on the larger set of subjects with different surgeon preferences along with different stem alignment techniques.

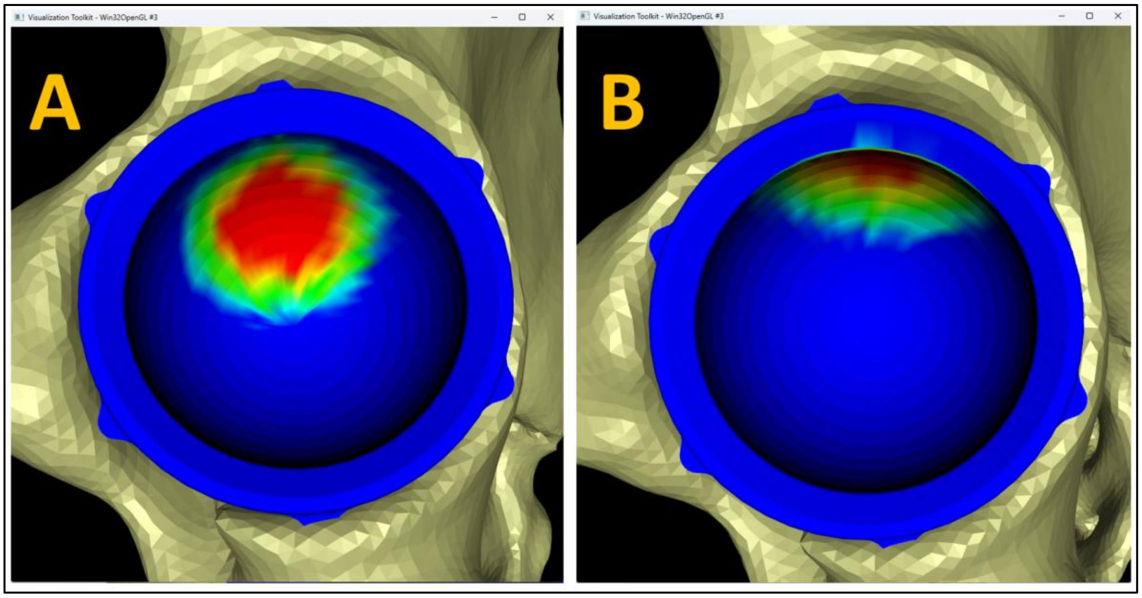

Figure 6-7: 3D cup contact map results: (A) Anatomical fit, (B) Canal fit. The images clearly show the edge loading in canal fit while anatomical fit does not have edge loading.

6.2. Canal fit and anatomical fit: Surgeon preferences evaluation results

Across the globe, surgeons have a variety of preferences with regards to surgical techniques, including component offsets, medializations, sizes, version control, and more [70]. This can result in a large array of outcomes for different patients implanted with the same implant system. To ensure that this population variability is adequately represented in the analysis presented in this dissertation, a cohort of eight subjects was selected from our patient-specific database based on distinct differences in bone shape, size, articulation, and muscle structures that are known to impact bone-to-bone articulation variation and kinematic profiles during walking (see Figure 6-8). The hip analysis software was used to conduct an analysis of all eight subjects under different stem alignment methods, including the anatomical fit and canal fit alignments, as well as other surgical technique preferences derived from four different surgeons (Table 2). Specifically, the analysis combined different alignment methods with two femoral head size preferences used in total hip arthroplasty (THA), specifically the smallest and largest head size preferences. The previous study on the standard subject shows the advantages and disadvantages of each stem alignment methods. The following study will further investigate the effect of canal fit and anatomical fit alignment positions on the outcome of THAs. The use of multiple subjects with varying bone structures and alignment methods provides a more comprehensive understanding of the effects of THA on hip mechanics and muscle forces. The results of this study will provide insight into the effects of different alignment methods and femoral head size preferences on hip joint mechanics and muscle forces.

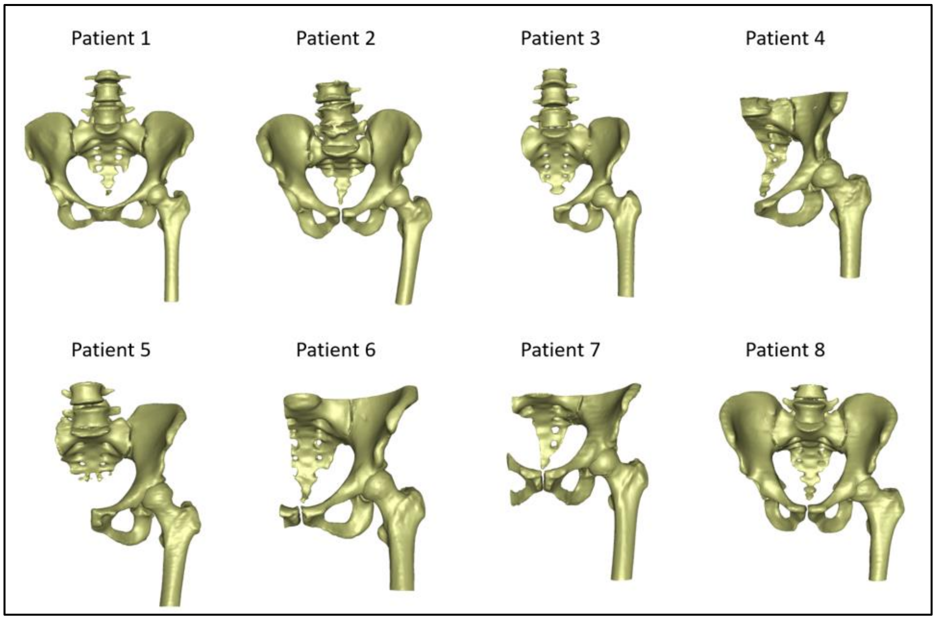

Figure 6-8: Eight bone models from our patient specific database.

Table 2: Four surgeon preferences profiles.

Surgeon profile	Stem type	Stem position	Cancellou s mantle (mm)	Cup type	Liner type	Head size
Surgeon 1	Emphasys	Anatomical fit	1.5	Emphasys	Neutral	Largest possible
Surgeon 2	Emphasys	Anatomical fit	1.5	Emphasys	Neutral	Smallest possible
Surgeon 3	Emphasys	Canal fit	1.5	Emphasys	Neutral	Largest possible
Surgeon 4	Emphasys	Canal fit	1.5	Emphasys	Neutral	Smallest possible

All four surgeon profiles utilized the same components from the novel EMPHASYS THA system, including the stem, femoral head, cup, and a neural liner, while maintaining a 1.5 mm cancellous mantle between the femoral stem and the cortical bone. The variations between the four surgeon profiles are as follows:

1. Surgeon 1: Anatomical fit with largest possible head size.
2. Surgeon 2: Anatomical fit with smallest possible head size.
3. Surgeon 3: Canal fit with largest possible head size.
4. Surgeon 4: Canal fit with smallest possible head size.

Femoral head size information for the eight subjects, ranging from 36 mm to 40 mm for the first two surgeon profiles and 28 mm to 32 mm for the other two surgeon profiles are defined in Table 3. In summary, surgeon 1 and surgeon 2 belong to a group of anatomical fit alignment preference, while surgeon 3 and surgeon 4 belong to a group of canal fit alignment preference.

6.2.1. Analysis database and parameters of interest

A summary of the results from this study, obtained from analyzing seven parameters for eight subjects during the stance phase of gait activity, with all four surgeon profiles is presented in Table 4. The parameters assessed were hip separation (measured in mm), bearing surface hip force (measured in proportional to the subject's body weight (BW)), bearing surface contact area (measured in mm^2), bearing surface contact stress (measured in MPa), and the muscle forces for the major muscles, Iliopsoas, Gluteus Medius, and Tensor Fasciae Latae (measured in xBW). For each of these parameters, two

Table 3: Stem head sizes information of 8 subjects.

Patient	Surgeon 1 & 3 (mm)	Surgeon 2 & 4 (mm)
1	36	28
2	40	28
3	36	28
4	40	28
5	40	28
6	36	28
7	40	28
8	40	32

Table 4: Simulation results of 4 surgeon preferences profiles for 8 subjects.

N = 8 subjects			Surgeon 1	Surgeon 2	Surgeon 3	Surgeon 4
Hip Separation (mm)	**Average**	Mean	0.502	0.539	0.556	0.601
		Std.Dev	0.062	0.047	0.102	0.082
	Max	Mean	0.560	0.595	0.609	0.657
		Std.Dev	0.066	0.055	0.107	0.088
Hip Force (*BW)	**Average**	Mean	2.752	2.758	2.906	2.837
		Std.Dev	0.522	0.518	0.660	0.580
	Max	Mean	3.084	3.093	3.302	3.199
		Std.Dev	0.569	0.554	0.772	0.652
Contact Area (mm^2)	**Average**	Mean	845.107	450.438	820.645	435.872
		Std.Dev	82.587	65.281	91.795	61.521
	Max	Mean	901.130	486.442	899.117	467.670
		Std.Dev	78.159	55.281	140.213	54.113
Contact Stress (MPa)	**Average**	Mean	2.840	5.372	3.101	5.756
		Std.Dev	0.403	0.745	0.636	1.261
	Max	Mean	3.278	5.991	3.560	6.483
		Std.Dev	0.508	0.845	0.648	1.456
Iliopsoas muscle force (*BW)	**Average**	Mean	0.555	0.555	0.604	0.588
		Std.Dev	0.242	0.239	0.279	0.263
	Max	Mean	0.696	0.696	0.760	0.738
		Std.Dev	0.317	0.313	0.365	0.346
Gluteus Medius muscle force (*BW)	**Average**	Mean	0.598	0.601	0.652	0.624
		Std.Dev	0.137	0.137	0.185	0.152
	Max	Mean	0.753	0.760	0.838	0.785
		Std.Dev	0.152	0.159	0.239	0.178
Tensor Fasciae Latae muscle force (*BW)	**Average**	Mean	0.310	0.310	0.336	0.327
		Std.Dev	0.095	0.093	0.127	0.110
	Max	Mean	0.352	0.352	0.389	0.376
		Std.Dev	0.101	0.098	0.143	0.121

specific values were analyzed: the average value, which is the average value of the parameter during the entire activity, and the maximum value, which is the maximum value of the parameter at any moment during the entire activity. Mean and standard deviation values are obtained for both average and maximum values from the data set of n = 8 subjects.

Hip separation was the measured distance between the stem head center and the acetabular cup center. These centers moved with respect to each other, hip separation was documented to have occurred. The hip force parameter represented the contact bearing force between the femoral head and the acetabular cup insert, measured in proportional to the subject's body weight. Contact area was calculated using a contact detection algorithm based on the position of the femoral head with respect to the acetabular cup liner and subsequently, the contact stress was derived by dividing the hip force by the contact area. The iliacus and psoas major muscles combine to form the Iliopsoas muscle, which represents the greatest influence for hip flexion. It originates from the lumbar vertebrae and inserts on the femur. The Gluteus Medius muscle is a hip abductor muscle that is located in the lateral hip region. It originates from the ilium and inserts on the greater trochanter of the femur. The Tensor Fasciae Latae (TFL) muscle is also a hip abductor muscle that originates from the iliac crest and inserts on the lateral tibial condyle via the iliotibial tract. Together, these muscles play important roles in hip movement and stability during various activities such as walking, running, and standing. The results of each parameter will be presented and discussed separately. Furthermore, to aid in comprehension, breakout tables displaying the results of each parameter will be included for ease of reference.

6.2.2. Hip Separation

The mean of average hip separation during stance phase of gait ranges from 0.50 mm to 0.60 mm. The combination of anatomical fit with the largest liner size exhibited the lowest mean value of average and maximum hip separation, with an average value of $0.50 \pm 0.06\ (mm)$ and a maximum value of $0.56 \pm 0.07\ (mm)$. In contrast, the combination of canal fit with the smallest liner size demonstrated the highest hip separation values, where the average and maximum hip separation was $0.60 \pm 0.08\ (mm)$ and $0.66 \pm 0.09\ (mm)$, respectively (Table 5). The results revealed that using the anatomical fit alignment position pertained to a 11% to 12% reduction in the average hip separation value compared to the canal fit alignment position (as seen in Table 5). The average hip separation profiles of the anatomical fit alignment position are consistently below the average hip separation profiles of the canal fit alignment position (as seen in Figure 6-9and Figure 6-10).

Overall, the order of surgeon profile with the average hip separation result from low to high is surgeon 1 ($0.50\ mm$), surgeon 2 ($0.54\ mm$), surgeon 3 ($0.56\ mm$), and lastly surgeon 4 ($0.60\ mm$). These results suggest that the surgical techniques and implant sizes can impact hip separation during the stance phase of gait, with the femoral stem fit using the anatomical fit approach using the larger stem head size associated with lower hip

Table 5: Hip separation results for 8 subjects.

N = 8 subjects			Anatomical fit		Canal fit	
			Surgeon 1	**Surgeon 2**	**Surgeon 3**	**Surgeon 4**
Hip Separation (mm)	**Average**	Mean	0.50	0.54	0.56	0.60
		Std.Dev	0.06	0.05	0.10	0.08
	Max	Mean	0.56	0.60	0.61	0.66
		Std.Dev	0.07	0.06	0.11	0.09

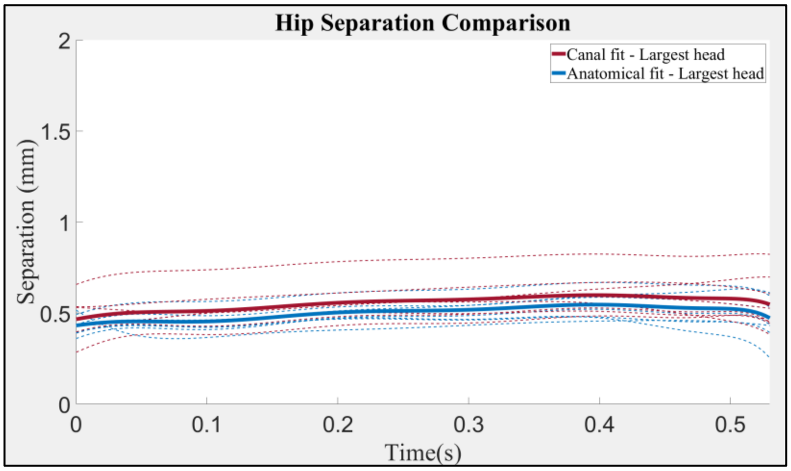

Figure 6-9: Hip separation comparison between canal fit and anatomical fit (largest head size preference).

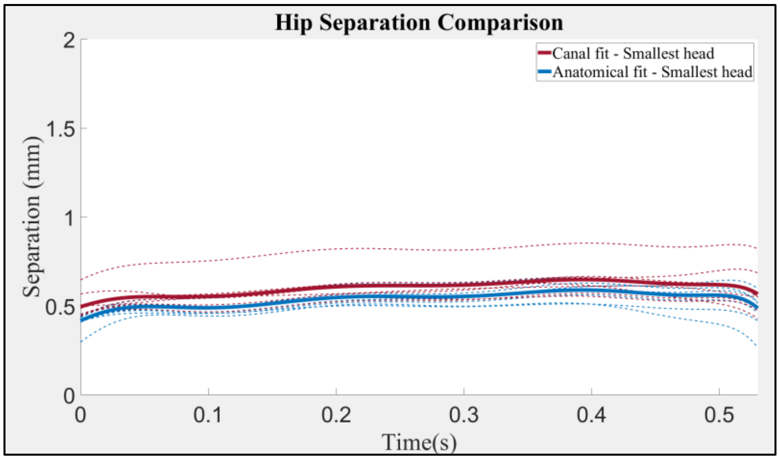

Figure 6-10: Hip separation comparison between canal fit and anatomical fit (smallest head size preference).

separation values. Specifically, the results further demonstrate that the anatomical fit alignment position resulted in lower hip separation in comparison to the canal fit alignment position, irrespective of the stem head sizes employed (Figure 6-9 and Figure 6-10).

6.2.3. Hip Force, Contact Area, and Contact Stress

From the results of hip forces, it can be observed that altering the preferences for head size has a negligible impact on the hip forces generated if the stem is aligned in the anatomical fit position. Specifically, in the anatomical fit position, the average hip force values for surgeon 1 and surgeon 2 were 2.75 xBw and 2.76 xBw, respectively, with a difference of less than 1%. Conversely, in the canal fit position, the average hip force values for surgeon 3 and surgeon 4 were 2.91 xBw and 2.84 xBw, respectively, with a difference of 2.46% (Table 6). Notably, a negligible difference exists between the average hip force values of surgeon 1 and surgeon 2 when the stem is in the anatomical fit position, with only a 0.22% variation. In contrast, when the stem is in the canal fit position (surgeon 3 and 4), the difference in average hip force value is more noticeable. Surgeon 3's average hip force value exceeds surgeon 4's by 2.43%, which is about 11 times greater than the difference between surgeon 1 and surgeon 2.

These findings indicate that head size preferences have a minimal effect on hip forces in the anatomical fit position. However, in the canal fit position, the differences between the two head size preferences are more noticeable. Furthermore, it was observed that the anatomical fit position resulted in lower hip forces compared to the canal fit position, irrespective of the head size preferences (Figure 6-11 and Figure 6-12). It is speculated that larger head sizes may induce muscle tightness in the vicinity of the hip

Table 6: Hip force, contact area, and contact stress results for 8 subjects.

N = 8 subjects			Anatomical fit		Canal fit	
			Surgeon 1	**Surgeon 2**	**Surgeon 3**	**Surgeon 4**
Hip Force (xBW)	**Average**	Mean	2.75	2.76	2.91	2.84
		Std.Dev	0.52	0.52	0.66	0.58
	Max	Mean	3.08	3.09	3.30	3.20
		Std.Dev	0.57	0.55	0.77	0.65
Contact Area (cm^2)	**Average**	Mean	8.45	4.50	8.21	4.36
		Std.Dev	0.83	0.65	0.92	0.62
	Max	Mean	9.01	4.86	8.99	4.68
		Std.Dev	0.78	0.55	1.40	0.54
Contact Stress (MPa)	**Average**	Mean	2.84	5.37	3.10	5.76
		Std.Dev	0.40	0.75	0.64	1.26
	Max	Mean	3.28	5.99	3.56	6.48
		Std.Dev	0.51	0.85	0.65	1.46

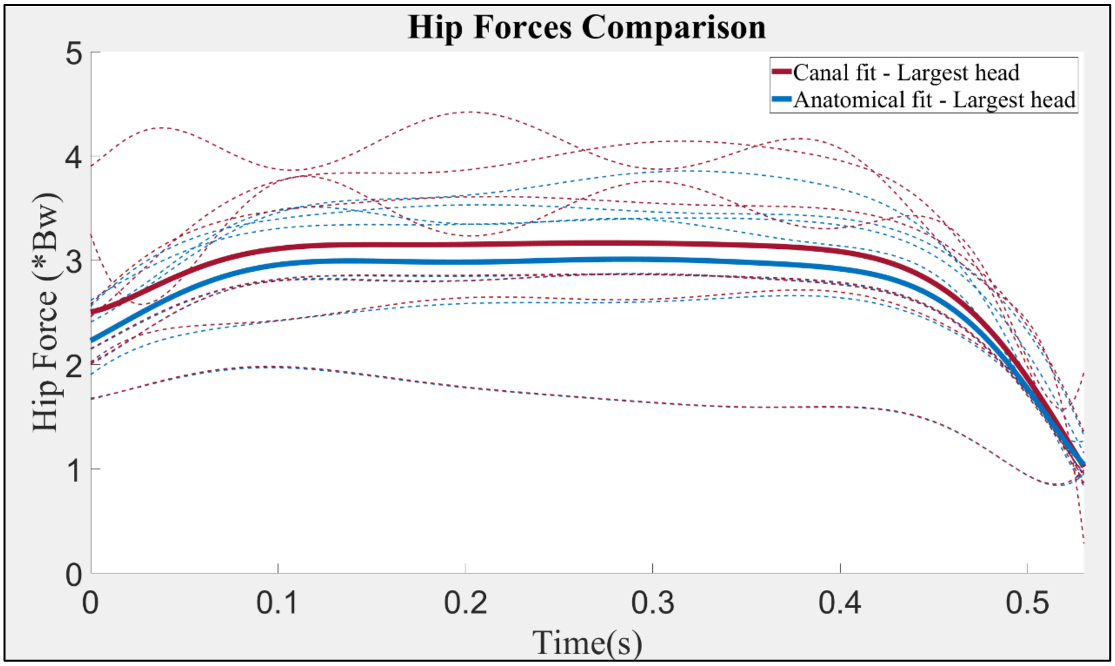

Figure 6-11: Hip forces comparison between canal fit and anatomical fit (largest head size preference).

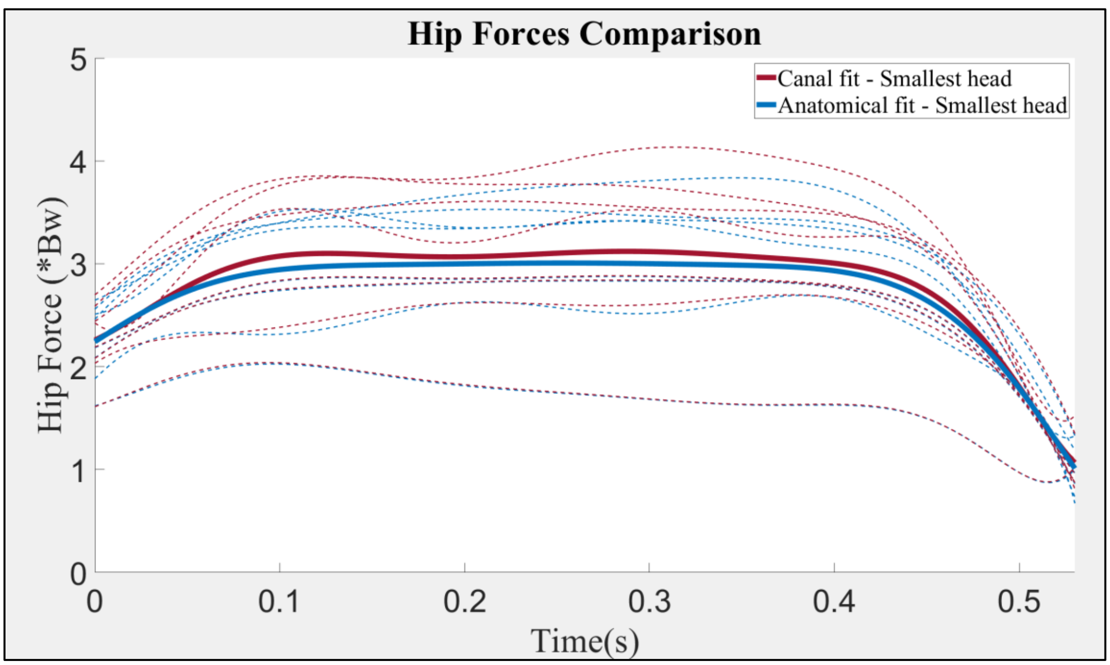

Figure 6-12: Hip forces comparison between canal fit and anatomical fit (smallest head size preference).

joint, given that they occupy more space. While this may not be a significant issue when the stem is aligned in the anatomical fit position, it becomes more apparent in the canal fit position.

In contrast to hip force, changes in head size preferences appeared to have a greater impact on contact area and contact stress. When the stem is in the anatomical fit position, choosing the largest liner size reduces the average contact stress value by 47.1% compared to choosing the smallest liner size, while in the canal fit position, it lowers the average contact stress value by 46.1%. Specifically, the utilization of a larger head size preference resulted in nearly twice the cup contact area and reduced contact stress by nearly half compared to a smaller head size preference (Table 6). Nonetheless, when analyzed individually, both head size preferences demonstrated improved hip mechanics in the anatomical fit position in comparison with the canal fit position (as seen in Figure 6-13, Figure 6-14, Figure 6-15, and Figure 6-16), characterized by greater cup contact area and reduced stress (Table 6). These findings mirror the results of a standard subject study outlined in the section 6.1, where the use of a canal fit led to increased edge loading and higher contact stresses.

6.2.4. Iliopsoas, Gluteus Medius, and Tensor Fasciae Latae Muscle Force

The average muscle forces result for the Iliopsoas, Gluteus Medius, and TFL muscles show minimal differences in the anatomical fit position, irrespective of head size preferences, with average forces of 0.56 xBw, 0.60 xBw, and 0.31 xBw respectively (Table 7, Table 8, and Table 9). However, in the canal fit position, larger head size preferences lead to slightly higher muscle forces for all three muscles compared to smaller head size

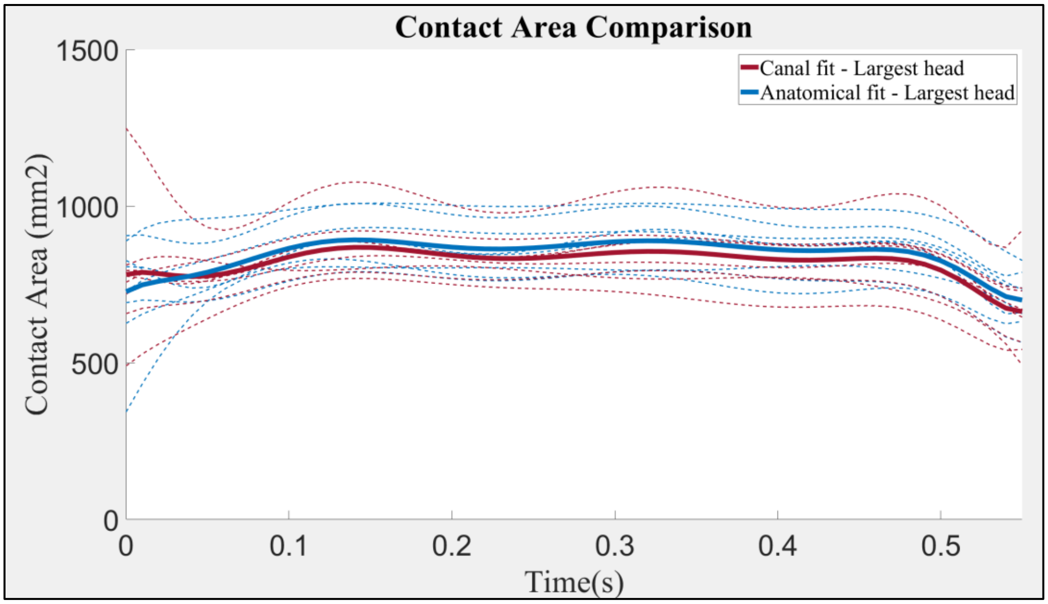

Figure 6-13: Contact area comparison between canal fit and anatomical fit (largest head size preference).

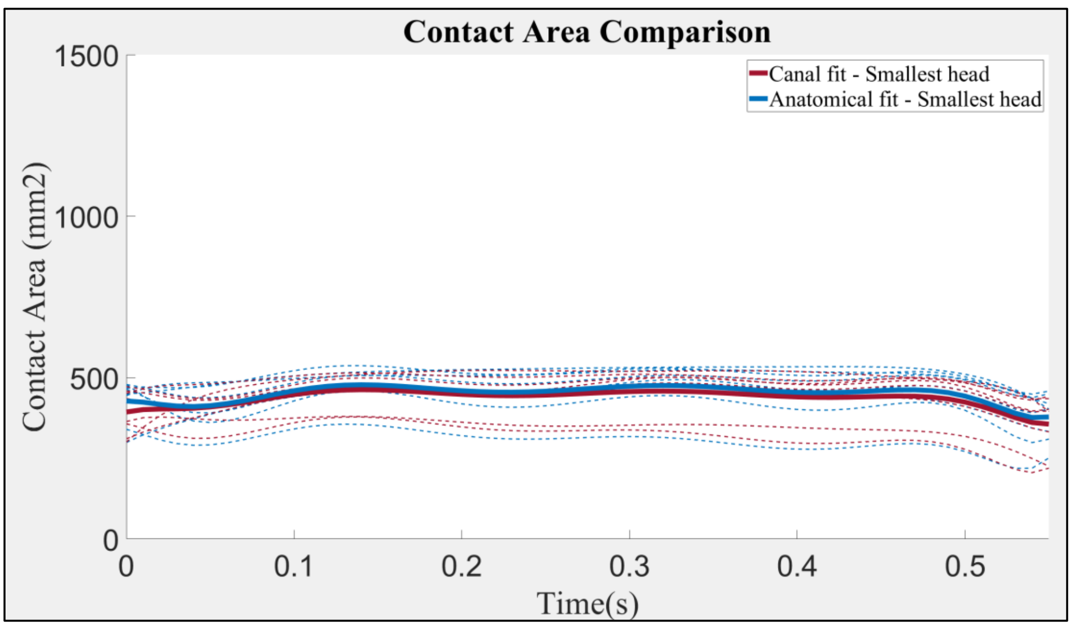

Figure 6-14: Contact area comparison between canal fit and anatomical fit (smallest head size preference).

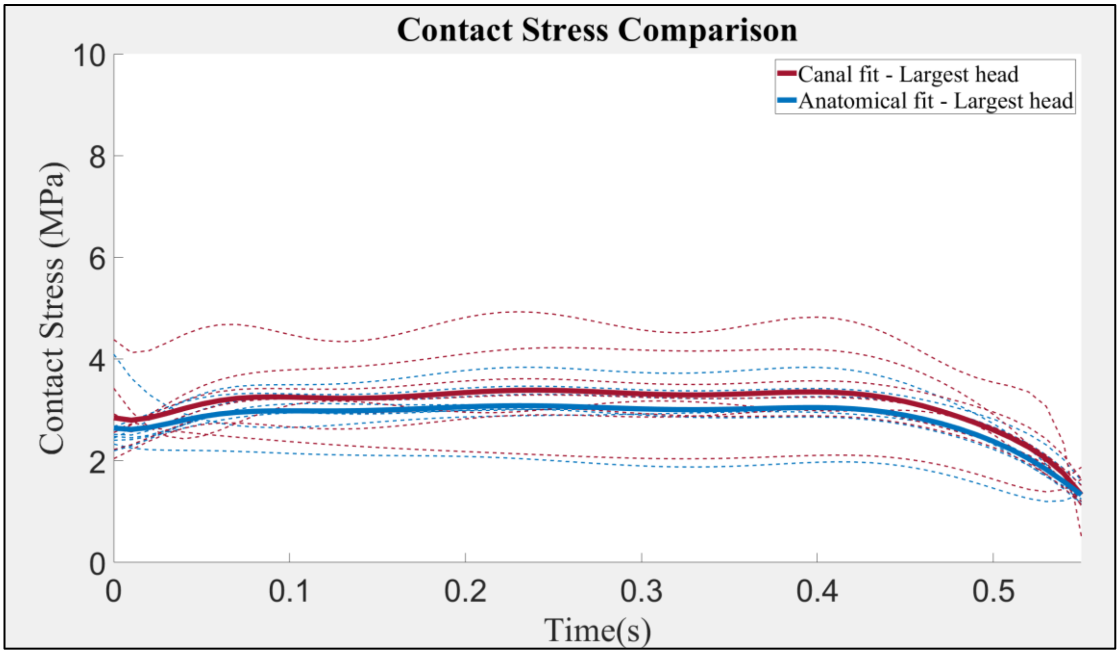

Figure 6-15: Contact stress comparison between canal fit and anatomical fit (largest head size preference).

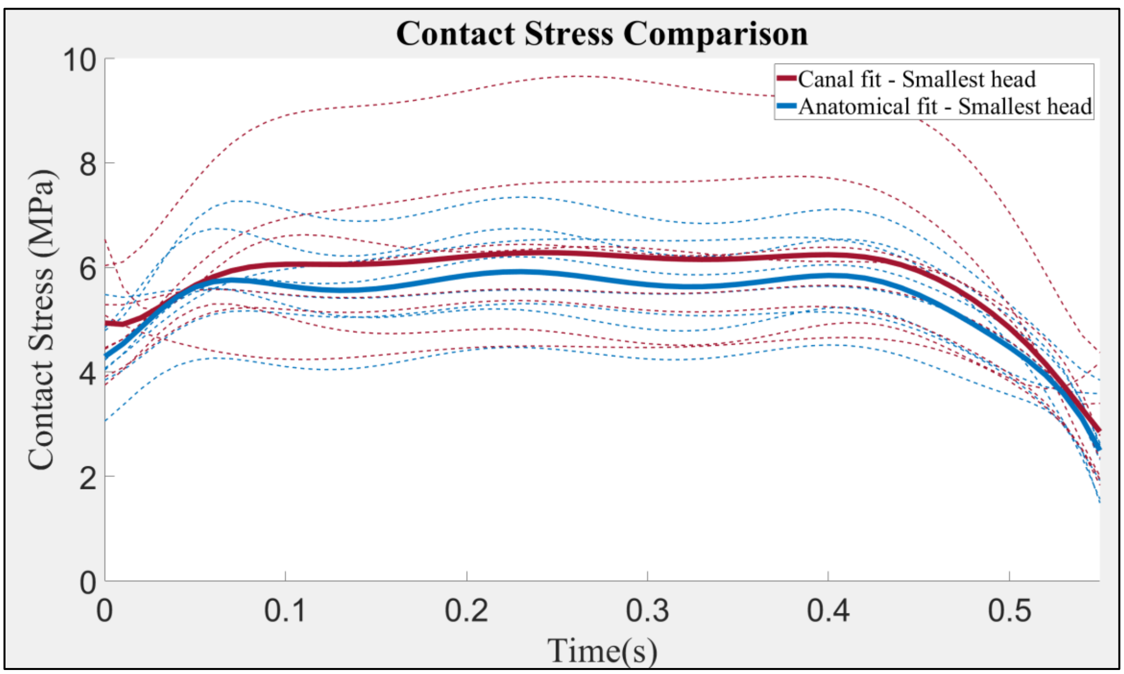

Figure 6-16: Contact stress comparison between canal fit and anatomical fit (smallest head size preference).

Table 7: Iliopsoas muscle force results for 8 subjects.

N = 8 subjects			Anatomical fit		Canal fit	
			Surgeon 1	Surgeon 2	Surgeon 3	Surgeon 4
Iliopsoas muscle force (xBW)	Average	Mean	0.56	0.56	0.60	0.59
		Std.Dev	0.24	0.24	0.28	0.26
	Max	Mean	0.70	0.70	0.76	0.74
		Std.Dev	0.32	0.31	0.37	0.35

Table 8: Gluteus Medius muscle force results for 8 subjects.

N = 8 subjects			Anatomical fit		Canal fit	
			Surgeon 1	Surgeon 2	Surgeon 3	Surgeon 4
Gluteus Medius muscle force (xBW)	Average	Mean	0.60	0.60	0.65	0.62
		Std.Dev	0.14	0.14	0.19	0.15
	Max	Mean	0.75	0.76	0.84	0.79
		Std.Dev	0.15	0.16	0.24	0.18

Table 9: Tensor Fasciae Latae muscle force results for 8 subjects.

N = 8 subjects			Anatomical fit		Canal fit	
			Surgeon 1	Surgeon 2	Surgeon 3	Surgeon 4
Tensor Fasciae Latae muscle force (xBW)	Average	Mean	0.31	0.31	0.34	0.33
		Std.Dev	0.10	0.09	0.13	0.11
	Max	Mean	0.35	0.35	0.39	0.38
		Std.Dev	0.10	0.10	0.14	0.12

preferences. This trend is similar to the results for hip forces with the stem is in the canal fit alignment position.

Overall, the anatomical fit alignment position produced reduced hip and muscle forces in all three muscles compared to the canal fit alignment. (Figure 6-17, Figure 6-18, Figure 6-19, Figure 6-20, Figure 6-21, and Figure 6-22). These findings further validate that surgical alignment preferences, in addition to implant sizing preferences, significantly impact the outcome of THAs.

6.3. Discussion

In this dissertation, we have incorporated different stem alignment positions with different head size preferences. It has been known or at least assumed that patients have a THA experience a benefit from having a larger femoral head size mated with a larger acetabular cup liner, but an analysis of femoral head has not been conducted that revealed specific results supporting these claims. Also, these head sizes were not analyzed for various surgical approaches to implantations. Although the anatomical fit requires more cortical bone removal compared to the canal fit position based on the results shown in section 6.1, the results from eight subject analysis clearly show the benefits of aligning the stem in the anatomical fit position. Obviously, there are more than just two factors that contribute to the outcome of THAs. The findings from this dissertation indicated that fitting the stem in the anatomical fit position resulted in a reduction of hip separation, an increase in femoral head contact area and contact stress within the acetabular liner compared to fitting the stem in the canal fit position. Additionally, the results also showed that using a larger femoral head reduced hip separation by 7% compared to the smallest stem head size,

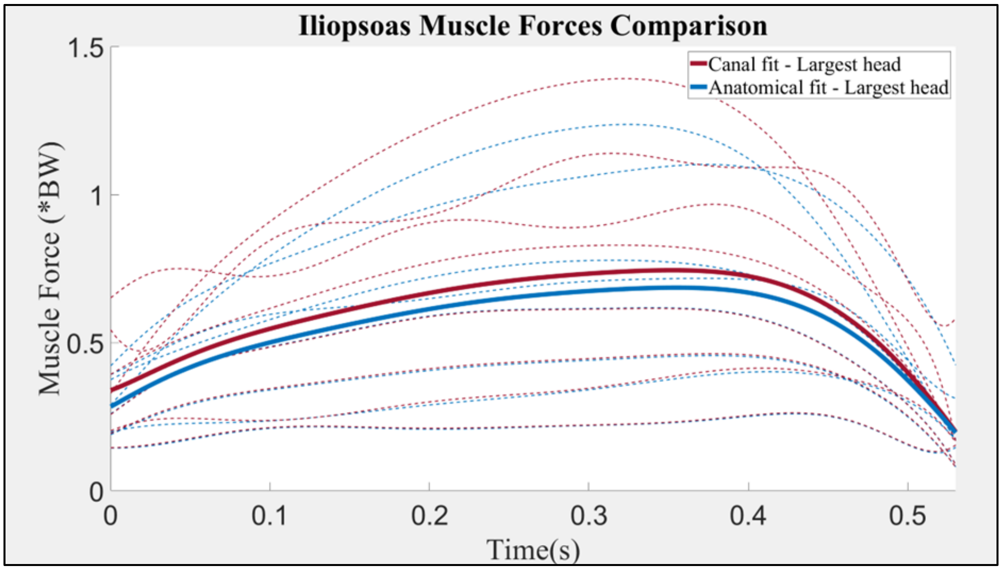

Figure 6-17: Iliopsoas muscle forces comparison between canal fit and anatomical fit (largest head size preference).

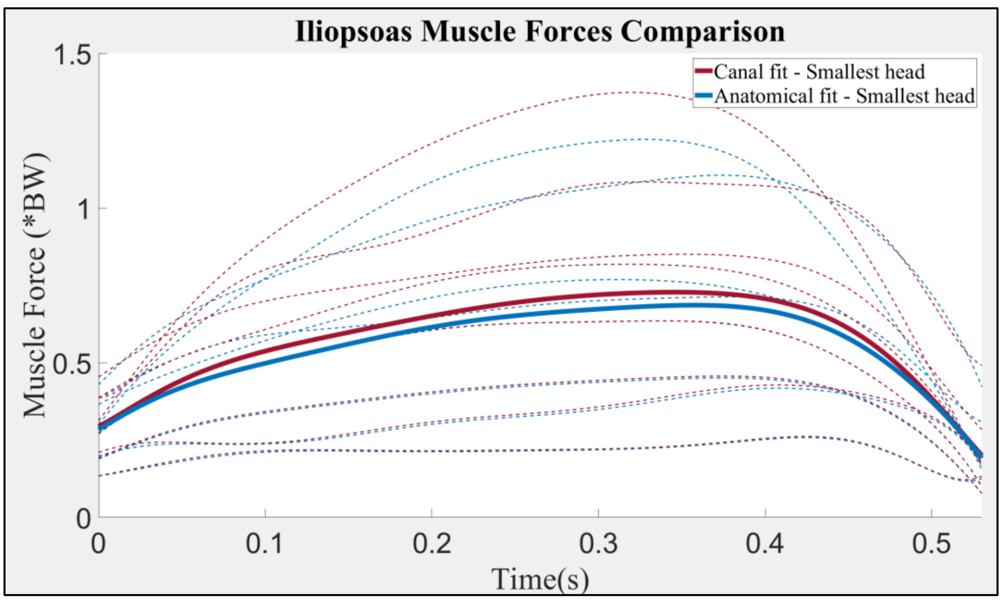

Figure 6-18: Iliopsoas muscle forces comparison between canal fit and anatomical fit (smallest head size preference).

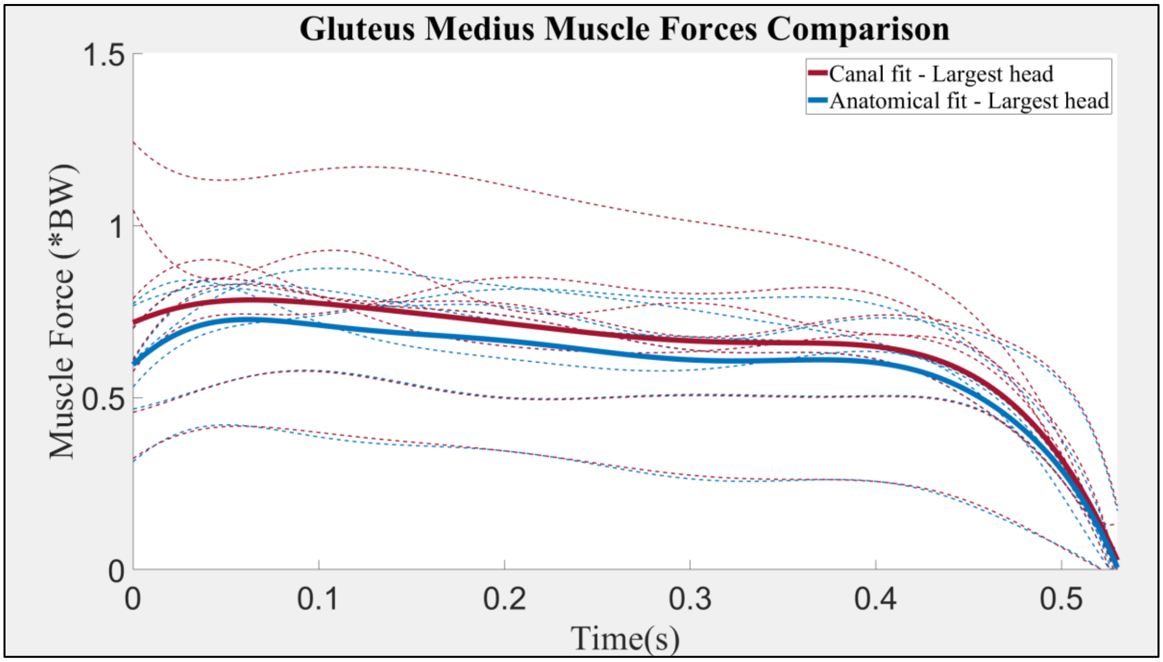

Figure 6-19: Gluteus Medius muscle forces comparison between canal fit and anatomical fit (largest head size preference).

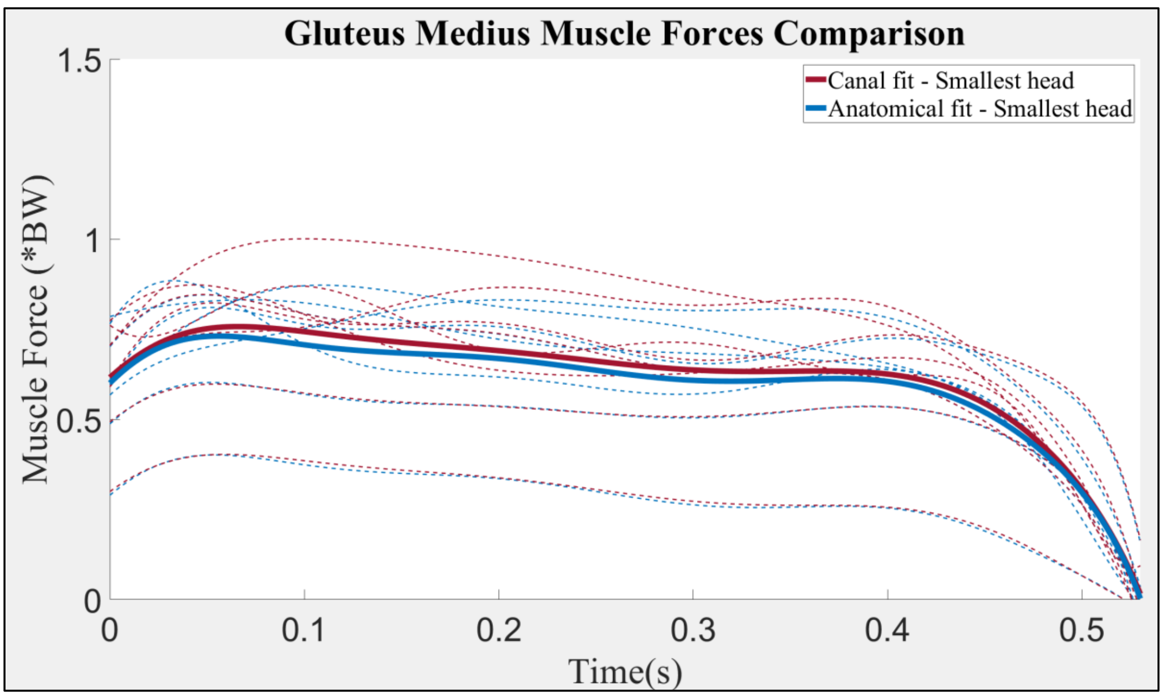

Figure 6-20: Gluteus Medius muscle forces comparison between canal fit and anatomical fit (smallest head size preference).

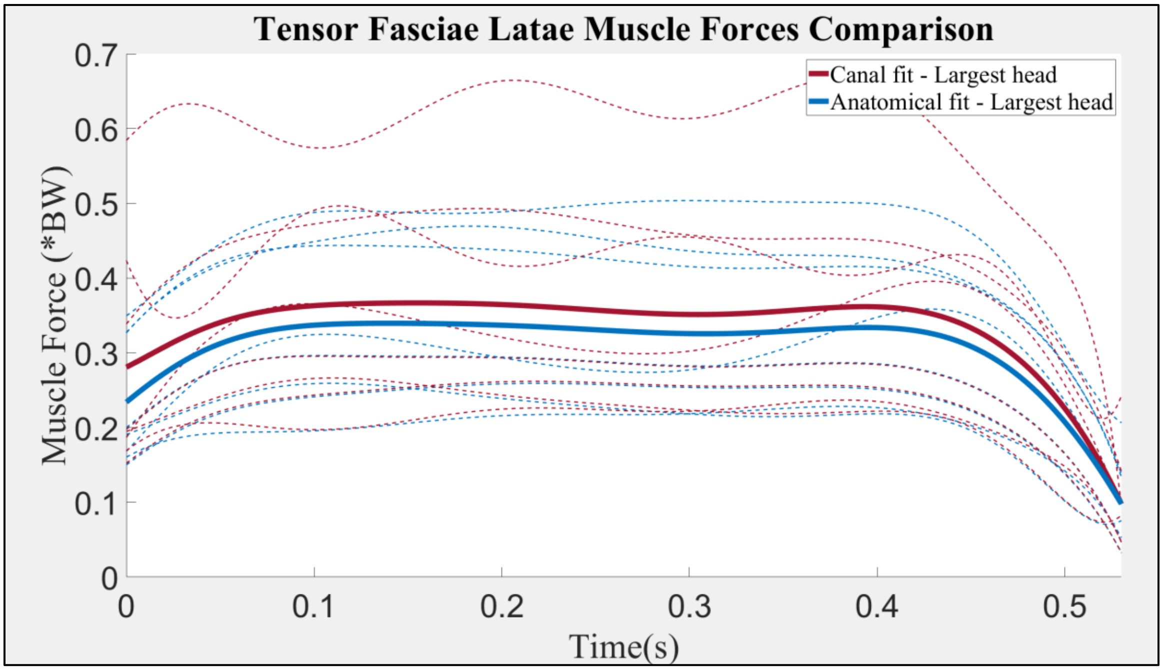

Figure 6-21: Tensor Fasciae Latae muscle forces comparison between canal fit and anatomical fit (largest head size preference).

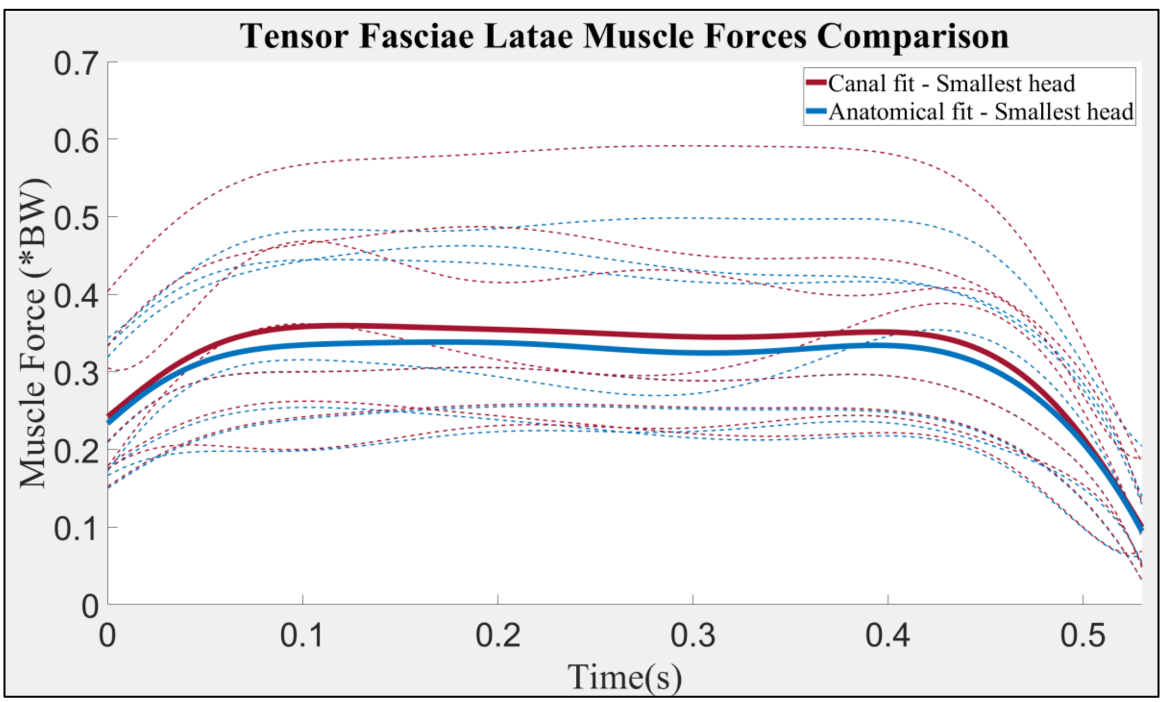

Figure 6-22: Tensor Fasciae Latae muscle forces comparison between canal fit and anatomical fit (smallest head size preference).

which aligns with the results of previous studies [68] [67]. Howie, et al. found that using a 36 mm stem head decreased the hip dislocation rate by 4.1% with a 95% confidence interval of 1.2% to 7.2% [67]. In a study conducted by John Fisher, et al., the authors concluded that there were significant increases in wear rate for both liner sizes (28 mm and 36 mm) under the microseparation conditions compared to the wear rate under conditions without introducing microseparation. Fisher, et al. also found that using larger liner size decreased the wear rate of the liner [68]. Our results showed a similar trend; in both head size preferences, the canal fit surgeons have higher hip separation and higher contact stress compared to the anatomical fit surgeons. Additionally, using larger head size resulted in larger contact area and lower contact stress.

Other studies have demonstrated in vivo hip separation and it is well-established that hip separation correlates with hip dislocation [68] [71] [49]. Our results also revealed that using the anatomical fit alignment position led to an increase in the contact area between the femoral head and the acetabular liner, compared to the canal fit alignment position. This leads to a reduction in the bearing surface contact stress by the femoral head on the acetabular liner surface, reducing the risk of polyethylene wear. In the canal fit position, using the largest femoral head sizes slightly increases hip force by 2.43% and muscle force values for the Iliopsoas, Gluteus Medius, and Tensor Fasciae Latae muscles by 2.72%, 4.49%, and 2.75%, respectively. In the anatomical fit position, there is no significant difference in hip and muscle forces between different femoral head sizes. The larger femoral head size in the canal fit position can cause impingement of adjacent muscles and increase pressure on the muscles around the hip, as demonstrated by J. Girard [72].

In the results sections, we examined the crucial factors that influence the success of a hip implant, namely the position of the stem and the stem head size preferences. Our focus was on the importance of maintaining the native hip anatomy, specifically with regard to the stem. Our findings from the previous results indicate that preserving the natural hip anatomy by positioning the stem anatomically leads to better hip mechanics, irrespective of the stem head size. We also recommend that orthopaedic companies integrate the stem's contact pattern with the cortical bone in the canal fit position to improve future implant designs. The ultimate objective of developing new stem designs is to achieve a better fit with the femoral canal while keeping the stem head center as close to the femoral anatomical head center as possible. By optimizing the head-to-head distances and component directions, implant design companies can create hip implants that emulate the natural mechanics of the hip joint, resulting in improved patient outcomes.

The hip analysis software applications are not only for implant design companies but also for surgeons. Poor stem alignment during surgery can lead to various complications such as instability, dislocation, and component wear, ultimately resulting in implant failure and the need for revision surgery. Therefore, it is critical for surgeons to pay close attention to implant alignment during the surgical procedure to optimize patient outcomes. Although it may be challenging to determine the “optimal” stem position within the canal, our findings suggest that anatomical fit alignment position offers superior hip mechanics compared to the canal fit position. However, the anatomical fit position requires more cortical bone removal, increasing the risk of bone fracture. Our hip analysis software could be a tool for surgeons to help them make their own decisions about what will be the “optimal” position when they fit the stem into the canal. Perhaps, the “optimal” position is somewhere in between the canal fit position and anatomical fit position.

CHAPTER 7: CONTRIBUTIONS

This dissertation focuses on the development and implementation of an implant algorithm in the hip analysis software package, with a specific emphasis on patient-specific component placement algorithms. The entire hip model software package contains a mathematical forward solution model of the hip joint, available for postoperative analyses of in vivo mechanics, along with various algorithms for component sizing suggestions, component positioning, and other analysis tools, which are useful tools for surgical technique evaluations and component designs. The contributions of this research include:

1. A novel concept of stem canal fit position that follows the natural shape of the femoral canal and requires minimal cortical bone removal.
2. New quantitative tools to assess different stem alignments, such as the stem contact map analysis in the medial and lateral sides of the stem, the cortical bone removal volume, and the anatomical distances data. These tools assist researchers in understanding the advantages and disadvantages of each stem alignment method.
3. A larger database with 63 additional Statistical Shape Model bones and 60 patient-specific bone models, capable of performing implant suggestion evaluations.
4. A database of patient specific bones of 10 subjects that can run simulations using the forward solution mathematical model of the hip joint, allowing for implant suggestion evaluations and additional evaluations with the forward solution model.
5. A new activity (the chair rise activity) within the forward solution mathematical model that expands the program's simulation capabilities.

6. A robust implant database that can be used to conduct analyses with any combination of stem type, cup type and implant positions.
7. A settling algorithm for the forward solution mathematical model to stabilize the system at the beginning of the activity.
8. The development of individual surgeon alignment preference profiles, which allow for clinical, surgeon-specific decisions typically made in the OR to be implemented into the hip model.
9. A User-friendly GUI containing various hip analysis tools, such as bone volume removal, stem contact map analysis, 3D and 2D cup contact map, 3D animation of activities, and bone cutting features. The GUI was redesigned that enhances the workflow of the hip analysis software and improves the User experience during program usage.
10. A fully functional hip analysis software that includes all the aforementioned tools. The integration of all these tools in a single software package helps in saving time during the training of new research personnel.

CHAPTER 8: SUMMARY AND FUTURE WORK

8.1. Summary

The primary objective of this dissertation was to develop a fully functional hip analysis software package capable of analyzing different implant types, comparing multiple component positioning scenarios, and running simulations of various activities. This software would be a valuable tool for orthopedic surgeons, as it would help them make informed decisions about the most suitable implant type, size, and orientation for a given patient, based on patient-specific bone anatomy and postoperative forward solution modeling predictions.

To achieve this objective, the research involved the development of multiple versions of the software, with each iteration being an improvement on the previous one. The software's development tasks included implementing the implant positioning algorithm, expanding the patient database, improving component sizing suggestion algorithms, adding analysis tools such as bone cutting and contact map calculation algorithms, and developing the program GUI, among others. Figure 3-1 in the dissertation provides a breakdown of the main objectives and tasks involved in developing the software. Over the course of almost four years of research, the software underwent continuous development and improvement. Each version was tested rigorously to ensure its accuracy and efficiency, with the feedback from the testing being used to guide the next iteration's development. The research team also collaborated with orthopedic surgeons to ensure that the software was meeting their needs and expectations.

The first objective was successfully achieved, as demonstrated by the hip analysis software GUI shown in Figure 4-19. The software is fully functional and capable of analyzing various implant types and component positioning scenarios. It can also simulate different activities, allowing surgeons to make informed decisions about the most suitable implant and component positioning for their patients. The tools developed for this dissertation can be used by implant design companies to improve future stem designs, cup designs, analyze existing hip implants and can be used by surgeons as preoperative planning and postoperative assessment tools. The software's accuracy and efficiency have been demonstrated through testing and validation against clinical data.

The second objective of this dissertation involved using the hip analysis software to conduct numerous studies with various scenarios. The most recent version of the software, as shown in Figure 4-19, was used in several analyses, including statistical shape model analyses, liner comparisons, stem comparisons, component positioning investigations, and surgeon preference analyses. The findings logically revealed that using different stem alignment techniques resulted in different outcomes, which helps provide insight into the future implant designs and surgical techniques. For instance, the anatomical fit alignment profile showed less hip separation, hip forces, contact stress, and muscle forces compared to canal fit alignments. However, achieving the anatomical fit position requires the surgeon to remove cortical bone from the femur, while the canal fit alignment requires less cortical bone removal, as the stem follows the natural shape of the canal to fit into the desired position.

8.2. Future work

In the future, we plan to continuously develop the hip analysis software and conduct further analyses to publish multiple journal articles. Future ideas and goals for program improvement are as follows:

1. Increase the total number of patient-specific subjects in the simulation database.
2. Add new activities to the software, including swing phase of gait, deep knee bend, walking upstairs and downstairs, etc.
3. Increase the duration of each activity simulation, such as a full gait cycle with at least 2 to 3 steps, or chair rise activities combined with sit down, walking upstairs/downstairs for 2 to 3 stairs.
4. Improve the running time of the implant positioning algorithm using a Ray Tracing algorithm to reduce the calculation time for contact between two meshes.
5. Implement a femoral head cutting algorithm to automatically cut the femoral head based on suggested stem size and stem position preferences.
6. Implement a cup polynomial calculation to the current program.
7. Implement automatic muscle and ligament attachment sites calculation for patient-specific data derived from the patient bone models.
8. Implement a cup positioning suggestion algorithm based on different surgeon preferences.
9. Implement the forward solution model for non-implanted hips.

These enhancements will improve the functionality and accuracy of the hip analysis software, making it a valuable tool for researchers, clinicians, and patients. Conducting further studies will improve our understanding of the hip joint and total hip arthroplasty, leading to a more powerful generation of the hip analysis software.

WORKS CITED

[1] Andreas Lösch, Felix Eckstein, Michael Haubner, Karl-Hans Englmeier,, "A non-invasive technique for 3-dimensional assessment of articular cartilage thickness based on MRI part 1: Development of a computational method," *Magnetic Resonance Imaging,* pp. 795-804, 1997.

[2] J. J. Callaghan, J. E. Templeton, S. S. Liu, D. R. Pedersen, D. D. Goetz, P. M. Sullivan, and R. C. Johnston, "Results of Charnley total hip arthroplasty at a minimum of thirty years: a concise follow-up of a previous report," *JBJS,* Vols. 86, no. 4, pp. 690-695, 2004.

[3] R. Otten, and H. Picavet, "Trends in the number of knee and hip arthroplasties: considerably more knee and hip prostheses due to osteoarthritis in 2030," *Nederlands tijdschrift voor geneeskunde,* vol. 154, pp. A1534-A1534, 2010.

[4] Ta, Manh Duc, "Development and Implementation of a Computational Surgical Planning Model for Pre-Operavite Planning and Post-Operative Assessment and Analysis of Total Hip Arthroplasty," *PhD diss., University of Tennessee*, 2019.

[5] RADIN, ERIC L. M.D, "Biomechanics of the Human Hip," *Clinical Orthopaedics and Related Research,* vol. 152, pp. 28-34, 1980.

[6] Jaffar, Akram Abood, Sadiq Jaffar Abass, and Mustafa Qusay Ismael, "Biomechanical aspects of shoulder and hip articulations: a comparison of two ball and socket joints.," *Al-Khwarizmi Engineering Journal,* vol. 2, no. 1, pp. 1-14, 2006.

[7] Ng KCG, Jeffers JRT, Beaulé PE, "Hip Joint Capsular Anatomy, Mechanics, and Surgical Management.," *Journal of Bone and Joint Surgery,* vol. 101, no. 23, pp. 2141-2151, 2019.

[8] Hewitt J, Guilak F, Glisson R, Vail TP, "Regional material properties of the human hip joint capsule ligaments," *Journal of orthopaedic research,* vol. 19, no. 3, pp. 359-364, 2001.

[9] Wagner FV, Negrão JR, Campos J, Ward SR, Haghighi P, Trudell DJ, Resnick D, "Capsular ligaments of the hip: anatomic, histologic, and positional study in cadaveric specimens with MR arthrography," *Radiology* , vol. 263, no. 1, pp. 189-198, 2012.

[10] R. D. Komistek, T. R. Kane, M. Mahfouz, J. A. Ochoa, and D. A. Dennis, "Knee mechanics: a review of past and present techniques to determine in vivo loads," *Journal of biomechanics,* Vols. 38, no. 2, pp. 215-228, 2005.

[11] Helwani, Mohammad A. MD, et al., "Effects of Regional Versus General Anesthesia on Outcomes After Total Hip Arthroplasty: A Retrospective Propensity-Matched

Cohort Study," *The Journal of Bone and Joint Surgery*, vol. 97, no. 3, pp. 186-193, 2015.

[12] Basques BA, Toy JO, Bohl DD, Golinvaux NS, Grauer JN, "General compared with spinal anesthesia for total hip arthroplasty," *The Journal of Bone and Joint Surgery*, vol. 97, no. 6, pp. 455-461, 2015.

[13] Learmonth ID, Young C, Rorabeck C, "The operation of the century: total hip replacement," *The Lancet*, vol. 370, no. 9597, pp. 1508-1519, 2007.

[14] Tsukayama DT, Estrada R, Gustilo RB, "Infection after total hip arthroplasty. A study of the treatment of one hundred and six infections," *The Journal of Bone and Joint surgery*, vol. 78, no. 4, pp. 512-523, 1996.

[15] Garvin, K L; Hanssen, A D, "Infection after total hip arthroplasty. Past, present, and future," *The Journal of Bone & Joint Surgery*, vol. 77, no. 10, pp. 1576-1588, 1995.

[16] Sikorski J, Hampson W, Staddon G, "The natural history and aetiology of deep vein thrombosis after total hip replacement," *The Journal of Bone & Joint Surgery* , Vols. 63-B, no. 2, pp. 171-177, 1981.

[17] Bauer, T., Schils, J., "The pathology of total joint arthroplasty: II. Mechanisms of implant failure," *Skeletal Radiology*, vol. 28, pp. 483-497, 1999.

[18] Lachiewicz, Paul F. MD; Kauk, Justin R. MD, "Anterior Iliopsoas Impingement and Tendinitis After Total Hip Arthroplasty," *JAAOS - Journal of the American Academy of Orthopaedic Surgeons,* vol. 17, no. 6, pp. 337-344, 2009.

[19] Trousdale, Robert T.; Cabanela, Miguel E.; Berry, Daniel J., "Anterior iliopsoas impingement after total hip arthroplasty," *The Journal of Arthroplasty,* vol. 10, no. 4, pp. 546-549, 1995.

[20] Sameer Jain and Peter V. Giannoudis, "Arthrodesis of the Hip and Conversion to Total Hip Arthroplasty: A Systematic Review," *The Journal of Arthroplasty,* vol. 28, no. 9, pp. 1596-1602, 2013.

[21] M.C.S. Inacio, E.W. Paxton, S.E. Graves, R.S. Namba, S. Nemes, "Projected increase in total knee arthroplasty in the United States – an alternative projection model," *Osteoarthritis and Cartilage,* vol. 25, no. 11, pp. 1797-1803, 2017.

[22] Kurtz, Steven; Ong, Kevin; Lau, Edmund; Mowat, Fionna; Halpern, Michael, "Projections of Primary and Revision Hip and Knee Arthroplasty in the United States from 2005 to 2030," *The Journal of Bone & Joint Surgery,* vol. 89, no. 4, pp. 780-785, 2007.

[23] LaCour, Michael Thomas, "Development and Implementation of a Forward Solution Hip Mathematical Model to Determine In Vivo Mechanics and Predict Hip Separation.," *PhD diss., University of Tennessee,* 2017.

[24] Carol A. Mancuso, Eduardo A. Salvati, Norman A. Johanson, Margaret G.E. Peterson, Mary E. Charlson, "Patients' expectations and satisfaction with total hip arthroplasty," *The Journal of Arthroplasty,* vol. 12, no. 4, pp. 387-396, 1997.

[25] Okafor Lauren; Antonia F. Chen , "Patient satisfaction and total hip arthroplasty: a review," *Arthroplasty,* vol. 1, no. 1, 2019.

[26] Ethgen, Olivier; Bruyère, Olivier; Richy, Florent; Dardennes, Charles; Reginster, Jean-Yves, "Health-Related Quality of Life in Total Hip and Total Knee Arthroplasty: A Qualitative and Systematic Review of the Literature," *Journal of Bone & Joint Surgery,* vol. 86, no. 5, pp. 963-974, 2004.

[27] Deborah M. Kennedy, PT, MSc, Paul W. Stratford, PT, MSc, Susan Robarts, PT, MSc, Jeffrey D. Gollish, MD, FRCSC, "Using Outcome Measure Results to Facilitate Clinical Decisions the First Year After Total Hip Arthroplasty," *Journal of Orthopaedic & Sports Physical Therapy,* vol. 41, no. 4, pp. 232-240, 2011.

[28] A team of JOSPT’s, "Total Hip Replacement: How Long Does It Take to Recover?," *Journal of Orthopaedic & Sports Physical Therapy,* vol. 41, no. 4, 2011.

[29] Stephen Richard Knight, Randeep Aujla, Satya Prasad Biswas, "Total Hip Arthroplasty - over 100 years of operative history," *Orthopedic reviews* , vol. 3, no. 2, 2011.

[30] Bota NC, Nistor DV, Caterev S, Todor A., "Historical overview of hip arthroplasty: From humble beginnings to a high-tech future," *Orthopedic Reviews*, vol. 13, no. 1, 2021.

[31] SALVATI, EDUARDO A. M.D.; BETTS, FOSTER PH.D.; DOTY, STEPHEN B. PH.D, "Particulate Metallic Debris in Cemented Total Hip Arthroplasty," *Clinical Orthopaedics and Related Research*, vol. 293, pp. 160-173, 1993.

[32] Huo, Michael H. M.D; Salvati, Eduardo A. M.D; Lieberman, Jay R. M.D; Betts, Foster Ph.D; Bansal, Manjula M.D, "Metallic Debris in Femoral Endosteolysis in Failed Cemented Total Hip Arthroplasties," *Clinical Orthopaedics and Related Research*, vol. 276, pp. 157-168, 1992.

[33] Lohmann CH, Singh G, Willert HG, Buchhorn GH, "Metallic debris from metal-on-metal total hip arthroplasty regulates periprosthetic tissues," *World J Orthop*, vol. 5, no. 5, pp. 660-666, 2014.

[34] A. Allisy, Henri Becquerel, "The Discovery of Radioactivity," *Radiation Protection Dosimetry*, vol. 68, no. 1-2, pp. 3-10, 1996.

[35] Paul R. Sierzenski, et al., "Applications of Justification and Optimization in Medical Imaging: Examples of Clinical Guidance for Computed Tomography Use in Emergency Medicine," *Annals of Emergency Medicine*, vol. 63, no. 1, pp. 25-32, 2014.

[36] Herminso Villarraga-Gómez, Ericka L. Herazo, Stuart T. Smith, "X-ray computed tomography: from medical imaging to dimensional metrology," *Precision Engineering*, vol. 60, pp. 544-569, 2019.

[37] Gunn, Therese and Rowntree, Pamela and Starkey, Deborah and Nissen, Lisa, "The use of virtual reality computed tomography simulation within a medical imaging and a radiation therapy undergraduate programme," *Journal of Medical Radiation Sciences*, vol. 68, no. 1, pp. 28-36, 2020.

[38] Douglas A. Dennis, Mohamed R. Mahfouz, Richard D. Komistek, William Hoff, "In vivo determination of normal and anterior cruciate ligament-deficient knee kinematics," *Journal of Biomechanics,* vol. 38, no. 2, pp. 241-253, 2005.

[39] Michael T. LaCour, Manh D. Ta, Richard D. Komistek, "Development of a hip joint mathematical model to assess implanted and non-implanted hips under various conditions," *Journal of Biomechanics*, vol. 112, 2020.

[40] P N T Wells, "Ultrasound imaging," *Physics in Medicine & Biology,* vol. 51, pp. R83-R98, 2006.

[41] Aldrich, John E. PhD, FCCPM, "Basic physics of ultrasound imaging," *Critical Care Medicine,* vol. 35, no. 5, pp. S131-S137, 2007.

[42] Mahfouz MR, Abdel Fatah EE, Johnson JM, Komistek RD, "A novel approach to 3D bone creation in minutes," *The bone and joint journal,* Vols. 103-B, no. 6, pp. 81-86, 2021.

[43] Louis Riglet, Anthony Viste, Tristan De Leissègues, Alexandre Naaim, Hervé Liebgott, Raphaël Dumas, Michel Henri Fessy, Laure-Lise Gras, "Accuracy and precision of the measurement of liner orientation of dual mobility cup total hip arthroplasty using ultrasound imaging," *Medical Engineering & Physics,* vol. 108, 2022.

[44] Abid Haleem, Mohd. Javaid, "3D scanning applications in medical field: A literature-based review," *Clinical Epidemiology and Global Health,* vol. 7, no. 2, pp. 199-210, 2019.

[45] Valeria Filippou, Charalampos Tsoumpas, "Recent advances on the development of phantoms using 3D printing for imaging with CT, MRI, PET, SPECT, and ultrasound," *Medical physics,* vol. 45, no. 9, 2018.

[46] Muraru D, Niero A, Rodriguez-Zanella H, Cherata D, Badano L, "Three-dimensional speckle-tracking echocardiography: benefits and limitations of integrating myocardial mechanics with three-dimensional imaging," *Cardiovascular Diagnosis and Therapy,* vol. 8, no. 1, pp. 101-117, 2018.

[47] Beckenbaugh RD, Ilstrup DM, "Total hip arthroplasty," *The Journal of Bone and Joint surgery. American Volume,* no. 649633 , pp. 60(3):306-313, 01 Apr 1978.

[48] Bedi A, Zaltz I, De La Torre K, Kelly BT, "Radiographic Comparison of Surgical Hip Dislocation and Hip Arthroscopy for Treatment of Cam Deformity in Femoroacetabular Impingement," *Radiographic Comparison of Surgical Hip Dislocation and Hip Arthroscopy for Treatment of Cam Deformity in Femoroacetabular Impingement,* vol. 39, no. 1, pp. 20-28, 2011.

[49] Komistek, Richard D. PhD; Dennis, Douglas A. MD; Ochoa, Jorge A. PhD; Haas, Brian D. MD; Hammill, Curt BS, "In Vivo Comparison of Hip Separation After Metal-on-Metal or Metal-on-Polyethylene Total Hip Arthroplasty," *The Journal of Bone & Joint Surgery,* vol. 84, no. 10, pp. 1836-1841, 2002.

[50] N. Subedi, N.S. Chew, M. Chandramohan, A.J. Scally, C. Groves, "Effectiveness of fluoroscopy-guided intra-articular steroid injection for hip osteoarthritis," *Clinical Radiology,* vol. 70, no. 11, pp. 1276-1280, 2015.

[51] Douglas A. Dennis, Richard D. Komistek, Eric J. Northcut, Jorge A. Ochoa, Allan Ritchie, "“In vivo” determination of hip joint separation and the forces generated due to impact loading conditions," *Journal of Biomechanics,* vol. 34, no. 5, pp. 263-629, 2001.

[52] M. R. Mahfouz, W. A. Hoff, R. D. Komistek and D. A. Dennis, "A robust method for registration of three-dimensional knee implant models to two-dimensional

fluoroscopy images," *IEEE Transactions on Medical Imaging,* vol. 22, no. 12, pp. 1561-1574, 2003.

[53] Bulat, Muge MSc; Korkmaz Can, Nuray PhD; Arslan, Yunus Ziya PhD; Herzog, Walter PhD, "Musculoskeletal Simulation Tools for Understanding Mechanisms of Lower-Limb Sports Injuries," *Current Sports Medicine Reports,* vol. 18, no. 6, pp. 210-216, 2019.

[54] Killen BA, Falisse A, De Groote F, Jonkers I, "In Silico-Enhanced Treatment and Rehabilitation Planning for Patients with Musculoskeletal Disorders: Can Musculoskeletal Modelling and Dynamic Simulations Really Impact Current Clinical Practice?," *Applied Sciences,* vol. 10, no. 20, 2020.

[55] Ajay Seth ,Jennifer L. Hicks ,Thomas K. Uchida, et al., "OpenSim: Simulating musculoskeletal dynamics and neuromuscular control to study human and animal movement," *PLOS Computational Biology,* vol. 14, no. 7, 2018.

[56] M Damsgaard, et al., "Analysis of musculoskeletal systems in the AnyBody Modeling System," *Simulation Modelling Practice and Theory,* vol. 2006, pp. 1100-1111, 2006.

[57] Le, Trung Bao, Mustafa Usta, Cyrus Aidun, Ajit Yoganathan, and Fotis Sotiropoulos, "Computational Methods for Fluid-Structure Interaction Simulation of Heart Valves in Patient-Specific Left Heart Anatomies," *Fluids ,* vol. 7, no. 3, 2022.

[58] Le, T., Elbaz, M.S.M., Van Der Geest, R.J. et al., "High Resolution Simulation of Diastolic Left Ventricular Hemodynamics Guided by Four-Dimensional Flow Magnetic Resonance Imaging Data," *Flow Turbulence Combust,* vol. 102, pp. 3-26, 2019.

[59] Castellazzi G, D'Altri AM, Bitelli G, Selvaggi I, Lambertini A, "From Laser Scanning to Finite Element Analysis of Complex Buildings by Using a Semi-Automatic Procedure," *Sensors,* vol. 15, no. 8, pp. 18360-18380, 2015.

[60] Ta Thi Thanh Mai, Le Van Chien, Pham Ha Thanh, "Shape optimization for Stokes flows using sensitivity analysis and finite element method," *Applied Numerical Mathematics*, vol. 129, pp. 160-179, 2018.

[61] Li-Xin Guo, Chi Zhang, "Development and Validation of a Whole Human Body Finite Element Model with Detailed Lumbar Spine," *World Neurosurgery,* vol. 163, pp. e579-e592, 2022.

[62] Y. Zhen, X. Cui, T. Lu, X. Li, C. Fang and X. Zhou, "3-D Finite-Element Method for Calculating the Ionized Electric Field and the Ion Current of the Human Body Model Under the UHVDC Lines," *IEEE Transactions on Power Delivery,* vol. 28, no. 2, pp. 965-971, 2013.

[63] Vavalle, N.A., Davis, M.L., Stitzel, J.D. et al, "Quantitative Validation of a Human Body Finite Element Model Using Rigid Body Impacts," *Annals of Biomedical Engineering* , vol. 43, pp. 2163-2174, 2015.

[64] Uzair N. Mughal, Hassan A. Khawaja and M. Moatamedi, "Finite element analysis of human femur bone," *Journal of Multiphysics* , vol. 9, no. 2, pp. 101-108, 2015.

[65] Russell H. Taylor, Arianna Menciassi, Gabor Fichtinger, Paolo Fiorini & Paolo Dario , "Medical Robotics and Computer-Integrated Surgery," in *Springer Handbook of Robotics*, Springer, 2016, pp. 1657-1684.

[66] Itaru Otomaru, et al., "Automated preoperative planning of femoral stem in total hip arthroplasty from 3D CT data: Atlas-based approach and comparative study," *Medical Image Analysis*, vol. 16, no. 2, pp. 415-426, 2012.

[67] Howie DW, Holubowycz OT, Middleton R, "Large Femoral Heads Decrease the Incidence of Dislocation After Total Hip Arthroplasty," *The Journal of Bone & Joint Surgery*, vol. 94, no. 12, pp. 1095-1102, 2012.

[68] Al-Hajjar M, Fisher J, Williams S, Tipper JL, Jennings LM, "Effect of femoral head size on the wear of metal on metal bearings in total hip replacements under adverse edge-loading conditions," *Journal of Biomedical Materials Research*, vol. 101B, no. 2, pp. 213-222, 2013.

[69] Lewinnek GE, Lewis JL, Tarr R, Compere CL, Zimmerman JR, "Dislocations after total hip-replacement arthroplasties.," *Journal of Bone and Joint Surgery,* vol. 60, pp. 217-220, 1978.

[70] Brian J. McGrory and Michael J. Stuart and Franklin H. Sim, "Participation in Sports After Hip and Knee Arthroplasty: Review of Literature and Survey of Surgeon Preferences," *Mayo Clinic Proceedings,* vol. 70, no. 4, pp. 342-348, 1995.

[71] Feng Liu, John Fisher, "Effect of an edge at cup rim on contact stress during micro-separation in ceramic-on-ceramic hip joints," *Tribology International,* vol. 113, pp. 323-329, 2017.

[72] J. Girard, "Femoral head diameter considerations for primary total hip arthroplasty," *Orthopaedics & Traumatology: Surgery & Research,* vol. 101, no. 1, pp. S25-S29, 2015.

VITA

Nguyen Dac Thang was born on July 4, 1996, in Bac Giang, Vietnam. He spent the first 6 years of his life there before moving to Bac Ninh city, where he grew up for 9 years. At the age of 15, Thang moved to Hanoi to attend the High School for Gifted Students, Hanoi National University of Education. It was during his time there that Thang's love for physics began to grow. He graduated from high school with the second prize in the Vietnam National Physics Olympiad in 2014. Thang then pursued his passion for mathematics by studying applied math at the Hanoi University of Science and Technology, School of Applied Mathematics and Informatics, for 5 years. In 2019, Thang received an offer from Dr. Komistek to continue his PhD studies at the University of Tennessee Knoxville. During his time at UTK, Thang used his knowledge of math and physics to solve problems related to the human skeleton structure, with a particular focus on the hip joint. Thang is fascinated by the beauty of mathematics and physics.

After completing his PhD in 2023, Thang intends to focus on his passions, which include studying math and physics, prioritizing his physical and mental health, and caring for his loved ones. Thang is a Vietnamese, and Thang loves living in Vietnam. Thang will be back in Vietnam one day eventually, so that he can spend time with important people in his life back in Vietnam.